# NANOPARTICLE-BASED APPROACHES IN CARDIOVASCULAR DISEASES

By

ANEETTA ELIZABETH KURIAKOSE

DISSERTATION

Submitted in partial fulfillment of the requirements

for the degree of Doctor of Philosophy at

The University of Texas at Arlington

August 2020

Arlington, Texas

**Dissertation Supervisor**

Dr. Kytai T. Nguyen

Professor of Bioengineering

**Dissertation Committee**

Dr. Liping Tang, Professor of Bioengineering

Dr. Yi Hong, Associate Professor of Bioengineering

Dr. Suchismita Acharya, Assistant Professor at University of North Texas Health Science Center

Dr. Hao Xu, Senior Lecturer of Bioengineering

# ABSTRACT


**NANOPARTICLE-BASED APPROACHES IN CARDIOVASCULAR DISEASES**

Aneetta E. Kuriakose, Ph.D.

The University of Texas at Arlington, 2020

Supervising Professor: Kytai T. Nguyen

Percutaneous coronary intervention (PCI) such as balloon angioplasty and stent placement are commonly employed for myocardial revascularization. These strategies, however, injure the arterial wall initiating a cascade of inflammatory responses that culminates in restenosis. Attempts are currently being made to improve the stents/balloon designs such that they suppress the inflammatory responses and support/enhance *in situ* reendothelialization. But the healing of the injured artery remains a major challenge. Therefore, in this work, we propose to characterize and identify a suitable fluorescent nanoparticle system that has potential to be used as vascular drug carriers. We also developed nanoparticles (NPs) that could enhance homing of more endothelial cells towards the injured arterial wall and facilitate their retention at that site, thereby promoting accelerated reendothelialization.

In the first approach, biodegradable photo-luminescent polylactone (BPLP) copolymers such as BPLP-co-poly (L-lactide) (BPLP-PLLA) and BPLP-co-poly(lactic-co-glycolic) acid (BPLP-PLGA50:50 and BPLP-PLGA75:25), that have intrinsic fluorescent properties were utilized to prepare fluorescent nanoparticles. These NPs would allow us to not only track their location following transplantation, but to also estimate the required dosing for administering and to assess the therapeutic outcome. Based on physical and *in vitro* compatibility properties of these investigated NPs, BPLP-PLGA NPs demonstrated as optimal fluorescent NPs with potential to be utilized for diagnosis and treatment of cardiovascular diseases. In the second approach, we created a nanoparticle system that enabled fast capture of endothelial cells by incorporating highly selective biorthogonal click chemistry between tetrazines and transcyclooctene. Our strategy of pre-targeting tetrazine modified nanoparticles demonstrates the specific binding of these NPs onto the injured arterial wall and then capturing and retaining transcyclooctene modified endothelial cells

to promote faster vascular healing. Taken together, these two approaches have outstanding potential applications in the detection and treatment of cardiovascular diseases.

## ACKNOWLEDGEMENT

I would like to express deepest appreciation to my mentor, Dr. Kytai T. Nguyen, for her persistent support, supervision and encouragement during my Ph.D. research. Dr. Nguyen is very considerate, always motivated me to strive through my challenges and difficulties, and without her mentorship, I would have never achieved my predoctoral fellowship. I am indeed blessed and grateful to have worked with Dr. Nguyen.

I would also like to thank Dr. Liping Tang for his invaluable suggestions, support, and guidance with the development of the multifunctional nanoparticles system to support cell homing. At this time, I would also like to acknowledge Dr. Min Kyung Khang with her sincere contribution towards this project.

I would like to express gratitude towards all of my committee members: Dr. Yi Hong, Dr. Suchismita Acharya, and Dr. Hao Xu for taking time out of their busy schedules to be a part of my dissertation committee and for helping me through the dissertation process. I would also like to acknowledge Dr. Jian Yang for providing me with biodegradable photoluminescent polymers and for his assistance with the publication of the first part of my research. In addition, I am truly grateful for all the co-authors in my publications for their help and support throughout the research.

I take this opportunity to thank Dr. Jyothi U. Men on for training me to be independent and instilling in me valuable lessons to become a good researcher. Additionally, I thank all the members at the Nanomedicine and Drug Delivery Lab, especially Vy Tran, Tam Nguyen, Harish Ramachandramoorty, Uday Chintapula, and Luis Soto for their help whenever I needed it. Special thanks to all my friends and colleagues, Dr. Nikhil Pandey, Dr. Roshni Iyer, Dr. Edidiong Inyang, Dr. Serkan Yaman, Thuy Thi Dang Truong, Dr. Duong Le, Dr. Linda Noukeu and Dr. Rachel Alex for their wonderful friendship and encouragement during my Ph.D program.

I would also like to thank the Bioengineering department and the staff for their help and assistance throughout my graduate study.

Lastly, I would like to acknowledge all my funding sources including T32 HL134613, F31 HL146118 and GAANN fellowships that made this work possible.

## DEDICATION

I would like to dedicate this dissertation to my family- my beloved parents Mr. Kuriakose and Mrs. Susan Kuriakose for their unconditional love and support throughout my journey; my loving husband, Sam Mathew; my wonderful sister, Ann Kuriakose and brother-in law Sibin Varghese; my brother Anoop Kuriakose and sister-in law Gisha Anoop for their constant encouragement and endless support to accomplish the thesis work; and my grandmother whose constant prayers and blessings have helped me to have the best things to occur in my life. Last but not the least, I dedicate this dissertation to my beautiful son, Benji and my awesome niblings, Johan, Aharon, Amos and Joanna for keeping my spirit up with all their innocence and making my world magical.

# TABLE OF CONTENTS

# LIST OF FIGURES

# LIST OF TABLES

# Chapter 1. INTRODUCTION

## 1.1 STATISTICS OF CARDIOVASCULAR DISEASE

Cardiovascular disease (CVD) accounts for the highest number of deaths in the United States. In fact, based on AHA statistics, CVD claims more lives each year than all forms of cancer and chronic lower respiratory diseases combined.[1] It is estimated that >130 million of the adult population of the U.S. will have some form of CVD by the year 2035.[2] The prevalence increases with advancing age and varies within racial, ethnic, geographic, and sociodemographic groups.[3] Among the different types of CVD, coronary heart disease mostly affects human lives, followed by stroke and heart failure. In 2015, 7.4 million out of the 17.7 million people that died from CVDs were due to coronary heart disease.[4] Although this trend in rate of deaths associated with coronary heart disease has declined since 2004, the burden and risk factors remain alarmingly high.[1] Furthermore, the medical costs associated with management and treatment of coronary artery disease were calculated to be >$100 billion annually; and they were expected to increase by about 100 percent by the year 2030.[1, 5] Overall, these statistics suggest the significance of developing effective, preventive care measures to substantially reduce the mortality and morbidity associated with CVD events.

## 1.2 CORONARY ARTERY DISEASE

Coronary artery disease (CAD) is characterized by the formation of atherosclerotic plaque within the lining of the coronary arteries resulting in constricted blood vessels. This limits the adequate supply of oxygen-rich blood to the heart muscle, thereby affecting functionality. Eventually, the reduced blood supply to the heart causes chest pain (angina), shortness of breath, myocardial infarction (MI), or sudden cardiac death. Some of the conventional risk factors that contribute to CAD include hypertension, hyperlipidemia, diabetes mellitus, smoking, and family history of CAD or MI; and it is estimated that these risk factors only account for 50% of the total risk of CAD, suggesting that some of the main causative factors have yet to be identified.[6, 7]

Atherosclerosis is initiated when the endothelium lining the blood vessel gets disrupted or activated as it encounters certain bacterial products or risk factors as diverse as dyslipidemia, vasoconstrictor

hormones inculpated in hypertension, the products of glycoxidation associated with hyperglycemia, or proinflammatory cytokines derived from excess adipose tissue.[8, 9] As a result, endothelial cells highly express the adhesion molecules such as P-selectin and vascular cell adhesion molecules-1 (VCAM-1), which mediate the attachment and recruitment of monocytes and lymphocytes to the region. Furthermore, low density lipoproteins (LDL) can permeate through the endothelial layer, accumulate in the intimal layer, and undergo oxidation. In response to the modified lipoproteins, vascular cells produce chemoattractant factors, which include monocyte chemoattractant protein-1 to direct the migration and diapedesis of adherent monocytes. Those monocytes that interact with endothelial cells increase their production of matrix metalloproteinase 9 (MMP-9) supporting the transmigration of leukocytes through the endothelial layer and their basement membrane. Within the intima, monocytes mature to become macrophages that scavenge the modified lipoproteins, leading to their formation of foamy cells. These foamy texture cells replicate and amplify the inflammatory response via secretion of various growth factors and cytokines. T cells that also recruit to the intimal region of blood vessels get activated and differentiate into T- helper 1 effector cells and amplify inflammatory activity with increased production of proinflammatory cytokines. As a result of increasing proinflammatory stimuli, smooth muscle cells (SMCs) get attracted to the site of a fatty streak; hence, they start to rapidly proliferate and produce extracellular matrix, mainly collagen and proteoglycans. This process leads to the progression of the lipid-rich lesion to fibrous plaque that encroaches the lumen of coronary vessels. As the lesion progresses, calcification occurs, and the final lesion formed consists of a fibrous cap with an overlying lipid rich core containing necrotic material that may be highly thrombogenic.[10]

### 1.2.1 Treatment Options and Limitations

Depending on the patient diagnosis and the extent of plaque buildup, current clinical treatments include medical therapy (MED), percutaneous coronary interventions (PCI) and coronary artery bypass grafting (CABG). In medical therapy, generally, antithrombotic drugs including aspirin and clopidogrel are prescribed aiming to control angina and prevent or reverse plaque progression. Although they have contributed towards substantial reduction of serious cardiovascular events and reduced all-cause mortality, there is a significant increase in risk of bleeding. Next to MED, PCI and CABG focus on re-establishing

adequate blood supply to the infarcted heart. CABG is a highly invasive procedure which utilizes the autologous arteries or veins as grafts to bypass the diseased coronary arteries to restore the blood flow.[11] It is generally recommended for many patients with the presence of severe left main stem artery stenosis, or left main equivalent disease and multi-vessels.[12, 13] Some of the main limitations with CABG include donor site morbidity, graft failure, and unavailability of suitable vessels for replacements especially with patients with underlying chronic conditions.[11, 14, 15]

PCI, on other hand, is a much less invasive procedure where the occluded arteries are opened using angioplasty balloons or stenting. Various clinical trials and meta-analyses have shown the improved outcomes of PCI when treated for acute coronary syndromes.[16] However, one of the main challenges with PCI is that it can inevitably damage and remove the endothelial cells lining the lumen of the blood vessel, initiating a cascade of inflammatory events culminating in thrombosis and restenosis. To overcome this, a new generation of drug eluting stents (DES) have been designed to locally deliver anti-proliferative drugs and have shown significant improvement in the clinical outcome.[17] Despite this, due to the non-specific action of these drugs on the endothelial cells, they prolong the healing of the vessel after implantation of DES resulting in late stage thrombotic events.[18] According to a recent *in vivo* case-controlled study, ~80% of patients diagnosed with late stent thrombosis were found to have uncovered struts that exposed foreign materials to the immune cells.[19] Furthermore, long-term anti-thrombogenic therapies increase the risk of serious bleeding complications in patients,[20] so rapid restoration of the functional endothelial layer can significantly prevent undesired late stage inflammatory responses following vascular interventions.

### 1.2.2 Restenosis and Intimal Hyperplasia

The vascular endothelium plays a pivotal role in maintaining homeostasis, regulates vascular tone as well as supports critical antithrombotic functions by producing various vasoactive molecules including nitric oxide, thrombomodulin, prostaglandins, tissue plasminogen activator and vasoconstrictors. When these endothelial cells get damaged due to a balloon injury or stent implantation, cells get activated to express the adhesion markers including ICAM-1, VCAM-1, and P-selectin or to detach to expose the underlying subendothelial collagen matrix. Platelets, under physiological conditions, are relatively inert circulating cells constantly 'surveying' the vasculature for any damage to the endothelium.[21] In response to

the endothelium denudation, the platelets adhere and activate to release mediators such as ADP and thromboxane, which eventually leads to platelet aggregation.[22] Platelet aggregates then interact with other inflammatory cells and support their infiltration. The initial tethering of platelets to the site of injury is mediated by the interaction of the glycoprotein (GP)Ib-IX-V complex on the platelet membrane with the A1 domain of vWF in the exposed sub endothelium.[22] This interaction further facilitates other platelet receptors including GPVI and $\alpha_2\beta_1$ engages with the collagen matrix for firmly adhering the platelets to the vasculature wall.[22] Due to this innate characteristic of platelets in recognizing the injury, it has paved the way to develop platelet mimicking drug delivery vehicles to treat various ailments such as wound healing, regeneration, thrombosis, and cancer. Following the platelet adherence, more leukocytes including monocytes and neutrophils are recruited and interact with the subendothelial matrix, thereby aggravating the inflammatory responses post PCI procedure.[23] In addition, smooth muscle cells (SMCs) in the medial layer of blood vessels respond to platelet derived growth factors (PDGF) and other growth factors released by adherent platelets by rapid proliferation, and deposition of extracellular matrix protein contributing to intimal thickening, neointimal hyperplasia and finally the development of restenosis following PCI.[24]

Delayed reconstruction of the endothelial layer has been identified as one of the major contributing factors for the late thrombosis.[25, 26] To improve reendothelialization, stent designs have been improvised to incorporate the following features: (a) stents with thin struts and streamlined geometry to improve the local vascular flow conditions[24]; (b) drug eluting stents to release anti-inflammatory agents including paclitaxel, dexamethasone, sirolimus or one of its analogues (everolimus, zotarolimus, or biolimus) to inhibit the progression of intimal hyperplasia[27]; and (c) cell-capturing stents that are immobilized with endothelial progenitor cells (EPCs) specific antibodies to support *in situ* endothelialization. For instance, the Genous® (OrbusNeich) stent, which is coated with anti-CD34 antibodies, is the first device of its kind evaluated in humans.[27-29] But the clinical data with the usage of Genous stents is not very promising, especially because CD34 is not an EPC specific marker, but rather a pluripotent stem cell marker. Hence, only a small population of CD34 positive cells form endothelial cells, whereas the rest can differentiate into various types of cells including inflammatory cells and vascular smooth muscle cells that exaggerate restenosis. Hence, other endothelial specific antibodies including anti-VEGFR2, anti-CD133 and anti VE-cadherin have been investigated for their potential to specifically capture progenitor cells to the injured site.[27-29] With the advent

of nanotechnology, newer modalities using magnetic targeting have also been explored to attract and capture transplanted endothelial cells effectively onto stents and vascular grafts.[30, 31]

### 1.3 NANOTECHNOLOGY IN TREATMENT AND DIAGNOSIS OF CVD

Nanoparticles (NPs) put forward many attractive features for drug delivery such as a high drug loading capacity, drug protection from a harsh biological environment, reduced off-target cytotoxicity of drugs, improved drug solubility, controlled drug release kinetics, and specific disease targeting.[32] Hence, in the past years, many efforts have been made to develop nanomedicines for treatment and diagnosis of various ailments including CVD. A diverse range of nanoparticle formulations of different composition, sizes and shapes have been utilized for this purpose. This includes liposomes, micelles, polymeric nanoparticles, dendrimers, gel like nanoparticles and magnetic nanoparticles.[33]

To minimize the harmful side effects and non-specific interaction of therapeutics, targeted delivery of nanomedicine is highly desirable. In targeted drug delivery, nanoparticles are expected to deliver payloads specifically to the diseased regions following systemic administration. To achieve this, nano systems were functionalized with proteins or antibodies to recognize their antigen or ligands highly expressed in the injured tissues. For instance, collagen IV represents 50% of the vascular basement membrane, and following PCI, this layer is generally exposed to the circulation. Chan et al. (2011) designed paclitaxel loaded nano burrs modified with collagen IV targeting peptides and showed them to be effective in suppressing stenosis following balloon angioplasty.[34] On the other hand, Kona et al. (2013) developed Gp1bα functionalized nanoparticles targeted towards vWF deposited onto a vascular basement membrane to deliver dexamethasone for inhibiting restenosis and intimal hyperplasia.[35] In another instance, alendronate loaded liposomes were modified with ligands to recognize the surface receptors present on activated platelets (e.g. GpIIb/IIIa and P-selectin) and demonstrated it to be effective in reducing in stent restenosis to 30% when compared to empty liposomes.[36] Biomimetic nano systems have also been increasingly researched in recent years, due to their innate characteristics to specifically accumulate at the diseased sites and their increased circulation time compared to other drug delivery systems. Hu et al. (2016) cloaked the docetaxel loaded PLGA nanoparticles with platelet membranes and demonstrated them to have platelet mimicking properties including selective adhesion to the damaged vasculature and improved

binding to platelet-adhering pathogens.[37] Docetaxel exhibited enhanced therapeutic efficacy in inhibiting restenosis when delivered by these platelet-mimetic nanoparticles. Xu et al. (2019) utilized similar biomimetic systems to deliver recombinant tissue plasminogen activator (rt-PA) to reverse thrombosis and simultaneously decreased potential side effects as well prolong the half-life of thrombolytic agents.[38] In another approach by Anselmo et al. (2014), they applied key attributes of natural platelets such as discoidal morphology, mechanical flexibility, biophysical and biochemical mediated aggregation; and heteromultivalent presentation of ligands to adhere onto vWF and collagen to develop synthetic platelets. Their "platelet-like" nanoparticles exhibited superior binding characteristics compared to spherical and rigid discoidal counterparts as well as demonstrated site selective adhesive and platelet-aggregatory properties under physiological flow conditions. Such nanoparticle systems were utilized to mimic and improve the hemostatic function of natural platelets.[39]

Localized drug delivery can also be achieved by coating the angioplasty balloons and stents with drug loaded nanoparticles. For instance, Iyer et al. (2019) transferred unconjugated nanoparticles to the arterial wall utilizing hydrogel coated angioplasty balloons and demonstrated long term retention on the vasculature, even under a physiological flow condition using *ex vivo* rat arteries.[40] Bioresorbable stents modified to elute the therapeutic loaded nanoparticles have also been developed to prevent stenosis after stent implantation.[41] Chorny et al. (2010) utilized magnetic nanoparticles and guided them to stented arteries using an external magnetic field for localized delivery of paclitaxel.[42] Such an approach also demonstrated an effective treatment efficacy by inhibiting in-stent stenosis at drug doses below those provided by paclitaxel-eluting stents. Furthermore, other stimuli responsive systems based on various triggers such as light irradiation, shear stress, pH alteration, change in temperature or response to redox potential were also investigated to support localized drug delivery for the treatment of cardiovascular disease.[33] An innovative strategy by Korin et al. (2012) was the development of shear-responsive microaggregates that break up into nanoscale components when exposed to abnormally high fluid shear stress present at highly constricted blood vessels.[43] These novel microaggregates were utilized to deliver tPA, which exhibited superior delivery of therapeutics at diseased regions with minimal side effects and maximum drug efficacy.

In addition to their capability as drug carriers, multifunctional nanoparticles are used to support cell delivery, capture, and retain at diseased sites for reendothelialization, angiogenesis and tissue regeneration. Magnetically mediated delivery of endothelial cells is one such instance where superparamagnetic nanoparticles (MNPs) were utilized to guide transplanted cells to the injured region. Polyak et al. (2016) and others have incorporated biodegradable MNPs into endothelial cells and localized them to stents using a brief exposure to a uniform magnetic field.[44, 45] It was proven that magnetically assisted delivery of endothelial cells had potential for homing cells to the injured vasculature and prevented in-stent stenosis. In another instance, bi-functionalized nano scaffolds were designed to engage with an injured artery, and at the same time, support the enrichment of endogenous or exogenously delivered therapeutic stem cells for *in* situ arterial wall regeneration following PCI.[46]

Increasing research focuses on utilizing nanoparticles to meet unmet needs in cardiovascular imaging. Especially due to the specific features provided by nanoparticles such as atypical size distribution, targeted specific delivery, high contrast capability, and an increased lifetime make them an indispensable tool in the future of medical imaging.[47] Nanoparticles can be labeled with a variety of imaging agents to enable their detection with computer tomography (CT), magnetic resonance imaging (MRI), optical methods, or nuclear imaging such as PET and SPECT. Most of the clinically applied contrast agents have two main limitations that can be improved with the use of nanoparticles: the first is toxic effects and the second is non-target specificity. For instance, the contrast agent gadolinium is used to detect plaque with cardiac resonance imaging; however, gadolinium releases free ions inducing toxic effects in the body.[48] Recently, it was found that self-assembled gadolinium nanoparticles have enhanced MRI contrast ability with reduced toxicity.[49] Another way to counteract the toxicity is by incorporating gadolinium into polymeric nanoparticles as demonstrated by Menon et al. (2016) and showing cytocompatibility and imaging capabilities following encapsulation within nanoparticles.[50] Superparamagnetic iron oxide nanoparticles were also utilized as contrast agents and served to be a safer alternative to gadolinium. Small sized dextran coated magnetic nanoparticles are clinically utilized to passively target intraplaque macrophages. However, these nanoparticles are amenable for surface modification, enabling them to actively target any biomarkers of interest for the diagnosis and imaging of cardiovascular diseases.[51] Iron oxide nanocrystals can also be incorporated into functionalized drug delivery systems such as micelles, liposomes, nano emulsion and

high-density lipoproteins to promote active targeting for *in vivo* imaging.[51] In addition to iron oxide nanoparticles, gold nanoparticles demonstrated favorable biocompatibility and versatility; hence, recently these particles have been applied to the cardiovascular field especially for CT and optical imaging.[52] Additionally, carbon nanotubes have been employed for the imaging application. Due to the high echogenic property of these nanostructures, they are able to be used as contrast agents for ultrasonography and demonstrated their capability to generate an ultrasound signal comparable with commercially available contrast agents without causing any toxicity.[53]

### 1.4 CELL THERAPY FOR TREATMENT OF CVD

Stem cell therapy has shown to be an attractive therapeutic approach to prevent and treat CVD.[54] A spectrum of stem cells from various sources has been investigated for their application in CVD. This includes skeletal myoblasts, bone marrow mononuclear cells, resident cardiac stem cells, adipose stem cells and embryonic progenitor cells.[55] Stem cell therapy has been used as treatment for various kinds of CVD; however, our focus in the following review will be upon their utilization in supporting the rapid reendothelialization process in preventing restenosis. Mostly, endothelial progenitor cells (EPCs), outgrowth endothelial cells (OECs), mesenchymal stem cells (MSCs) or induced pluripotent stem cells (iPSCs) are administered to treat an arterial injury following PCI.[31, 45, 56-60] A successful regeneration occurs when these exogenously delivered stem cells or endogenous cells differentiate into functional endothelial cells. Although MSCs were shown to be promising due to their high adhesive capacity and regeneration-promoting paracrine activities, these cells can potentially differentiate into smooth muscle cells and aggravates the arterial injury.[61] Therefore, Wang et al. (2007) co-delivered both MSCs along with OECs, and demonstrated that OECs can significantly modulate and attenuate intimal hyperplasia contributed by MSCs following vascular injury.[61] In another instance, Chang et al. (2018) utilized genetically modified MSCs secreting growth factors that not only supported increased reendothelialization and reduced restenosis, but also helped in specific differentiation of MSCs into mature endothelial cells lining the arterial lumen.[62]

Upon an arterial or tissue injury, stem cells mobilize from bone marrow into circulation and accumulate in diseased regions due to their interaction with chemokines and growth factors released by

injured tissues or inflammatory cells. To improve their homing, stents have been modified to express EPC specific antibodies as earlier mentioned. In another approach, Li et al. (2018) developed click chemistry moieties tagged antibodies to interlink circulating stem cells to the activated platelets at the site of the arterial injury.[63] Some of the issues utilizing endogenous stem cells are: 1) a decrease in cell signaling molecules that direct stem cell mobilization over time following the injury, and 2) poor functionality of mobilized stem cells in aged patients or patients with underlying health conditions. However, for the exogenous transfer of stem cells, the primary concern is still due to the poor cell homing and engraftment in the diseased regions following transplantation.[55] Several methodologies are investigated to overcome this challenge. The application of MNP laden stem cells is one such approach that has demonstrated the feasibility of using external stimuli to direct the homing of transplanted cells to the desired region.[31, 45, 64] Another novel approach is by modifying the stem cell surface to present receptors to target one of the biomarkers of the injured sites. Giordano et al. (2016) generally modified ECs to highly express interleukin (IL)-8 receptors such as IL8RA and RB on their membrane to attract the cells towards injured arteries that overexpress IL-8 following PCI.[60] Non-genetic mediated approaches were also employed to incorporate the desired proteins on the cell surface that may improve stem cells' homing.[65] For instance, Lo et al. (2013) integrated P-selectin glycoprotein ligand-1 onto MSCs using palmitated protein G and demonstrated their effective capture and rolling onto injured endothelial cell monolayers at physiological relevant wall shear stress.[66] Tang et al. (2018), on other hand, had an interesting approach to improve the homing of stem cells to injured tissue.[67] In their work, platelet vesicles were fused with cardiac stem cells to instill the platelets' natural homing capability into the stem cell to recognize and accumulate onto the denuded endothelium.

## 1.5 RESEARCH OVERVIEW

Our long-term goal of our research is to develop a multifunctional nanoparticle system to be used for treatment and imaging applications for better management of cardiovascular disease. To achieve our goal, in this research project, two different kinds of novel nanoparticle systems that have potential application in CVD were developed: (1) nanoparticles that can be utilized for *in vivo* imaging purposes by utilizing biodegradable photoluminescent polymers, and (2) nanoparticles that can support rapid cell capture to promote reendothelialization following PCI procedures by incorporating highly selective

biorthogonal click chemistry with nanotechnology and cell therapy. Our strategy will ensure *in vivo* tracking as well as a cell homing system to improve the therapeutic outcomes of cell therapy.

To achieve our long-term goal, the following specific aims were developed:

**Aim 1. Fabrication and evaluation of photoluminescent polylactones for their potential as theranostic vascular nanoparticles.** In this aim, we will fabricate and screen three different photoluminescent polylactones such as BPLPL-PLGA 50:50, BPLPL-PLGA 75:25 and BPLPL-PLLA for their physical properties including sizing, stability, degradation, and payload release kinetics. In addition, the cyto-/hemocompatibility of these fluorescent nanocarriers will be evaluated in terms of cellular growth and immune cells' activation.

**Aim 2. Development of multifunctional nanoparticles to mediate endothelial cell homing to the injured vasculature.** In this aim, we will fabricate multifunctional nanoparticles that can target a vWF coated surface representing the injured vasculature as well as interlink with engineered endothelial cells via click chemistry coupling. Nanoparticles with different amounts of surface tetrazine moieties will be fabricated and characterized for their biological properties *in vitro*. In parallel, endothelial cells will be engineered to present transcyclooctene (TCO) hooks and evaluated for their functional properties. In addition, the capability and specificity of multifunctional nanoparticles to home engineered cells will be evaluated using *in vitro* and *ex vivo* models.

The **main innovative highlights and significant aspects** of our research are as follows:

- The utilization of biocompatible polylactones with an intrinsic and stable photoluminescent capability to synthesize vascular drug carriers. The optimal nanoparticle system that can potentially be utilized to monitor their pharmacokinetics and distribution after *in vivo* delivery. Furthermore, it helps us to estimate the required dosing of the therapeutic candidates to be administered at the injured site and assess the outcome of the therapy.
- The combination of nanotechnology and cell therapy mediated by a click chemistry-based interaction is the first of its kind. Our approach can promote stable interaction of the cells to the extracellular matrix and promote efficient cell homing and retention onto the injured vasculature.

# Chapter 2. CHARACTERIZATION OF PHOTOLUMINESCENT POLYLACTONE-BASED NANOPARTICLES FOR THEIR APPLICATIONS IN CARDIOVASCULAR DISEASES

## 2.1 SIGNIFICANCE

The real time, non-invasive monitoring of transplanted cells and nanocarriers after delivery would help us to determine their pharmacokinetics and tissue distribution *in vivo*. In addition, we can estimate the required dosing of the therapeutic candidates to be administered at the injured site, assess the outcome of the therapy, and develop more efficient treatment/ delivery strategies. A common strategy employed in labeling cells or drug carriers for imaging applications is by directly incorporating fluorophores, radioisotopes, quantum dots, and paramagnetic nanoparticles within them. However, major concerns involved with these imaging agents are often associated with their poor photobleaching-resistance and substantial cytotoxicity, which limit their applications for long-term *in vivo* tracking of cells and/or drug carriers. Another technique to image living cells involves genetic modification by introducing reporter genes into the cells' genome to express specific fluorescent/bioluminescent proteins or enzymes required for signal generation. This approach is less favorable as it produces gene alteration, and often requires viral vectors for gene transduction, which may cause immunogenicity and mutagenesis. Therefore, this strategy of imaging is only approved in terminally ill patients.[68] Considering the issues associated with the tracking of cells and/or drug carriers using the aforementioned strategies, the development of biodegradable and biocompatible materials that allows non-invasive, stable and long-term imaging capabilities has become increasingly desirable.

Earlier, we developed citrate-based biomaterials, known as biodegradable photoluminescent polymers (BPLPs), that possessed a strong and tunable photoluminescence phenomenon; and we demonstrated their potential use in bioimaging, drug delivery and tissue engineering.[69] Unlike other imaging agents that are not degradable, BPLPs are created from biocompatible monomers via a convenient thermal polycondensation reaction and are shown to have controlled degradability properties. However, the main challenge of using BPLPs for nanoparticle fabrication was associated with their low molecular weight, which

resulted in nanoparticle aggregation in physiological conditions, hence limiting their use as an imaging probe. To overcome this, we synthesized new polymers by incorporating BPLPs into the widely used biodegradable polylactones, referred to as biodegradable photoluminescent polylactones (BPLPLs) that showed higher molecular weight, improved mechanical strength, and had favorable processability over BPLPs.[70, 71] The intrinsic and stable fluorescent property of BPLPs is well preserved in BPLPLs. Furthermore, the BPLPLs fluorescence emission ranging from blue to red can be adjusted by varying different amino acids in the syntheses of BPLPs.[69, 72]

In this research, we developed three different nanoparticles based on BPLPLs including BPLP-co-poly (L-lactic acid) (BPLPL-PLLA) and BPLP-co-poly (lactic-co-glycolic acid) copolymers with lactic acid and glycolic acid ratios of 75:25 (BPLPL-PLGA75:25) as well as 50:50 (BPLPL-PLGA50:50). Furthermore, we characterized their physical properties and biocompatibility with the blood cells and endothelial cells and investigated their bioimaging applications. Our preliminary characterization studies would help us to identify a suitable BPLPL-based material to synthesize theranostic NPs that can be utilized both as an imaging agent to track the EC delivery and as a vascular drug carrier to promote *in situ* reendothelialization post arterial injury.

## 2.2 MATERIALS AND METHODS

Synthesis of BPLPLs such as BPLPL-PLLA (1:100), BPLPL-PLGA50:50 (1:100), BPLPL-PLGA75:25 (1:100) was described previously.[70, 71] The ratio of 1:100 represents the feeding molar ratio of BPLP either with lactic acid or a combination of lactic acid and glycolic acid. PLGA50:50 of molecular weight 55-65kDa was purchased from Akina, Inc (West Lafayette, IN). Other reagents including bovine serum albumin (BSA) and polyvinyl alcohol (PVA) of molecular weight 31-50kDa were bought from Sigma-Aldrich (St. Louis, MO). MTS reagent (CellTiter 96®AQueous One Solution Cell Proliferation Assay) and Pierce BCA protein assay were obtained from Promega (Madison, WI) and ThermoFisher Scientific (Grand Island, NY), respectively. OxiSelect™ Intracellular Nitric Oxide (NO) Fluorometric Assay Kits were purchased from CellBioLabs, Inc (San Diego, CA). Furthermore, human umbilical vein endothelial cells (HUVECs) were purchased from American Type Culture Collection (ATCC, Manassas, VA), while the culture media

(Vasculife Basal Medium) and supplemental kits (Vasculife VEGF Lifefactors) were purchased from Lifeline Cell Technology (Frederick, MD). Other chemicals, if not specified were purchased from Sigma Aldrich.

### 2.2.1 Synthesis of BPLPL-based Nanoparticles

BSA was selected as the model protein to be encapsulated into BPLPL nanoparticles, which were synthesized by a standard double emulsion technique. For this procedure, BSA solution (20 mg of BSA dissolved in 0.2 ml of DI water) was emulsified into 2% (w/v) BPLP-polylactones solution prepared in 5 ml of chloroform and sonicated. This primary emulsion was added drop wise into 12 ml of 5% (w/v) PVA and sonicated again at 30 W for 5 minutes. Following the overnight stirring to evaporate organic solvents, the nanoparticles were washed and isolated by centrifugation at 15,000 rpm for 30 minutes, and protein (BSA)-loaded BPLPL based NPs were collected via freeze-drying. Blank BPLPL NPs as well as PLGA50:50 NPs were also fabricated using similar procedures without adding BSA to be utilized for *in vitro* cells- and blood-based studies.

### 2.2.2 Physical Characterization of BPLPL-based Nanoparticles

The nanoparticles were characterized for their particle size, polydispersity and zeta potential via a dynamic light scattering (DLS) method using Zeta PALS zeta potential analyzer (Brookhaven Instruments, Holtsville, NY). The size and morphology of the nanoparticles were also observed using transmission electron microscopy (TEM). The stability of particles was determined by observing the variation in their size while suspended in various formulations such as DI water, saline (0.9% sodium chloride solution), 10% Fetal Bovine Serum (FBS, Atlanta Biological, Lawrenceville, GA), or simulated body fluid with similar composition of blood plasma, prepared as described previously).[73] The particles were incubated at 37$^{o}$C and their sizes were measured using DLS every 12 hours up to 3 days. Furthermore, the amount of BSA encapsulated into BPLPL-based particles was estimated based on unentrapped BSA in PVA solution after centrifugation. The percentage of loading efficiency was calculated as actual amount of BSA loaded with respect to the initial amount of BSA used to prepare NPs. For the *in vitro* release study of BSA, 1 mg/ml of particle solution in PBS suspended in a 100 kDa dialysis bag (Spectrum Laboratories Inc., Rancho Dominguez, CA) was dialyzed against phosphate buffer saline (PBS) solution. At each predetermined time point, 1 ml of dialysate solution was collected and replaced with fresh PBS solution. BSA content in the

collected solution was quantified using BCA protein assays following manufacturer's instructions, and cumulative BSA release over the time was analyzed based on BSA standards. *In vitro* degradation of nanoparticles in DI water was analyzed over a period of 4 weeks. Briefly, NPs were suspended in DI water and incubated at 37$^{o}$C for predetermined times. At each time point, particles were collected and freeze dried. The degradation was determined based on the remaining mass of NPs.

### 2.2.3 *In Vitro* Cell Studies of BPLPL-based Nanoparticles

**Cytocompatibility:** To evaluate the cytotoxicity of BPLPL-based nanoparticles with human umbilical vein endothelial cells (HUVEC), cells were seeded in 96 well plates at a seeding density of 30,000 cells/cm$^2$ and incubated in 37$^{o}$C for 24 hours. Following incubation, cell culture media was replaced with increasing concentrations of nanoparticle suspension (in media) for 24 hours. The cells were then washed and incubated with MTS assay reagents for 3 hours. Absorbance readings were measured at 490 nm using UV-Vis spectrophotometer (Infinite M200 plate reader, Tecan, Durham, NC), and the percent of cell viability was determined with respect to untreated cells.

**Cellular uptake:** The efficiency of HUVECs to internalize BPLPL-based nanoparticles was determined. Briefly, HUVECs of density 30,000 cells/cm$^2$ were initially seeded in to 96 well plates and allowed to attach for 24 hours. The cell culture media was then replaced with nanoparticle suspensions of various concentrations, and the plates were incubated for 4 hours. After treatment, cells were washed with PBS and lysed with 1% Triton X-100 for 30 minutes at 37$^{o}$C, and lysate was utilized to measure the nanoparticles' fluorescence intensities at excitation and emission wavelengths of 377 nm and 431 nm, respectively. These measurements were analyzed against a nanoparticle standard. These fluorescence intensity values were then normalized with the total protein content per sample using BCA assays following manufacturer's instructions. In parallel, the nanoparticle interactions with endothelial cells were imaged using a fluorescence microscope under a FITC channel.

**Cellular functionality:** HUVEC functionality in the presence of BPLPL-based nanoparticles was determined based on nitric oxide (NO) production. Nanoparticles (1 mg/ml) were incubated with cells for 24 hours, following which nitric oxide production of exposed cells was quantified using Intracellular Nitric Oxide Fluorometric Assay kits (Cell Biolabs, Inc., San Diego, CA) following the manufacturer's instructions. In

brief, an NO fluorometric probe (provided with the kit) enters the cells and deacetylates by intracellular esterase to a non-fluorescent intermediate, which is rapidly oxidized by nitric oxide into a fluorescent triazolo-fluorescein analog. The fluorescence intensity is proportional to NO levels within the cell cytosol, which can be quantified at a wavelength of 480 nm (excitation)/530 nm(emission) using UV/vis spectrophotometer (Infinite M200 plate reader, Tecan, Durham, NC). Cells grown on tissue culture plates without any treatment served as control.

### 2.2.4 *In Vitro* Blood Studies of BPLPL-based Nanoparticles

**Blood collection:** Whole blood was drawn from healthy adult volunteers into acid citrate dextrose anticoagulant tubes (ACD, Solution A; BD Franklin Lakes, NJ). Consent from the volunteers was obtained prior to the blood collection, and all the procedures strictly adhered to the IRB standards approved at the University of Texas at Arlington.

**Whole blood clotting kinetics and hemolysis:** Briefly, in hemolysis, 10 µl of various concentrations of nanoparticles ranging from 0-1000 µg/ml were incubated with 200 µl of blood for 2 hours at 37$^{o}$C. The nanoparticles were centrifuged at 1000 rpm for 5 minutes and absorbance of the supernatant was obtained using UV-Vis Spectrophotometer at a wavelength of 545 nm. Blood diluted in DI water served as the positive control, whereas saline diluted blood as the negative control for hemolysis studies. Percentage of hemolysis due to each sample was quantified based on Eq. (1). In the whole blood clotting study, we studied the effects of particles on normal blood clotting kinetics, which was measured as blood clotting index (BCI). Here, whole blood initially activated by adding 0.01 M of calcium chloride, and 50 µl of activated blood was then treated with 10 µl of 0.5 mg/ml of nanoparticles at predetermined time points. At each time point, 1.5 ml of DI water was added to lyse the un-clotted blood, and absorbance of the supernatant was measured at 540 nm. Untreated blood served as a control. The absorbance of whole blood (without any addition of calcium chloride) in water at 540 nm was applied as a reference value. The BCI can be quantified from Eq. (2).

$$(1)\quad Hemolysis\ (\%) = \frac{Absorbance\ of\ sample - Absorbance\ of\ negative\ control}{Absorbance\ of\ positive\ control - Absorbance\ of\ negative\ control} X\ 100\%$$

(2) $BCI = \frac{Absorbance\ of\ blood\ in\ contact\ with\ samples\ at\ set\ time\ points\ at\ 545nm}{Absorbance\ of\ whole\ blood\ in\ water\ at\ 545nm\ at\ time\ 0}$

**Platelet adhesion and aggregation:** We further investigated the hemocompatibility of BPLPL materials based on the platelet adhesion and activation. For this study, platelet rich plasma (PRP) was collected by centrifuging whole blood at 190 g for 12 minutes. PRP was incubated with BPLPL films for 1 hour at 37°C under static conditions. After 1 hour, films were rinsed carefully with PBS and attached platelets were lysed using a cell lysis solution for 1 hour. The LDH release corresponding to platelet adhesion was quantified by detecting the amount of lactate dehydrogenase (LDH) present in the lysate solution using CytoTox 96® Non-Radioactive Cytotoxicity Assays according to the manufacturer's instructions. Glass served as the positive control for comparison. The morphology of platelet adhesion on the polymer films was also visualized using scanning electron microscopy (SEM) imaging. Briefly, platelets on films were fixed with 2.5% glutaraldehyde (Electron Microscopy Science, 16536-15) overnight, post fixed with 1% Osmium tetroxide in 0.1M Cacodylate buffer (Electron Microscopy Sciences, 19150) for 1 hour, dehydrated with a graded series of ethanol (50%, 75%, 95%, 100%) for 15 minutes at each step, and further dried using varying ratios of hexamethyldisilane (HMDS) in ethanol (1:2, 1:1, 2:1) for 15 minutes at each step. Finally, the films were dried using 100% HMDS for 30 minutes and then sputter-coated with silver for SEM. In addition, after incubating PRP with polymer films for 1 hour, 5 µl of suspension was collected and incubated with saturating concentrations of CD42b-PE (platelet marker) and PAC1- FITC (activated glycoprotein GP IIb/IIIa receptor marker) for 20 minutes. The antibodies were obtained from BD Biosciences. The platelets were fixed with 1% paraformaldehyde for 2 hours in 4°C and were analyzed on a BD LSRII flow cytometer. At least 10,000 events per sample were analyzed and identified based on their forward and side scattering characteristics and by positive staining with anti-CD42b-PE antibodies. The percentage of GpIIb/IIIa expressing platelets was calculated relative to the total number of platelets (CD42b positive cells).

### 2.2.5 Statistical Analysis

All the experiments were performed with n = 3–6 if not specified. Data were expressed as mean ± SEM. The statistical analysis was assessed using ANOVA followed by post hoc Pairwise Multiple Comparisons using the Holm-Sidak method on GraphPad Prism (GraphPad Software Inc, CA). A significant difference was considered where P values appeared < 0.05.

## 2.3 RESULTS

### 2.3.1 Physical Characterization of BPLPL-based Nanoparticles

DLS results show that the BPLPL-PLGA50:50, BPLPL-PLGA75:25 and BPLPL-PLLA based nanoparticles suspended in DI water have hydrodynamic sizes of 157 nm, 149 nm and 145 nm, respectively (**Table 2.1**). The polydispersity values ranging from 0.10-0.17 suggest the particles were well dispersed. TEM images of BPLPL nanoparticles also confirm the uniform distribution of NPs with smooth and spherical morphology (**Figures 2.1 A-C**). Zeta potential for BPLPL-PLGA 50:50, BPLPL-PLGA 75:25 and BPLPL-PLLA based nanoparticles were -24.7, -23.9, and -21.9 mV, respectively, suggesting that the particles might be stable in physiological solutions.[74] In addition, the stability of BPLPL based nanoparticles was evaluated at various formulations including DI water, 10% FBS, 0.9% saline and simulated body fluid by recording the nanoparticles diameter at fixed time intervals. We have observed that BPLPL-PLGA NPs were stable in all

***Table 2.1. DLS measurements of BPLPL based NPs***

| Polymeric Nanoparticles | Size (nm) | Polydispersity | Zeta potential (mV) |
|---|---|---|---|
| BPLP-cys-PLLA (1:100) NPs | 145 ± 26 | 0.129 ± 0.035 | -21.85 ± 2.16 |
| BPLP-cys-PLGA75:25 (1:100) NPs | 149 ± 37 | 0.116 ± 0.032 | -23.85 ± 1.32 |
| BPLP-cys-PLGA50:50 (1:100) NPs | 157 ± 44 | 0.164 ± 0.010 | -24.72 ± 0.82 |

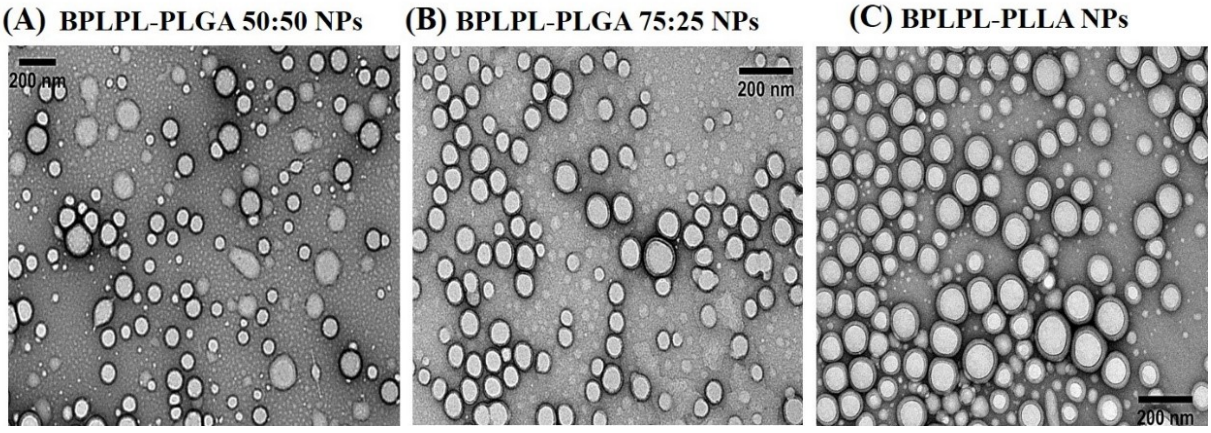


***Figure 2.1 Morphological characterization of BPLPL-based NPs.*** *TEM images of (A) BPLPL-PLGA50:50 (1:100), (B) BPLPL-PLGA75:25(1:100), (C) BPLPL-PLLA (1:100) show uniform sized and spherical morphology of nanoparticles. The scale bar represents 200 nm.*

formulations for 48 hours with no significant aggregation or change in size. Although BPLPL-PLLA NPs

remained relatively stable in DI water, saline and serum, they tended to have some aggregation in simulated body fluid at 48 hours (**Figure 2.2**).

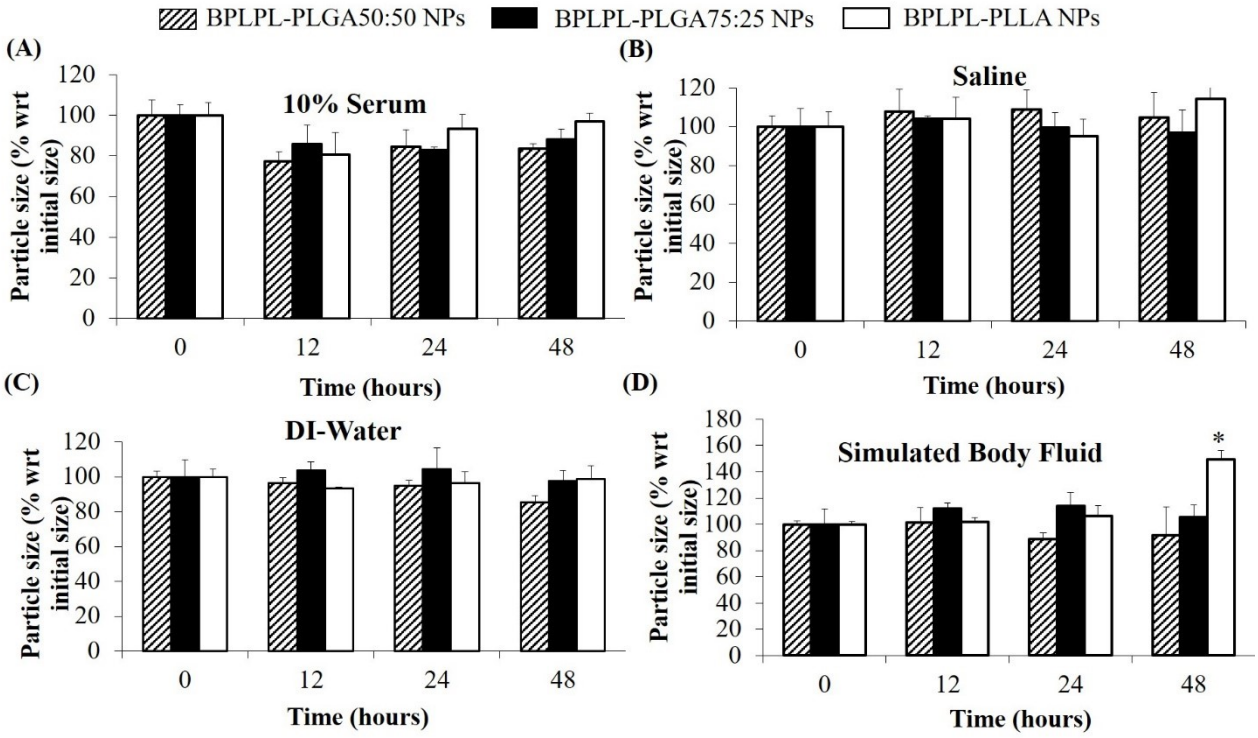


***Figure 2.2 Stability of BPLPL-based NPs.*** *NP stability in various formulations such as (A) 10% serum, (B) Saline (0.9% NaCl), (C) DI-water, and (D) Stimulated body fluid based on particle size measured over periods of 48 hours. Graph plot as average ± SD of n = 3 samples. Asterisk (*) represents p < 0.05 in comparison to size of BPLPL-PLLA NPs at the initial time point.*

To determine if these nanoparticles could be utilized for drug delivery applications, their drug release kinetics and degradation studies were conducted. BSA was chosen as the model growth factor. BPLPL-PLGA 50:50, BPLPL-PLGA 75:25 and BPLPL-PLLA showed a loading efficiency of 70%, 69%, and 77%, respectively. **Figure 2.3A** showed that both BPLPL-PLGA nanoparticles could release ~50% content within 24 hours, and the complete release was achieved in 7 days. On the other hand, BPLPL-PLLA nanoparticles demonstrated comparatively lower release kinetics, and only 50% BSA release was achieved in 2 weeks (**Figure 2.3A**). The *in vitro* degradation study also emphasizes the role of polymer composition on particle behavior (**Figure 2.3B**), where BPLPL-PLGA particles showed a similar degradation rate and almost ~80% degraded in 4 weeks. However, BPLPL-PLLA degraded slowly with only ~30% lost in weight when observed after 4 weeks. Furthermore, all BPLP-cys-polylactone based nanoparticles showed maximum excitation and emission wavelength at 374 and 441 nm, respectively (**Figure 2.3C**).

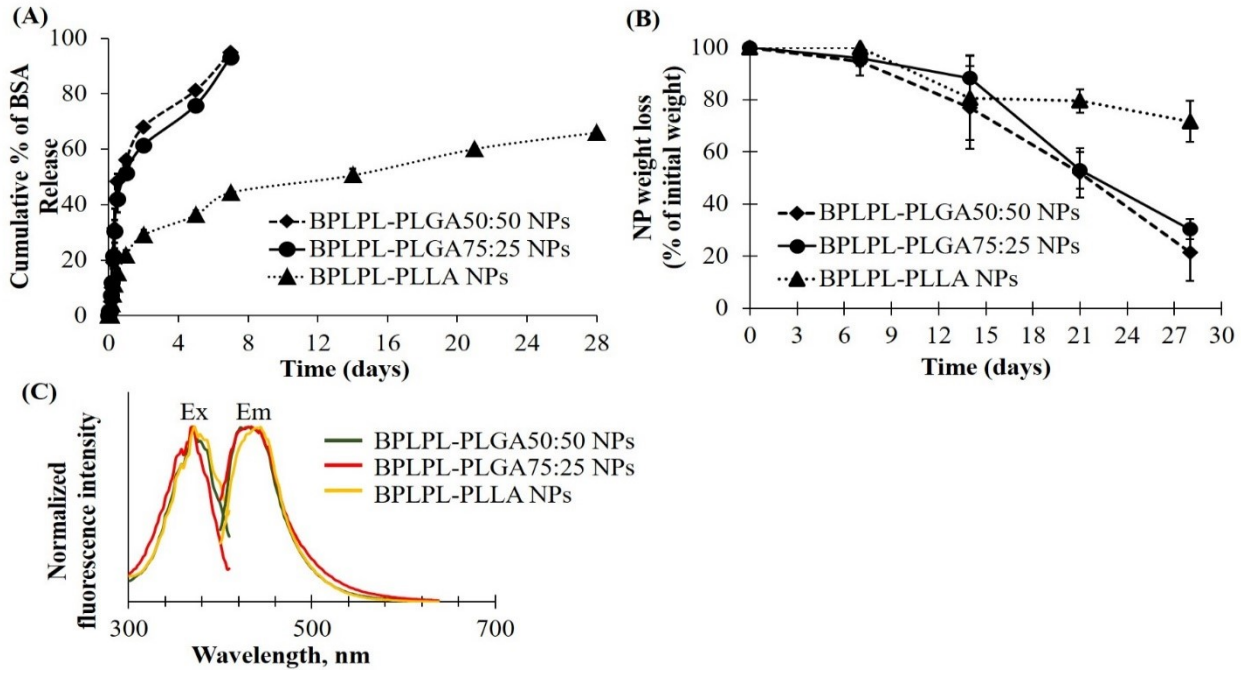


***Figure 2.4 Physical characterization of BPLPL-based NPs.*** *(A) BSA release kinetics from BPLPL-based nanoparticles in PBS solution at 37°C for 2 weeks, (B) Degradation of NPs in water at 37°C for 4 weeks, and (C) Fluorescence spectrum of cysteine derived BPLPL-based NPs (1 mg/ml) has an excitation and emission at 377 and 441 nm, respectively. Graph plot as average ± SD of n = 3 samples.*

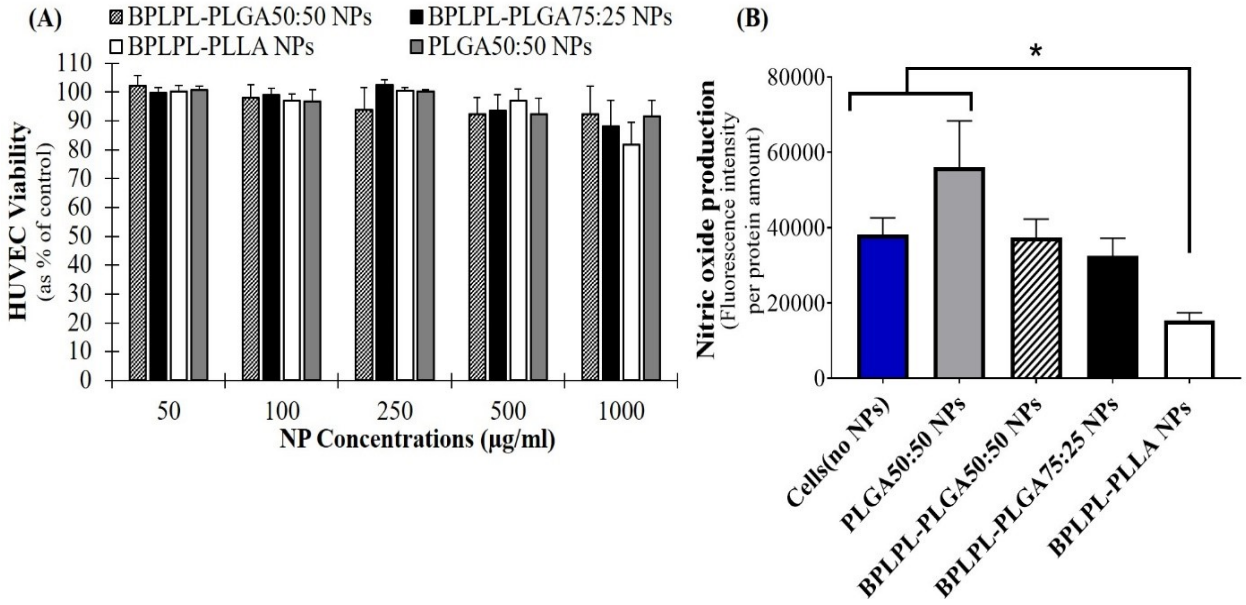


***Figure 2.3 Cytocompatibility of BPLPL-based nanoparticles.*** *(A) HUVEC viability in the presence of various concentrations of nanoparticles as quantified using MTS assays. (B) Intracellular NOS activity within HUVECs was quantified after incubation with 1,000 µg/ml of BPLPL-based NPs for 24 hours. Fluorescence intensity correlates with NOS activity or NO production within cells. *Represents significance with respect to cells treated to BPLPL-PLLA. Graph plotted in terms of average ± standard error mean (SEM).*

### 2.3.2 *In Vitro* Cell Studies with BPLPL-based Nanoparticles

Cytocompatibility evaluation of BPLPL-based NPs at various concentrations after 24 hours incubation with HUVECs was conducted. Accordingly, BPLPL NPs at all concentrations ranging from 50-1000 µg/ml was shown to be compatible with HUVECs with >80% viable cells after NP exposure (**Figure 2.4 A**). In addition, the functional status of endothelial cells in the presence of BPLPL-based NPs was studied by assessing the nitric oxide (NO) production. Accordingly, we noted that NO production by HUVECs treated with BPLPL-PLLA NPs at 1000 µg/ml for 24 hours was significantly lower than that of cells treated with BPLPL-PLGA NPs and untreated cells (**Figure 2.4 B**). On the other hand, NOS activity quantified for HUVECs in the presence of both BPLPL-PLGA50:50 and BPLPL-PLGA75:25 demonstrated no negative effects on cellular function.

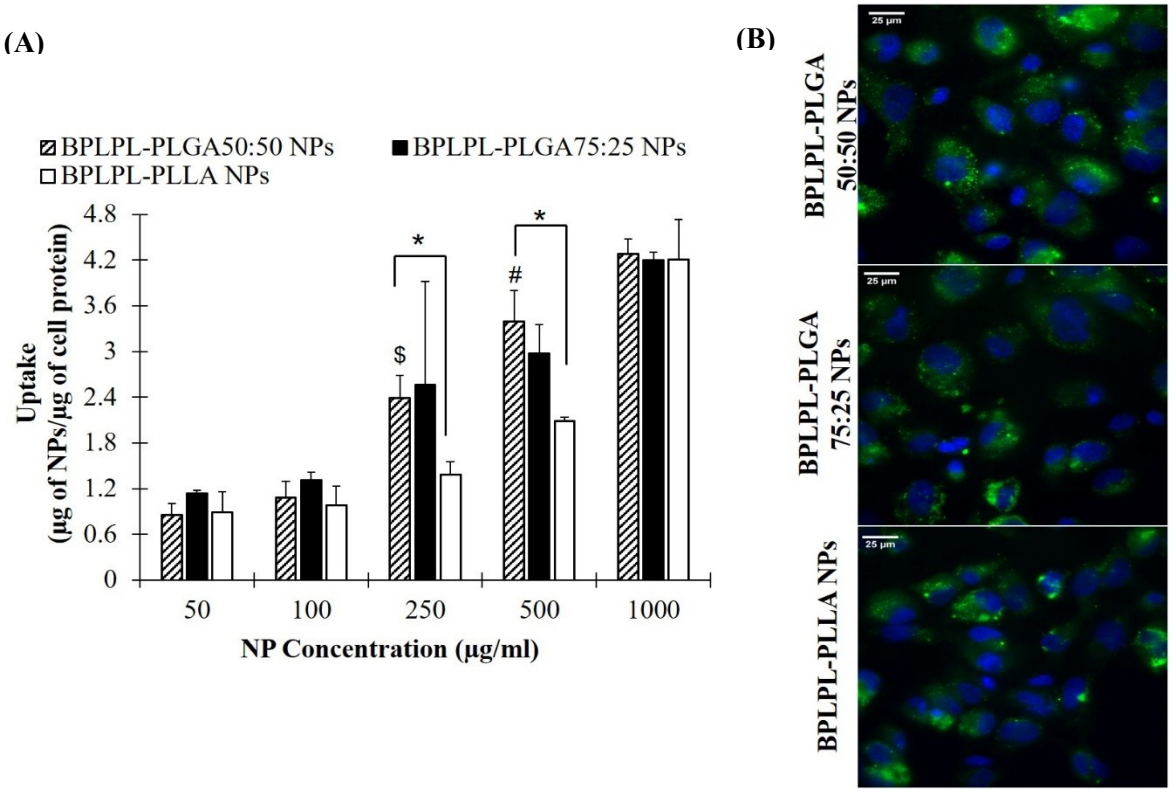


***Figure 2.5 Cellular uptake of BPLPL-based nanoparticles.*** *(A) Nanoparticle uptake by endothelial cells (HUVECs) at various concentrations after incubation for 4 hours in 37°C was quantified in terms of amount of nanoparticles relative to protein amount per sample. $ and # represent significance with respect to BPLPL-PLGA50:50 NPs at concentrations of 100 and 250 µg/ml, respectively; whereas * represents significance between BPLPL-PLGA50:50 NPs and BPLPL-PLLA NPs. (B) Fluorescent images of nanoparticles internalized HUVECs at 60X, green represents nanoparticles and blue for cell nuclei. The scale bar is 25 µm in length. Graph plotted in terms of average ± SEM.*

Lastly, the uptake of BPLPL-based NPs by vascular endothelial cells (HUVECs) was studied by incubating cells with various concentrations of NPs over 4 hours. All NP formulations showed dose-dependent cellular uptake up to a concentration of 1000 µg/ml (**Figure 2.5 A**). Fluorescence images also showed the internalization of BPLPL-based nanoparticles by endothelial cells and their subsequent localization in the cytoplasmic region of cells after a 4-hour incubation with particles (**Figure 2.5 B**).

### 2.3.3 Hemocompatibility of BPLPL-based Nanoparticles

Hemocompatibility of nanoparticles was determined based on whole blood clotting kinetics, a hemolysis study, and platelet responses. Blood clotting time reflects the thromboresistance property of nanoparticles, and high thromboresistance; (Blood clot index, BCI value) means high blood compatibility. All BPLPL-based nanoparticles showed similar BCI values with each other and when compared to untreated blood samples (**Figure 2.6A**). This suggests that particles have no significant effect on the normal

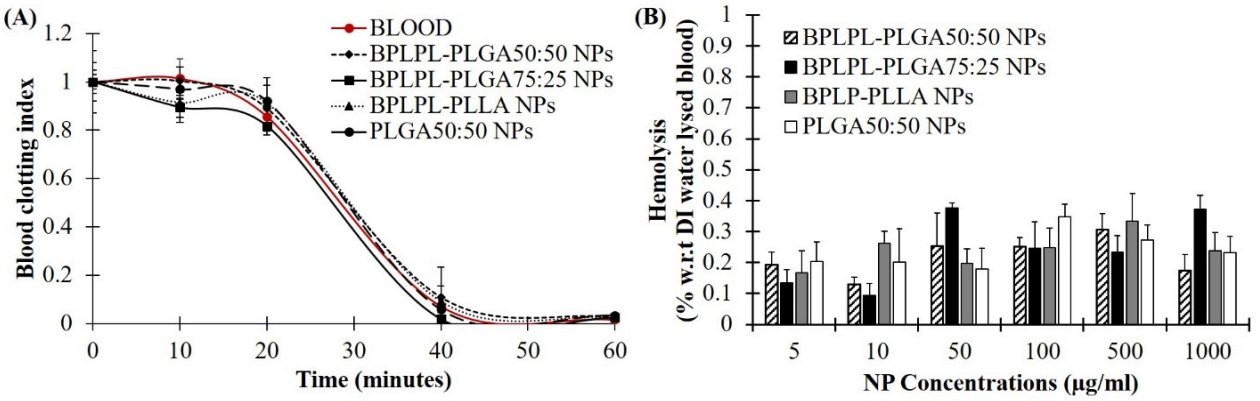


***Figure 2.6 Hemocompatibility of BPLPL-based NPs.*** *NP compatibility in whole blood was assessed based on (A) the clotting kinetic profile in the presence of 1 mg/ml of NPs and (B) hemolysis after incubating with nanoparticles of various concentrations for predetermined timepoints. Graph plot as average ± SEM*

blood clotting kinetics. Furthermore, BPLPL-based NPs at all tested concentrations proved to be nonhemolytic with a maximum of 0.4%, which was well within the standardized ISO values for nonhemolytic materials, which is 0-2% (**Figure 2.6B**).[75] To assess the compatibility of BPLPL-based materials with platelets, BPLPL films were incubated with PRP at 37°C for 1 hour. Based on the analysis, BPLPL-PLLA showed a significantly higher number of platelets adhered onto its surface than those of BPLPL-PLGA counterparts (**Figure 2.7A**). As platelets get activated, P-selectin translocates from intracellular granules to the external membrane, whereas fibrinogen aggregates platelets by bridging glycoprotein GPIIb/IIIa

between adjacent platelets [76]. Based on flow cytometric analysis, a significant amount of platelet activation was seen on the glass surface as a positive control (**Figure 2.7B**). The amount of activation seen on the BPLPL-PLGA surface was similar to those on PLGA surfaces. In accordance with these observations, SEM images also showed significantly higher platelet attachment on glass and BPLPL-PLLA surfaces than others. Closer observation of these images (**Figure 2.7C**) shows that platelets are spreading and aggregating on glass and BPLPL-PLLA surfaces. Other surfaces such as PLGA 50:50, BPLPL-PLGA 75:25 and BPLPL-PLGA 50:50 also presented a platelet shape change representing the early stage of platelet activation, which was characterized by transformation from a discoid to spheroid form with small bulbous protrusions distributed over the platelet surface [77].

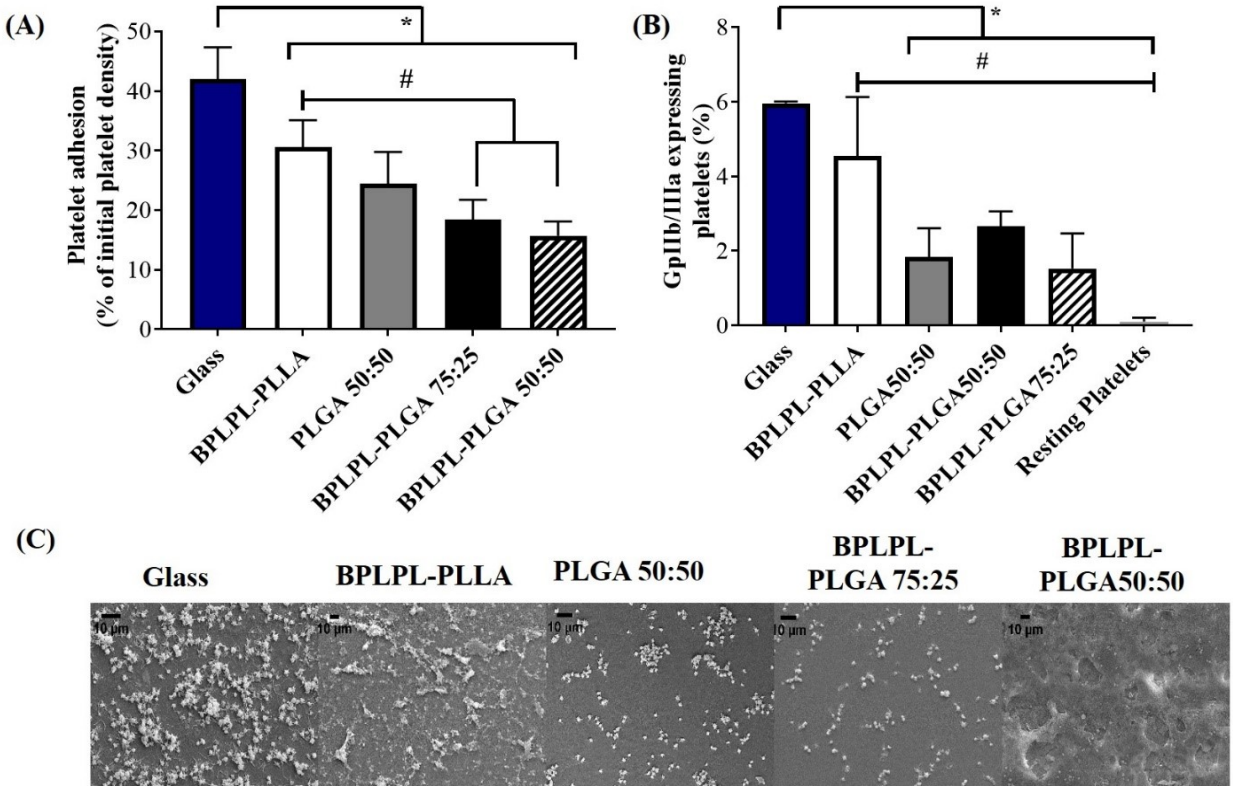


***Figure 2.7 Platelet responses to BPLPL-based materials.*** *(A) Platelet adhesion to BPLPL-based materials after 1 hour incubation at 37°C quantified using LDH assays, (B) Platelet activation quantified based on expression of GPIIb/IIIa surface markers using flow cytometry, and (C) SEM images to demonstrate platelet morphological changes and interactions with BPLPL-based materials. *and # represent significance value of p < 0.05 with respect to glass and BPLPL-PLLA, respectively. Graph plot as average ± SEM, and scale bar for SEM images represents length of 10 µm.*

## 2.4 DISCUSSION

Bioimaging holds huge potential in the field of drug delivery, tissue engineering and regenerative medicine. During the last decade, several functional polymers with imaging capabilities were investigated to understand the biological processes and their potential applications for image-guided surgery and therapy.[78, 79] The BPLP is one such novel biomaterial with intrinsic and excellent photoluminescent properties that can be used as a label-free *in vivo* imaging tool for disease detection and treatment. The components that are utilized to develop BPLPs include citric acid, amino acids, and aliphatic diols, which are all commonly used in many FDA-regulated devices.[69, 80] Recently, a family of biodegradable photoluminescent polylactones based on BPLP have been reported.[71] This new class of materials can be utilized to fabricate theranostic nanoparticles which can be tracked with a variety of microscopy techniques, including fluorescent microscopy, confocal laser scanning microscopy and two-photon microscopy.[80]

In our present work, we screened three different BPLPL-based nanoparticles (BPLPL-NPs) including BPLPL-PLLA, BPLPL-PLGA50:50, and BPLPL-PLGA75:25 to determine the most promising formulation that can be utilized for theranostic applications in treating cardiovascular diseases. Our characterization showed that most BPLPL-NPs maintained uniform, spherical morphology with 150 nm in diameter and higher negative zeta potential values compared to PLGA 50:50 nanoparticles due to inclusion of the citric acid component in BPLP. This increased surface charged group of BPLPL-based NPs not only provides additional functional motifs required for the conjugation of targeting ligands, but also improves NPs stability in physiological fluids. To evaluate this, the diameter of BPLPL-NPs in various formulations including DI water, serum, saline and simulated body fluid was monitored for 48 hours. Accordingly, we found that most of the BPLPL-NPs, except BPLPL-PLLA at 48 hours in simulated body fluids, were relatively stable with no signs of aggregations. It is plausible that long-term incubation of BPLPL-PLLA in simulated body fluids alters the colloidal stability of particles due to enhanced interactions of these NPs with various salts and enzymes that constitute the solvent. Lazzari et al. (2012) have observed similar aggregation behavior for PLLA NPs in simulated body fluids after prolonged incubation.[81] In such instances, simple modifications of BPLPL-PLLA NPs surface with PEG chains might be able to prevent the docking of enzymes or ions on nanoparticle surfaces, thereby improving their colloidal stability in physiological conditions.[82]

The presence of PLLA in BPLPs also seem to affect the protein loading efficiency, protein release kinetics and degradation profile of BPLPL-PLLA NPs. It was noted that BPLPL-PLGA NPs released ~50% of BSA within 24 hours, whereas BPLPL-PLLA achieved a similar amount of BSA release within 2 weeks. In addition, BPLPL-PLLA NPs demonstrated a slower degradation rate with ~30% lost weight compared to BPLPL-PLGA NPs which showed ~80% degradation within 4 weeks. Hu et al. (2016) explained that BPLP incorporation into polylactones could enhance water permeability, which in turn, accelerates the drug release rate and degradation of copolymers.[70] Also, the percentage of hydrophilic glycolic acid in BPLPL would also attribute to faster degradation and thereby drug release from the particles. We speculate that the hydrophobic nature of PLLA may have improved their protein encapsulation compared to its PLGA counterparts by forming a hydrophobic wall to retard BSA leakage into the outer water phase during the NP synthesis.[83] Furthermore, the photoluminescent property of BPLP was retained in BPLPL-based NPs, with maximum excitation and emission wavelength at 344 and 441 nm, respectively. Previously, we have shown that depending on the amino acids used in BPLP syntheses, the fluorescence emission could be broadened up to 725 nm, highlighting the versatility of these polymers for biomedical imaging.[84]

Following the physical and chemical characterization of BPLPL NPs, their cytotoxicity with endothelial cells was investigated. BPLPL NPs exhibited excellent cytocompatibility with >80% of HUVECs viability post treatment with NPs at all concentrations. Xie et al. (2014) also reported similar values for cell viability using 3T3 fibroblasts exposed to BPLPL-PLLA nanoparticles at concentrations ranging from 1-500 µg/ml.[71] Due to the presence of a high number of carboxylic groups on the BPLP backbone, it was noted earlier about reduced cell survival in the presence of BPLP NPs.[71, 85] In our study, BPLPL-based NPs showed a similar cytocompatibility profile as seen for PLGA NPs with minimal cytotoxicity on HUVECs. Similar to our observation, Hu et al. (2016) also reported comparable *in vitro* cytotoxicity by mesenchymal stem cells as well as *in vivo* foreign body response towards BPLPL and PLGA materials.[70] This suggests that inclusion of BPLP into commonly used polymers such as PLGA did not significantly affect the cell survival, while the newly synthesized polymers can still inherit the florescent properties from BPLP, which could possibly be utilized for theranostic applications in CVD treatment.

Next, the proper functioning of endothelial cells in the presence of BPLPL-based NPs in terms of nitric oxide production was evaluated. Nitric oxide (NO) is an important signaling molecule released by endothelial cells to regulate vascular inflammation, platelet function, angiogenesis, and protection from ischemia reperfusion injury. Any dysregulation of NO production due to NOS uncoupling is known to cause cardiovascular diseases (e.g. atherosclerosis, diabetes, and hypertension).[86] Inorganic nanoparticles including fluorescent silica NPs, superparamagnetic iron oxide NPs, titanium dioxide NPs generally investigated to be utilized for bioimaging applications demonstrated to induce EC toxicity and dysfunction with impaired NO production.[87-89] When compared to these NP types, BPLPL-PLGA NPs could be a better alternative since they demonstrated to be inert with no effect on normal cell activities. However, this is not the case with BPLPL-PLLA NPs. Nitric oxide production by endothelial cells was significantly reduced when compared to cells exposed to PLGA NPs. The mechanism that influenced the cellular behavior in the presence of BPLPL-PLLA NPs is not clear. However, it is plausible that the BPLPL-PLLA nanoparticles may have upregulated oxidative stress within the cells that can activate autophagy and eventually lead to endothelial dysfunction via the PI3K/Akt/mTOR pathway as seen for silica NPs.[90] Similar to our observation, Wang et al. (2014) also noted that exposure of PLLA particles to human coronary artery endothelial cells decreased their NO production and induced inflammatory adhesion molecule expression such as ICAM-1 and VCAM-1, which might facilitate immune cell adhesion and recruitment.[91] Furthermore, several studies reported that stents coated with PLLA impairs endothelial cell functions and impaired their recovery on the luminal side of stents that promoted in late stent thrombosis.[92, 93]

To investigate the utilization of BPLPL-based NPs as an imaging probe to track HUVECs, we incubated BPLPL-based NPs with vascular endothelial cells (HUVECs) over time. Dose-dependent uptake of NPs was observed for all NP formulations. Fluorescence images demonstrated the internalization of BPLPL-based nanoparticles by endothelial cells and their subsequent localization in the cytoplasmic region of cells after a 4-hour incubation. Our results agreed with previous reports from other groups that tested various nanoparticle formulations on a different cell line. For instance, Menon et al. (2014) demonstrated increasing uptake of PLGA nanoparticles by Type I alveolar epithelial cells up to 1000 μg/ml.[94] Kona et al. (2012) also observed dose-dependent uptake of GpIbα conjugated PLGA nanoparticles and unconjugated nanoparticles by human aortic endothelial cells, which were saturated at 300 μg/ml.[35] Even BPLP particles

were shown to have dose-dependent uptake characteristics.[95] In this study, they observed BPLP particles being uptake by the human dermal fibroblast without any saturation up to 500 μg/ml. It was also noted that hydrophilic and hydrophobic versions of BPLP polymers impacted the amount of nanoparticles being internalized by the different cell lines, thereby exhibiting variation in NP cellular uptake. Similarly, we have observed a significant difference in BPLPL-PLLA and BPLPL-PLGA50:50 based NPs uptake by endothelial cells, especially at concentrations of 250 μg/ml and 500 μg/ml. We speculate that such difference is due to the differential composition of PLLA and PLGA50:50 in BPLPLs materials, where PLLA is more hydrophobic in nature than PLGA50:50, and thereby affected the NP uptake by the endothelial cells. Cells continued to exhibit significant uptake of these nanoparticles at 1000 μg/ml, and as a result, almost similar amounts of NPs in the cells were observed at high concentrations despite the polymer types. On the other hand, we did not observe cells demonstrate any dose-dependent NP uptake for BPLPL-PLLA NPs at concentrations <250 μg/ml. In line with our results, it is plausible that the serum proteins in the media interact with the nanoparticles and modulate their uptake kinetics by the endothelial cells at low concentrations.[96, 97] Also, at these small concentrations, the measured levels of fluorescence intensity produced by NPs in the cells may be more difficult to discriminate.

In addition to the intrinsic fluorescence property of BPLPLs, we investigated whether the citric acid composition endows them with hemocompatibility suitable for blood contacting applications as previously seen for poly(diol-citrate) (POC) prepared from citric acid and 1,8-octanediol.[84, 98-100] First, *in vitro* hemostatic properties of BPLPL-based NPs were evaluated by whole blood clotting experiment. At various time points, absorbance of RBCs that were not trapped in clots were determined at 540 nm. Higher BCI values represent reduced blood clotting kinetics, and we observed blood treated with BPLPL-based NPs did not exhibit a different rate of clotting when compared with either untreated blood or blood incubated with PLGA NPs. Second, hemolytic results of BPLPL-based NPs demonstrated them to be nonhemolytic material that is safe to be utilized for drug delivery applications without causing any adverse effects. Lastly, platelet behaviors towards BPLPL-based materials indicate that BPLPL-PLGA consisted of better or comparable platelet attachment and activation as seen in those of PLGA surfaces; whereas a higher number of platelets adhered and expressed GPIIb/IIIa markers on BPLPL-PLLA surfaces. Many studies previously observed that PLLA in its unmodified form or without incorporation of therapeutic agents induced

increased inflammatory responses mainly due to its hydrophobic nature.[101-104] Our speculation is that since incorporating BPLPs into PLLA is shown to increase the wettability of the polymer[70]; the effect we have observed for platelets to BPLPL-PLLA could be minimal than its unmodified form of PLLA, which must be investigated further.

## 2.5 CONCLUSION

We have formulated three different photoluminescent polylactone based NPs, and characterized their physical and chemical properties, protein encapsulation, *in vitro* hemocompatibility, cytocompatibility and particle uptake. Among these formulations, BPLPL-PLGA NPs exhibited stability in physiological conditions, bi-phasic release kinetics, excellent cytocompatibility with no negative influence on cellular functions, optimal uptake characteristics, and hemocompatibility similar to PLGA nanoparticles. Most importantly, BPLPL-based NPs showed intrinsic fluorescence capability inherited from the precursor BPLP. In short, herein we have demonstrated that BPLPL-based NPs are a safe, biocompatible material with imaging capability that can potentially be used to fabricate targeted, therapeutic loaded nanocarriers for theranostic applications or utilized as an imaging agent to tag transplanted cells.

# Chapter 3. BIOORTHOGONAL CLICK CHEMISTRY MEDIATED ENDOTHELIAL CELL HOMING ON TO INJURED VASCULATURE

*Min Kyung Khang, Ph. D and Aneetta E. Kuriakose contributed equally on this project. Dr. Khang performed conjugation of Tz-Gp1bα onto PLGA NPs and subsequent analysis of NP targeting and cell capturing. Ms. Kuriakose conducted engineering of endothelial cells with TCO and optimization of NP targeting and cell capturing studies.*

## 3.1 SIGNIFICANCE

Rapid healing of lost endothelial cells from the arterial wall due to PCI procedures has been recommended to be a promising therapeutic strategy to prevent undesired inflammatory responses and restore arterial function.[24] Effective and early reendothelialization is also significant to improve the overall patency rate of small-diameter vascular grafts.[105, 106] Several strategies have been explored to achieve a functional endothelial layer following an arterial injury or while using artificial conduits for tissue engineering applications. Cell transplantation including stem cells, endothelial progenitor cells or endothelial cells is one such method. However, the homing of the transplanted cells to the injured regions has been a challenging issue.[107] Following the intravenous injection of the cells, most of them get trapped within the lung capillaries; and in certain instances, the amount of homing molecules expressed on transplanted cells were too low or may have been lost during the *in vitro* expansion process.[107] To counter these limitations, some of the few approaches could include local administration of cells, cell pre-conditioning, genetic modification, cell surface engineering with targeting agents, and incorporation of magnetic nanoparticles into cells to guide them to the injured regions, and these methods have been explored previously.[107]

In the past decade, increasing interest is focused on bioorthogonal chemical reactions, which are covalent chemical modifications performed on biological entities to understand their dynamics and functions in living systems.[108, 109] The reactant pairs involved in these reactions are mutually reactive but remain inert with biological functionalities or processes in a cell. Their reactions are highly specific and rapid; and thus, the formed products are stable and non-toxic under physiological settings.[108, 109] Inspired from nature's simple and powerful connecting reactions, click chemistry is the most specific bioorthogonal reaction that utilizes readily available reagents that are not sensitive to oxygen or water.[109] Among the various available biorthogonal click chemistry reactions, inverse-electron-demand [4+2] cycloaddition of 1,2,4,5-tetrazines

with strained alkenes including trans-cyclooctene (TCO) and norbornene is the fastest biorthogonal transformation on record, with rate constants ranging from $10^3$ to $10^6 M^{-1}s^{-1}$.[110, 111] Due to the high selectivity and unprecedented speed reactivity between Tz and TCO, they have been explored for bioimaging, diagnostics, cell tracking, tissue engineering and drug delivery applications.[112-117]

In this work, we have investigated whether click chemistry would enable effective capture and homing of the transplanted cells to the injured vasculature wall following angioplasty procedures. To achieve this, we have developed a nanoparticle system that would be pretargeted towards the injury site via association of Gp1bα with vWF on the subendothelial matrix (**Fig. 3.1A and 3.1B**). Gp1bα which is also modified with Tz based hooks can engage with TCO engineered endothelial cells transplanted to the denuded

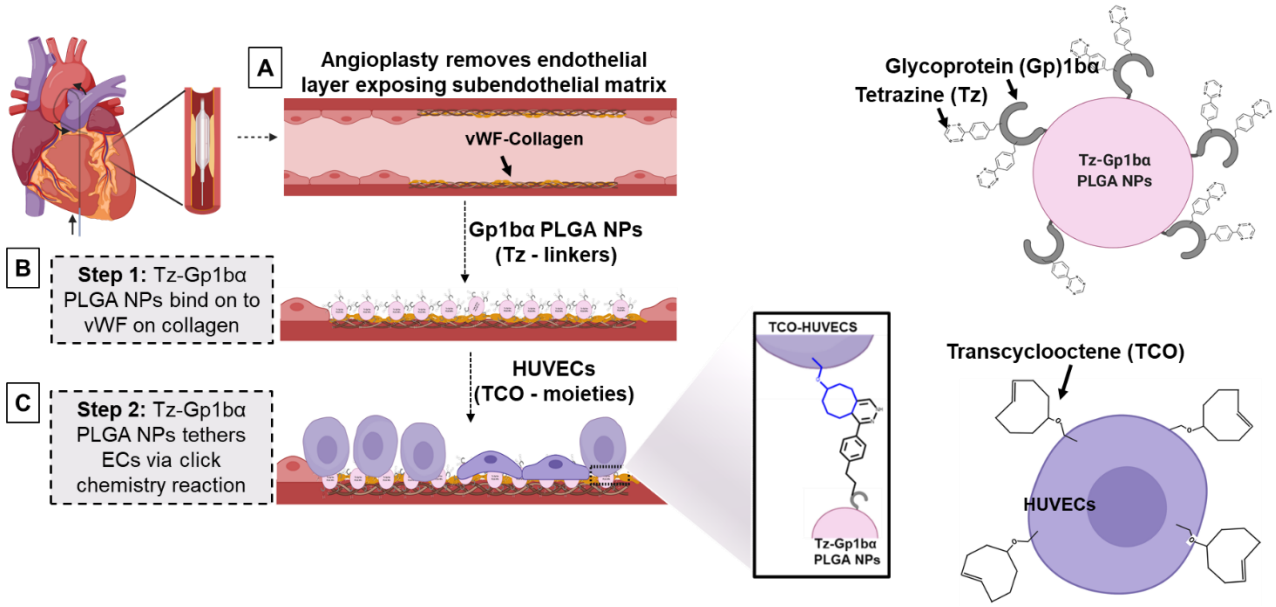


***Figure 3.1 Biorthogonal click chemistry mediated EC regeneration post PCI.*** *A) Angioplasty/stent procedures inflict vascular wall damage exposing its underlying collagen matrix. vWF multimers bound on to collagen surfaces may attract inflammatory cells like platelets. B) Our strategy is to deliver Tz-Gp1bα PLGA NPs to attach onto vWF molecules and reduce the immune response. C) In parallel, our Tz-Gp1bα PLGA NPs have the capability to capture TCO engineered endothelial cells in circulation via click chemistry reactions. These ECs cover the injured arterial wall and rapidly restore normal endothelial functions.*

endothelium to support rapid reendothelialization (**Fig. 3.1C**). Our novel, two step pre-targeting approach to capture cells has the following advantages: (1) strong, fast and stable interaction of cells to the targeted region; (2) selectivity over conventional antigen-antibody based reactions; and (3) a nanoparticle platform that allows site specific delivery of growth factors that supports endothelial retention and growth at the targeted site.

## 3.2 MATERIALS AND METHODS

Poly (lactic-co-glycolic acid) (PLGA, L/G 50:50, Mw: 15,000-25,000 Da) with carboxyl end groups was obtained from Akina Inc (West Lafayette, IN). Chloroform, polyvinyl alcohol (PVA, Mw: 13,000 Da, 85-89% hydrolyzed), Coumarin 6, 1-Ethyl-3-(3 dimethylaminopropyl)carbodiimide (EDC), N-Hydroxysuccinimide (NHS), 2-(N-morpholino)ethanesulfonic acid (MES), Dulbecco's Phosphate-Buffered Saline (DPBS), Giemsa stain, paraformaldehyde, Triton X-100, Indocyanine green (ICG)- and dimethyl sulfoxide (DMSO) were purchased from Sigma (St. Louis, MO). mTz-PEG$_4$-NHS, TCO-PEG$_4$-NHS, TCO-Cy5, Tz-Cy5 and Tz-Cy3 were obtained from Click Chemistry Tools (Scottsdale, AZ). Human GP1bα protein and von Willebrand factor (VWF) were obtained from Sino Biological (Wayne, PA). CellTracker™ Red CMTPX and NucBlue were purchased from ThermoFisher Scientific (Waltham, MA). All chemicals were used without further purification. Milli-Q grade deionized water was used for all the experiments. Human umbilical cord derived endothelial cells (HUVECs) were obtained from ATCC (Manassas, VA). HUVECs were cultured in M199 (Life Technologies, 11995-065) supplemented with 1% PenStrep (G1146 Sigma), 5% fetal bovine serum (Life Technologies, 12483-020, Frederick, MD), 2 ng/ml fibroblast growth factor (0.1%), 1 ng/ml epidermal growth factor (0.2%), 1 µg/ml ascorbic acid (0.1%), 1 µg/ml hydrocortisone (0.1%), and 90 µg/ml heparin (1%). Unless specifically stated, HUVECs were suspended and cultured in complete M199 media. Umbilical cord derived endothelial outgrowth cells, a population of progenitor cells (EOCs), were obtained from AngioBiocore (Indianapolis, IN) and cultured in EGM2 media replenished with growth medium 2 supplement mix (Promocell, Germany) and 1% Mycozap (Lonza, Houston, TX).

### 3.2.1 Development and Characterization of Tz Tagged Gp1bα-Conjugated PLGA NPs (Tz-Gp1bα PLGA NPs)

*Fabrication of PLGA Nanoparticles*. PLGA NPs were fabricated using our standard single emulsion procedure with slight modifications.[40, 118] To allow for fluorescent imaging and tracking of the particles, Coumarin 6 was loaded into PLGA nanoparticles (C6 PLGA NPs). Briefly, PLGA (100 mg) and Coumarin 6 (0.5 mg) were dissolved in 3 ml of chloroform to form the organic (oil) phase. This solution was then added dropwise to 20 ml of poly vinyl alcohol (PVA) 5% (w/v) solution (water phase) and sonicated at 40W for 5 minutes on ice. The particle suspension was then stirred overnight at room temperature to ensure

complete organic solvent evaporation. NPs were then recovered by centrifugation at 15,000 rpm for 20 minutes at 25ºC. All NPs were lyophilized and stored in powder form at -20ºC for further use. Blank PLGA nanoparticles were also prepared as formerly described without the addition of Coumarin 6. ICG loaded PLGA nanoparticles were also synthesized utilizing the standard double emulsion method as previously described to perform preliminary *ex vivo* studies.[119]

*Conjugation of Tz Tagged Gp1bα onto PLGA NPs.* Tz-conjugated Gp1bα (Tz-Gp1bα) was prepared by reacting amines on Gp1bα with mTz-$PEG_4$-NHS. Following this, modified Gp1bα was surface conjugated onto PLGA NPs using carbodiimide chemistry to synthesize Tz-Gp1bα PLGA NPs.[46, 118] Briefly, 50 µg of Gp1bα powder was completely dissolved in PBS of pH 7.4 to achieve a concentration of 1 mg/ml, and then Tz-$PEG_4$-NHS (100-fold molar excess with respect to Gp1bα) in a 2 µl DMSO was added. The mixture was shaken gently at room temperature for 1 hour and Tz-Gp1bα was purified by using a sterilized centrifuging column (MWCO 300,000) at 5,000 rpm for 5 minutes. The conjugation degree of Tz moieties on the Gp1bα were determined by reacting them with an equivalent molar amount of TCO-Cy3 and measuring its fluorescence at excitation and emission wavelength of 550 nm and 580 nm, respectively using UV/Vis spectrophotometer (Infinite M200 plate reader, Tecan, Durham, NC).

To surface immobilize the Tz-Gp1bα on to PLGA NPs, 1 mg of the PLGA NPs was activated with 12 mg of EDC and 18 mg of NHS in a 5 ml of MES buffer (0.1 M, pH 4.75) for 2 hours at room temperature with gentle shaking. The activated NPs were collected by centrifugation at 5000 rpm for 5 minutes and washed once with PBS (pH 7.4). These activated NPs were then added into Tz-Gp1bα solution to achieve a final NP concentration of 2 mg/ml in PBS (pH 7.4), and the mixture was incubated at 4ºC overnight. Finally, Tz-Gp1bα PLGA NPs were collected by centrifugation and utilized for the studies. The degree of Tz-Gp1bα conjugated onto PLGA NPs was indirectly quantified from the supernatant using Bradford assay (Bio-Rad, Hercules, CA) following manufacturer's protocol. PLGA NPs with or without Gp1bα served as controls for the studies described in this work.

The optimal amount of Tz to modify Gp1bα protein was determined based on the performance of Tz-Gp1bα C6 PLGA NPs to target an injury mimicking surface and their subsequent capability to capture the click reagent counterpart, which was TCO engineered cells. In brief, mTz-PEG4-NHS was dissolved in

DMSO and added into 10 µg of Gp1bα to achieve a final molar coupling ratio of 25:1, 50:1, 75:1 and 100:1. Unmodified Gp1bα served as a control. Tz-Gp1bα of various ratios was separately conjugated on to C6 PLGA NPs via carbodiimide chemistry. Following the conjugation, NPs were used to investigate their binding capacity to vWF coated surfaces and ability to immobilize HUVECs modified with 10 µm of TCO-PEG4-NHS. To perform this study, the hydrophobic surface was initially coated with 10 µg/ml of vWF and let dry overnight. 1 mg/ml of either Tz-Gp1bα- or Gp1bα- or un-conjugated C6 PLGA NPs were then added onto vWF coated surfaces and incubated at 37ºC for 30 minutes. The NP-bound surface was washed twice with 1X PBS solution to remove unattached NPs. Following this, 10,000 TCO-HUVECs (labeled with NucBlue and Cell tracker Red CMPTX) were added on to NP-bound surfaces and incubated further for 30 minutes at 37ºC. The surface was washed again to remove loosely attached cells and imaged using a Leica fluorescence microscope under an FITC channel to visualize C6 PLGA NPs and a DAPI and Cy3 channel to observe TCO-HUVECs attachment. The captured images were analyzed using ImageJ software to determine the fluorescence intensity of bound NPs and the number of cells captured by NPs. Lastly, to further determine whether the amount of protein immobilized on the NPs surface influenced the nanoparticles' targeting and capturing properties, 1 mg of C6 PLGA NPs were conjugated with 30 µg and 60 µg of Gp1bα modified with 100 molar excess of Tz. These NPs were used to evaluate their binding efficiency to vWF coated surfaces as well as to interact with TCO-HUVECs as described above. NPs tagged with 60 µg of Gp1bα and unconjugated NPs served as a positive and negative control, respectively.

*Characterization of Tz-Gp1bα PLGA NPs.* The hydrodynamic diameter, polydispersity and zeta potential of the particles were quantified via dynamic light scattering (DLS) method using ZetaPALS zeta potential analyzer (Brookhaven Instruments, Holtsville, NY). NPs hydrodynamic diameters were reported as the mean of the diameter distribution. High-resolution transmission electron microscopy (HRTEM) images were used to confirm homogeneous and round-shaped morphology of the samples. 10 µl of NP solution in DI water (2 mg/ml) was placed on a CF400-CU TEM grid (Electron Microscopy Sciences, Hatfield, PA) and imaged with a Tecnai T12 HRTEM microscope (FEI, Hillsboro, OR). *In vitro* cytocompatibility of NP formulations was performed as previously described.[32] In brief, HUVECs were seeded onto a 96-well plate at the density of 8000 cells/well and the cells were treated with different concentrations (0, 100, 250, 500, 1000, and 2000 µg/ml) of either Tz-Gp1bα- or Gp1bα- or un-conjugated

blank PLGA NPs for 24 hours. Following the incubation, the NP suspension from the wells was discarded, and cells were clearly washed and incubated with MTS reagents for 2 hours at 37°C (CellTiter 96® AQueous One Solution Cell Proliferation Assay, Promega, Madison, WI). Absorbance readings were measured at 490 nm using UV-Vis spectrophotometer (Infinite M200 plate reader, Tecan, Durham, NC), and the percent of cell viability was determined with respect to untreated cells.

### 3.2.2 Development and Functional Evaluation of TCO-Modified Endothelial Cells (TCO-HUVECs)

*Fabrication of TCO-HUVECs*. TCO-$PEG_4$-NHS was utilized to modify the surface of HUVECs. For this, 50,000 HUVECs were washed and suspended in 1 ml of 1X PBS solution (pH 7.4). The cell suspension was then treated with a predetermined amount of TCO-$PEG_4$-NHS for 30 minutes at room temperature. Following the treatment, TCO-HUVECs were collected at 1000 rpm for 5 minutes and washed with PBS at least once to remove any traces of unreacted TCO-$PEG_4$-NHS. Unless specified, newly modified TCO-HUVECs were then utilized for the studies described in this work. The optimal amount of TCO-$PEG_4$-NHS suitable for cell surface engineering was determined based on cell growth, viability, and functional properties post modification process.

50,000 cells suspended in 1 ml of PBS solution was treated with different concentrations of TCO-PEG4-NHS (0, 1, 5 and 10 μM) for 30 minutes. To determine the presence and quantify the amount of TCO moieties labeled on the membrane of HUVECs, cells were treated with 10 μM of Tz-Cy5 for 30 minutes. After the treatment, TCO-HUVECs were washed, fixed with 1% paraformaldehyde for 2 hours in 4°C and analyzed on a BD LSRII flow cytometer. At least 10,000 events per sample were analyzed and cell population was identified based on their forward and side scattering characteristics. Median fluorescence intensity (MFI) of APC (for Tz-Cy5) positive endothelial cells was graphed and calculated. Next, HUVECs modified with 10μM of TCO-PEG4-NHS and unmodified HUVECs were stained with 10μM of Tz-Cy5 for 15 minutes. The cell nuclei were then stained with NucBlue and fixed to images using a Leica DMi8 fluorescence microscope (Leica, Wetzlar, Germany) under Cy5 and DAPI channel.

TCO availability on the HUVEC cell membrane post modification was measured against time. HUVECs were seeded onto a 96-well plate at a cell density of $1\times10^4$ cells/well and cultured overnight. Following this, HUVECs were treated with 100 μl of 1X PBS supplemented with 10μM of TCO-PEG4-NHS

for 30 minutes at room temperature. Cells were then washed with PBS solution and replaced with 100 µl of fresh media. At predetermined time points (0, 2, 4, 6, and 24 hours), culture medium was discarded and HUVECs were treated with fresh culture media containing 10 µM of Tz-Cy3 for 15 minutes. Cells were then washed and lysed using 1% Triton X-100 for 30 minutes at 37ºC. The fluorescence intensity of Cy3 labeling on the cells was quantified at a wavelength of 550 nm (excitation)/580 nm (emission) using UV/Vis spectrophotometer. DNA content in lysate was also quantified using Picogreen DNA assays (ThermoFisher, Waltham, MA) following the manufacturer's instructions. Furthermore, the presence of TCO groups on the cell surface following several days of modification was conducted in a similar manner. Here, cells were seeded in a black 96 well plate and tagged with TCO as formerly described. Following this, TCO-modified cells were incubated with 10 µM of Tz-Cy5. These cells were imaged, and their fluorescence intensity was quantified using a UV/Vis spectrophotometer (Infinite M200 plate reader, Tecan, Durham, NC). The TCO-HUVECs were then supplemented with 100 µl of fresh media and cultured until predetermined time points including 2,4, and 6 days. At the specified time, cells were washed and treated with 10 µM of Tz-Cy3. Cells were then imaged, and the fluorescence intensities of both Tz-Cy3 and Tz-Cy5 were quantified, respectively.

*Evaluation of TCO-HUVECs Properties*. The viability and growth of HUVECs post TCO modification were evaluated based on the cell metabolic activity. In brief, HUVECs tagged with various concentrations of TCO-$PEG_4$-NHS (1, 10, 20 and 50 µM) were seeded into 96 well plates at a density of 10,000 cells/well and were cultured for 24 and 72 hours. At the specified timepoints, HUVECs were washed and the metabolic status of the cells was determined using MTS assays (CellTiter 96® AQueous One Solution Cell Proliferation Assay, Promega, Madison, WI) following the manufacturer's instructions. Unmodified HUVECs seeded at a similar cell density were used as a control for this study. Cellular viability was expressed as a percentage relative to the unmodified cells at 24 hours. The absorbance for the unmodified HUVECs cultured at day 1 was set at 100%.

Furthermore, the functional performance of TCO-HUVECs was assessed based on nitric oxide (NO) production, LDL uptake and migratory properties. HUVECs modified with different concentrations of TCO-$PEG_4$-NHS (1, 10 and 25 µM) were seeded into 96 well plates as formerly described. Following a 24

hour culture, NO production by HUVECs was determined using Nitric Oxide Fluorometric Assay kits (Cell Biolabs Inc., San Diego, CA).[86] In brief, an NO fluorometric probe (provided with the kit) was incubated with HUVECs at 37°C for 2 hours. As the NO fluorometric probe enters the cells, it is deacetylated by intracellular esterase to a non-fluorescent intermediate, which is rapidly oxidized by nitric oxide into a fluorescent triazolo-fluorescein analog. After 2 hours of incubation, cells were lysed using 1X cell lysis buffer (provided with the kit) for 30 minutes, and fluorescence for NO production was measured at a wavelength of 480 nm (excitation)/530 nm (emission) using UV/Vis spectrophotometer (Infinite M200 plate reader, Tecan, Durham, NC). Unmodified HUVECs either treated with NOS (nitric oxide synthase) inhibitor L-NNA (N5-[imino(nitroamino)methyl]-L-ornithine) at 50 μM or without served as controls.

To determine the cells' ability to uptake LDL (low-density lipoproteins), HUVECs labeled with various amount of TCO-$PEG_4$-NHS (1, 5, 10, and 25 μM) were seeded into 96 well plates as formerly described. After 24 hours of culture, cells were incubated with Dil-Ac-LDL (ThermoFisher, Waltham, MA) at a concentration of 10 μg/ml for 6 hours at 37°C. Fluorescence imaging of Dil-Ac-LDL internalized within TCO-HUVECs was captured using a Leica DMi8 fluorescence microscope (Leica, Wetzlar, Germany) and quantified using ImageJ software. LDL uptake by HUVECs correlates with corrected total cell fluorescence of Dil stain[120]. Unmodified HUVECs served as a control. Cells were also co-stained with NucBlue to identify the cell nuclei. In addition, HUVEC migratory properties post modification compared to unmodified cells were also conducted. For this, 20,000 HUVECs modified with 10 μM of TCO-$PEG_4$-NHS and unmodified cells were suspended in Basal M199 media and seeded onto each fibronectin coated transwell insert with 8 μm pore size. These cells were then exposed to M199 media either supplemented with growth factors or without for 24 hours. Following this, migrated cells were fixed, stained with Giemsa, imaged using an inverted light microscope (Leica TCS SP8 SMD, Leica, Buffalo Grove, IL) and analyzed with ImageJ.

### 3.2.3 Verification of Click Chemistry Mediated Interactions of NPs with Engineered Cells

For this study, HUVEC cells were seeded into 24-well plates at a density of 50,000 cells/well overnight. HUVECs were then treated with Basal M199 medium supplemented with either 10 μM of TCO-$PEG_4$-NHS or without for 30 minutes. Following the treatment, cells were washed and incubated with either 1 mg/ml of Tz-Gp1bα- or Gp1bα- or un-conjugated C6 PLGA NPs for 20 minutes at 37ºC. Cells were then

washed to remove unbound NPs and imaged using a Leica DMi8 fluorescence microscope (Leica, Wetzlar, Germany) under bright light and an FITC channel. To further confirm the specificity of the click chemistry approach to form a NP-cell complex, TCO-HUVECs were pretreated with 10 μM of Tz-Cy5 for 20 minutes and then incubated with Tz-Gp1bα C6 PLGA NPs as described before. These cells were also imaged under a Cy5 channel to visualize Tz-Cy5 interacting with TCO-HUVECs.

To confirm the attachment of nanoparticles to TCO tagged endothelial cells via a click chemistry reaction, flow cytometric analysis was conducted. In brief, 200,000 TCO-HUVECs suspended in 200 μl of 1X PBS was incubated with either 1 mg of Tz-Gp1bα- or Gp1bα- or un-conjugated C6 PLGA NPs for 20 minutes at 37ºC followed by treatment. In a separate study, TCO-HUVECs treated with 1 mg of Tz-Gp1bα- or Gp1bα- or un-conjugated blank PLGA NPs were labeled with 10 μM of Tz-Cy5. These NP bound HUVECs were then fixed with 1% paraformaldehyde and were analyzed on a BD LSRII flow cytometer. At least 5,000 events per sample were analyzed and the population was gated based on their forward and side scattering characteristics. MFI of FITC (for C6 PLGA NPs) and APC (for Tz-Cy5) positive endothelial cells was graphed and calculated.

### 3.2.4 *In Vitro* Evaluation of Tz-Gp1bα PLGA NPs Efficiency Under Static and Flow Condition

The efficacy of Tz-Gp1bα PLGA NPs was determined by their ability to recognize and adhere onto a vWF coated surface as well as to capture endothelial cells via a click chemistry mediated approach. To perform this study, a hydrophobic surface was initially coated with 10 μg/ml of vWF and let dry overnight. 1 mg/ml of either Tz-Gp1bα- or Gp1bα- or un-conjugated C6 PLGA NPs was then added onto a vWF coated surface and incubated at 37ºC for 30 minutes. The NP-bound surface was washed twice with 1X PBS solution to remove unattached NPs. Following this, 10,000 TCO-HUVECs (labeled with NucBlue and Cell tracker Red CMPTX) were added onto the NP-bound surface and incubated further for 30 minutes at 37ºC. The surface was washed again to remove loosely attached cells and imaged using a Leica DMi8 fluorescence microscope (Leica, Wetzlar, Germany) under an FITC channel to visualize C6 PLGA NPs, and DAPI and Cy3 channels to observe TCO-HUVECs attachment. The captured images were analyzed using ImageJ software to determine the fluorescence intensity of bound NPs and the number of cells captured by NPs.

The targeting and cell capturing capabilities of Tz-Gp1bα PLGA NPs were also verified under flow conditions. Here, collagen coated Ibidi μSlides VI$^{0.4}$ were immobilized with 30 μg/ml of vWF for 1 hour at 37$^{o}$C. After coating, 1 mg of either Tz-Gp1bα- or Gp1bα- or un-conjugated C6 PLGA NPs was perfused through the channels of the flow slide using a syringe pump (Harvard Apparatus Infuse/Withdraw Syringe Pump) that was set to withdraw solution at 0.17125 ml/min to give a corresponding shear stress of 0.25 dyne/cm$^2$ according to manufacturer's specifications. Following the NPs attachment, 200,000 of NucBlue and Cell tracker$^{TM}$ Red CMPTX-labeled, TCO-HUVECs was perfused at 0.25 dyne/cm$^2$ for 6 minutes. Upon the completion of flow, the microslides were imaged using a Leica fluorescent microscope at the FITC channel to observe NP attachment and at DAPI or Cy3 channels to visualize the captured cells. The obtained images were then analyzed using ImageJ software.

### 3.2.5 Preliminary Analysis of Click Chemistry Mediated Stem Cell Capture Using an *Ex Vivo* Model

As a proof-of-concept, we have conducted *ex vivo* studies utilizing a rat carotid artery with denuded endothelium. In brief, a fresh rat carotid artery was recovered from a sacrificed animal, following which the endothelial layer was removed by treatment with 0.25% Trypsin in PBS as previously described.[121] The injured section of the artery was closed with surgical clamps and then followed with a pre-targeting treatment of Indocyanine green (ICG)-loaded Tz-Gp1bα PLGA NPs that were incubated for 10 minutes, washed with PBS three times to remove unbound NPs, and then 200,000 TCO-endothelial progenitor cells (TCO-EPCs) were injected and incubated with the arterial segment for 10 minutes. Post incubation, the tissue was rinsed with PBS and then imaged using a Kodak In Vivo Imager (Carestream Health Inc., New Haven, CT).

### 3.2.6 Statistical Analysis

The statistical analysis for *in vitro* cell studies including cytocompatibility of NP formulation and evaluation of TCO-HUVEC properties was assessed using one-way ANOVA followed by post-hoc pairwise multiple comparisons using the Tukey method on GraphPad Prism (GraphPad Software Inc., CA). The data for NP adhesion and number of TCO-HUVECs captured by bound NPs on a vWF surface were statistically analyzed using a two-tail student t-test in Excel. A significant difference was noted when p-values appeared

< 0.05. Unless specified, all data was represented as Average ± Standard Deviation with a sample size (n) of 3-5 replicates.

## 3.3 RESULTS

### 3.3.1 Characterization of Tz Tagged Gp1bα-Conjugated PLGA NPs (Tz-Gp1bα PLGA NPs)

DLS measurements show that the fabricated unconjugated PLGA NPs have an average diameter of 173 nm (polydispersity 0.134) while the other two conjugates, Gp1bα-PLGA NPs and Tz-Gp1bα PLGA NPs, have 171nm (0.117) and 173 nm (0.152), respectively (Table 1). The HRTEM images (**Fig. 3.2A**) show that the Tz-Gp1bα PLGA NPs have a uniform sized spherical morphology. The zeta potential values for unconjugated PLGA NPs, Gp1bα PLGA NPs and Tz-Gp1bα PLGA NPs were -23.28, -10.03 and -7.95 mV, respectively (**Table 3.1**). Decreases in zeta potential values were observed for Gp1bα conjugated NPs with respect to unconjugated ones, suggesting the effective conjugation process. To evaluate toxicity of the Tz-Gp1bα PLGA NPs to HUVEC cells *in vitro*, MTS assays were performed in cell samples when they were exposed to various concentrations of NPs. The results show that none of the nanoparticle formulations

***Table 3.1 Size, charge, polydispersity of nanoparticle formulations***

| Batch | Size (nm) | Polydispersity | Zeta Potential (mV) |
|---|---|---|---|
| PLGA NPs | 173 ± 68 | 0.134 ± 0.041 | -23.28 ± 3.20 |
| Gp1bα PLGA NPs | 171 ± 44 | 0.117 ± 0.022 | -10.03 ± 2.86 |
| Tz-Gp1bα PLGA NPs | 173 ± 64 | 0.152 ± 0.063 | -7.95 ± 3.27 |

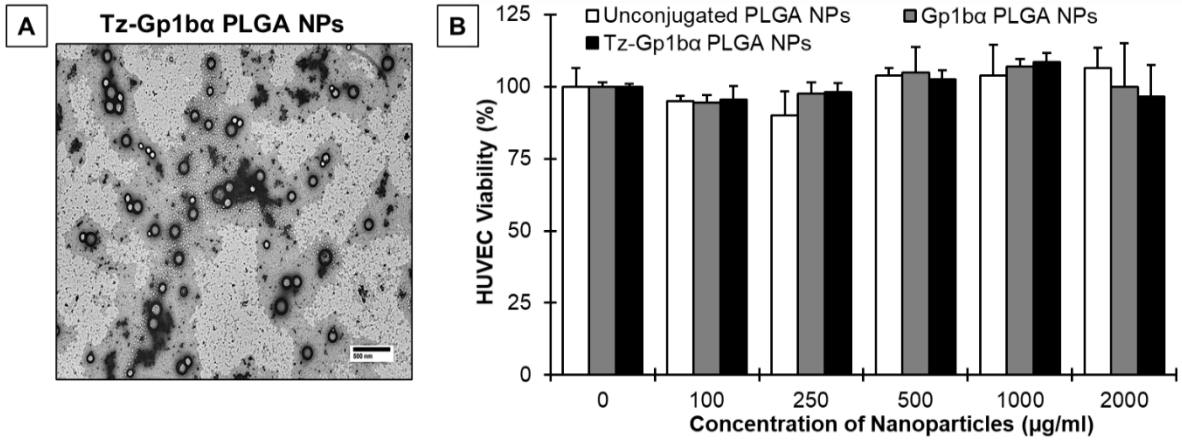


***Figure 3.2 Characterization of Tz tagged Gp1bα (Tz-Gp1bα) conjugated PLGA NPs.*** *A) TEM image of Tz-Gp1bα PLGA NPs shows spherical and uniform nanoparticles. The scale bar represents 500 µm. B) Cytocompatibility of Tz-Gp1bα PLGA NPs of various concentrations with HUVECs were determined by MTS assays. Percentage of cell viability was quantified with respect to untreated cells. No significant toxicity was seen, and their responses were comparable to unconjugated NPs and Gp1bα-conjugated PLGA NPs.*

show any indication of toxicity even at high concentrations. Tz-Gp1bα PLGA NPs were cyto-compatible with endothelial cells and suitable for our application (**Fig. 3.2B**).

### 3.3.2 Functional Characterization of TCO-Modified Endothelial Cells (TCO-HUVECs)

HUVECs were surface modified with various concentrations of TCO-PEG$_4$-NHS and their functional properties including growth, NO production, LDL uptake and migratory behavior were evaluated. Viability and growth of TCO-HUVECs was conducted using MTS assays (**Fig. 3.3A**). At least 90% of TCO-HUVECs were metabolically active post 24 hours of modification with ≤10μM of TCO-PEG$_4$-NHS. However, cell

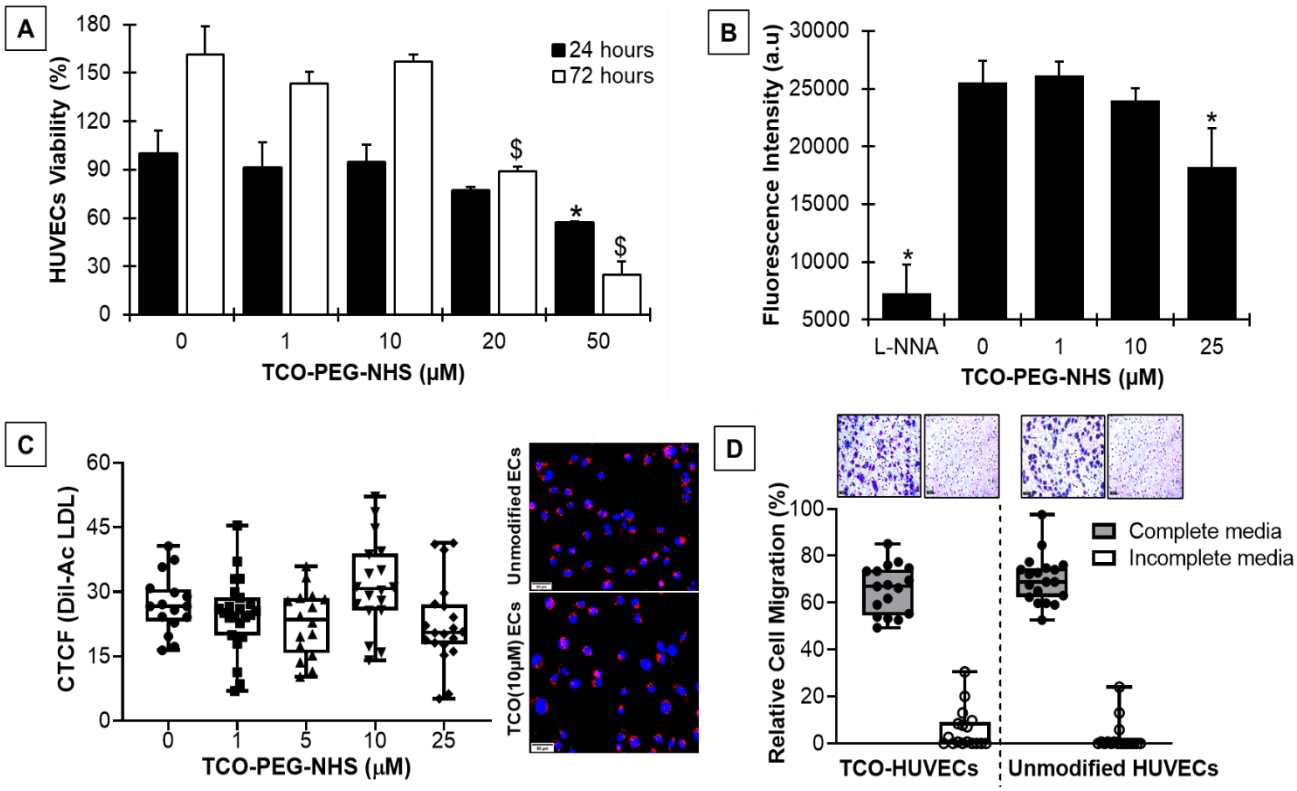


***Figure 3.3 Functional evaluation of TCO-HUVECs.*** *A) TCO-HUVECs viability over time was determined using MTS assay. Percentages of metabolically active cells were quantified with respect to unmodified cells post 24 hours of culture. B) Fluorescence intensity quantifies the amount of NO release from TCO-HUVECs post 24 hours of culture. L-NNA, a NOS inhibitor, downregulated NO production in cells served as a negative control. Data in A) and B) were represented as Average ± SD. Significance marked as * or $ when p <0.05 with respect to unmodified HUVECs on 24 and 48 hours of culture, respectively. C) Ac-LDL uptake by TCO-HUVECs represented as corrected total cell fluorescence (CTCF) of DiI stain within cells quantified using ImageJ. Fluorescence images of cells which was stained for Ac-LDL particles (red) and nuclei (blue), respectively. Scale bar is 50 μm in length. D) Migratory behavior of unmodified HUVECs and TCO-HUVECs in response to M199 basal media supplemented with growth factors post 24 hours of incubation. The percentage of cell migration was calculated with respect to initial number of cells. Graphs in C) and D) were box plots showing the data distribution with median, minimum, and maximum values.*

viability of HUVECs that were treated with 20μM and 50μM of TCO-$PEG_4$-NHS, decreased to 77% and 57% respectively. These HUVECs also significantly reduced their growth rate when assessed after 72 hours post modification compared to other HUVECs that were modified with ≤10μM of TCO-$PEG_4$-NHS. Furthermore, NO release from TCO-HUVECs modified with 25μM post 24 hours modification were substantially decreased compared to unmodified HUVECs (**Fig. 3.3B**). This impairment in NO production by TCO-HUVECs may have negatively affected their viability and growth following the post modification process. On the other hand, no reduction in NO production was observed when cells were modified with ≤ 10μM of TCO-$PEG_4$-NHS.

The endothelial cells process of internalizing LDL particles has been widely characterized. These cells uptake relatively small amounts of LDL via endocytosis and later metabolize to acquire cholesterol for their membrane synthesis.[122] However, in pathological conditions, LDL particles are modified with oxidative changes and contribute towards the progression of atherosclerosis.[123-125] Such modified LDL can be specifically recognized by endothelial cells and monocytes via their scavenger receptors.[126] Thus, the oxidized, or acetylated form of the LDL particle has been utilized as a marker to identify endothelial cells or EPC population. Nevertheless, when the endothelial cells are dysfunctional or diseased, they internalized more modified LDL particles as observed by Fournet-Bourguignon et al. (2000).[127] To evaluate whether TCO conjugation on the HUVECs impairs endothelial cells or not, we treated the cells post 24 hours of TCO-modification with 10 μg/ml of acetylated LDL (Ac-LDL) for 6 hours. The amount of Ac-LDL taken up by the cells directly correlates with the fluorescence intensity of Dil (lipophilic stain) that was tagged on to Ac-LDL. Unmodified HUVECs served as a control. According to our results, all TCO-HUVECs internalized Ac-LDL particles in similar amounts with unmodified HUVECs (red, **Fig. 3.3C**).

Lastly, TCO-HUVECs and HUVECs migratory properties in response to the growth factors were conducted using Boyden chamber assay. The number of HUVECs that migrated with respect to the initial number of cells seeded into the cell culture insert was analyzed (**Fig. 3.3D**). When unmodified HUVECs and TCO-modified cells in cell culture inserts were exposed to basal M199 media without any growth factors, we observed a negligible percentage of cell migration. However, in the presence of growth factors supplemented media, at least ~67% of both TCO-HUVECs and unmodified HUVECs migrated towards the

lower chamber of the Boyden chamber. Our results suggest that TCO conjugation of HUVECs did not affect the migratory response of the cells and performed in a similar fashion as the unmodified HUVECs.

### 3.3.3 Click Chemistry Mediated Interaction of NPs with Engineered Cells

The interaction between Tz-Gp1bα PLGA NPs and TCO-HUVECs via a click chemistry-based reaction is a very selective and efficient process. To determine this, HUVECs and TCO-HUVECs cultured in 24 well

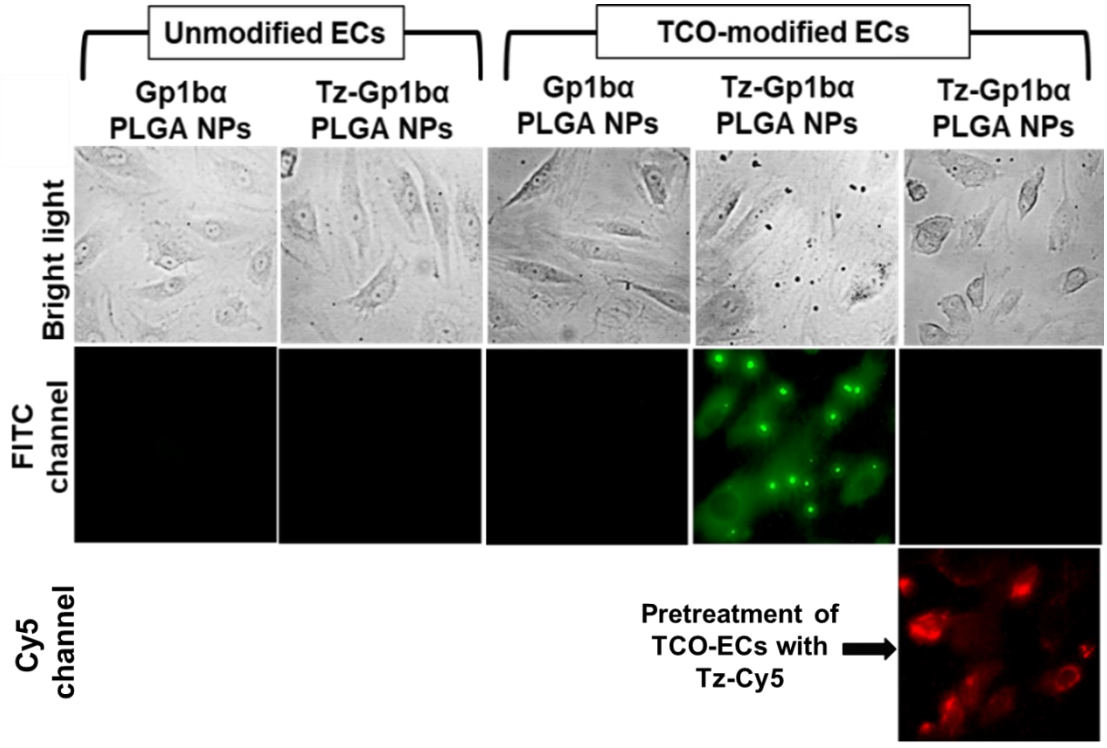


***Figure 3.4 Tz /TCO mediated NPs-HUVECs interaction.*** *HUVECs cultured in TCPS overnight were either modified with 10μM of TCO-PEG-NHS or without and were treated with C6 loaded PLGA NPs (green) conjugated with Gp1bα or Tz-Gp1bα. Qualitative images demonstrate that the presence of both Tz and TCO moieties on NPs and HUVECs respectively were required to form the NP-cell complex. Such interaction was blocked when TCO-HUVECs were pretreated with 10μM of Cy5-Tz (red).*

plates were separately treated with various formulations of NPs including Tz-Gp1bα-, Gp1bα-, and un-conjugated C6 PLGA NPs. As expected, C6 loaded Tz-Gp1bα PLGA NPs (green) only attach on the surface of TCO-HUVECs and not the unmodified ones (**Fig. 3.4**). Very minimal interaction of Gp1bα-, and un-conjugated C6 PLGA NPs with TCO-HUVECs were present. Furthermore, when TCO-HUVECs were treated with Tz-Cy5 prior to their treatment with Tz-Gp1bα C6 PLGA NPs, no complex formation between cells and NPs was seen. Fluorescence images shows the presence of Tz-Cy5 (red) on the TCO-HUVECs,

but no NPs were bound to these cells. These results suggest that the binding force between the cells and NPs is mainly due to the click chemistry reaction between Tz and TCO.

### 3.3.4 *In Vitro* Evaluation of Tz-Gp1bα PLGA NPs Efficiency Under Static and Flow Conditions

To investigate the Gp1bα capability to specifically target injured regions and arrest engineered TCO-HUVECs, various formulations of NPs including Tz-Gp1bα-, Gp1bα-, and un-conjugated C6 PLGA NPs were exposed to vWF-coated slides under static (**Fig. 3.5A**) and flow conditions of 0.25dyn/cm$^2$ (**Fig. 3.6A**). Accordingly, Tz-Gp1bα PLGA NPs accumulate efficiently on to vWF surfaces at the same rate as Gp1bα PLGA NPs, whereas unconjugated PLGA NPs have almost a negligible targeting capability towards

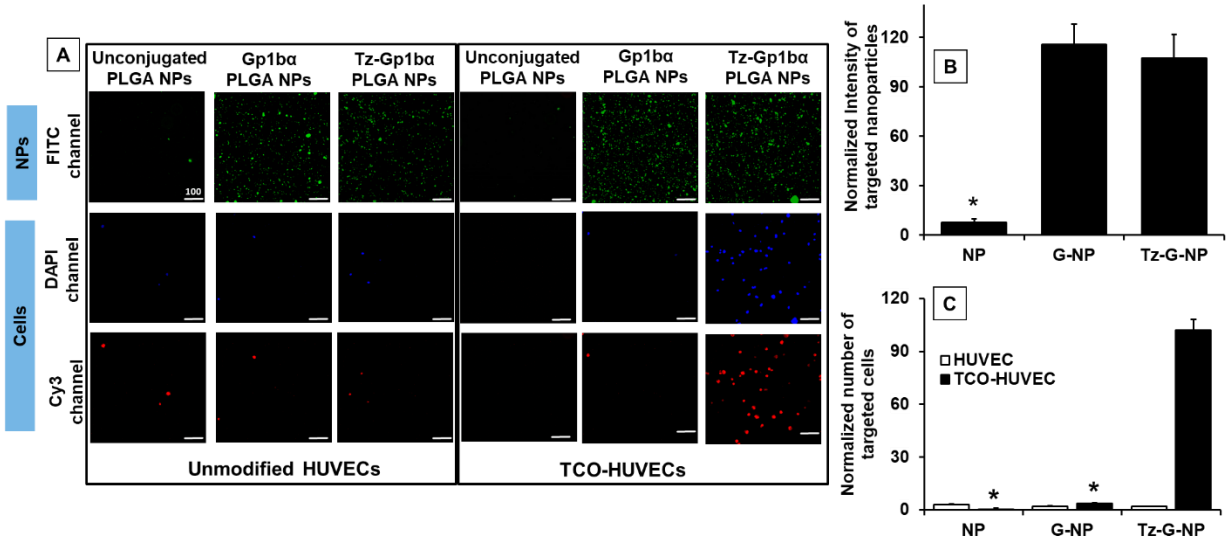


***Figure 3.5 Evaluation of Tz-Gp1bα PLGA NPs efficiency under static condition.*** *A) Fluorescent images show the ability of Tz-Gp1bα PLGA NPs (green) to target a vWF coated surface and their specificity to capture TCO-HUVECs (red) under static conditions. PLGA NPs were loaded with Coumarin 6 and cells were labeled with Nucblue (blue) and CMPTX red stain. The scale bar represents 100 μm in length. Significance marked as * when p<0.05 with respect to Tz-Gp1bα PLGA NPs. B) Quantitative data represents the fluorescent intensity of C6 loaded PLGA NPs bound to a vWF surface. C) The graph shows the number of TCO-HUVECs and unmodified HUVECs captured by NPs bound on the vWF- surface. Data represented as Average ± SD with sample size (n) = 3. Significance is indicated as * when p value is < 0.05 with respect to TCO-HUVECs captured by Tz-Gp1bα PLGA NPs.*

the coated surface signifying the efficiency of Gp1bα at recognizing the injured arterial wall (**Fig. 3.5B & 3.6B**). Furthermore, only Tz-Gp1bα conjugated PLGA NPs accumulated on to vWF surfaces subsequently captured and arrested TCO engineered cells both under static conditions and from circulation (**Fig. 3.5C & 3.6C)**. On the other hand, only <10% of TCO-HUVECs were adhered on to Gp1bα- or unconjugated PLGA

NPs treated vWF surface. Similarly, a negligible number of unmodified HUVECs interacted and were captured onto Tz-Gp1bα PLGA NPs coated surfaces, demonstrating the overall specificity of our approach in homing engineered transplanted cells towards an injured mimicking surface.

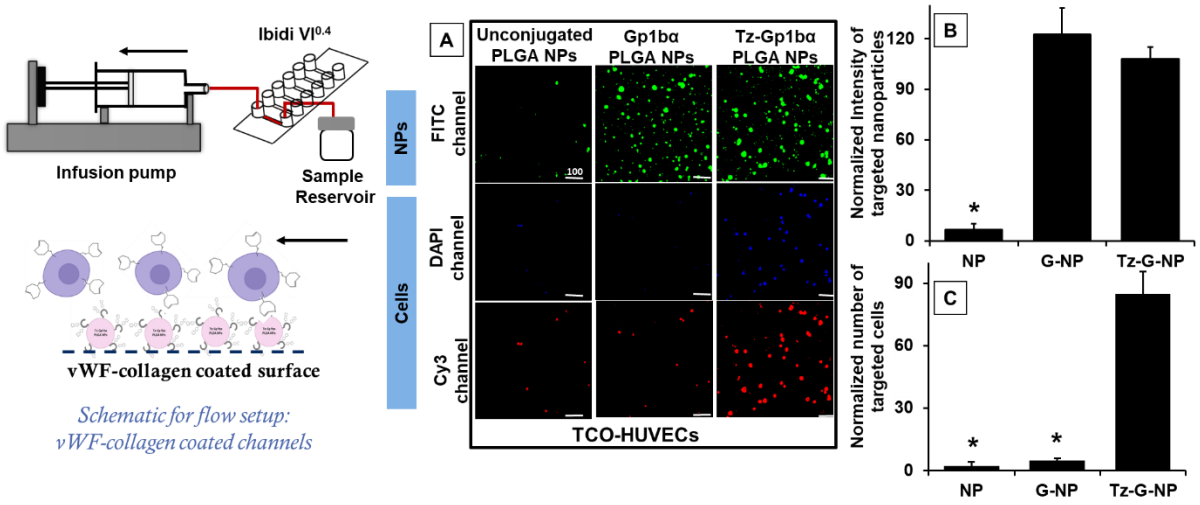


***Figure 3.6 Evaluation of Tz-Gp1bα PLGA NPs efficiency under flow conditions.*** *A) Fluorescent images show the ability of Tz-Gp1bα PLGA NPs (green) to target vWF immobilized collagen coated Ibidi VI$^{0.4}$ channel and their capability to capture TCO-HUVECs (red) under flow conditions when shear stress of 0.25 dyne/cm$^2$ for 6 minutes was applied. PLGA NPs were loaded with Coumarin 6 and cells were labeled with Nucblue (blue) and CMPTX red stain. The scale bar represents 100 µm in length. B) Quantitative data represents the fluorescent intensity of C6 loaded PLGA NPs bound to the vWF surface after flow conditions. Significance marked as * when p<0.05 with respect to Tz-Gp1bα PLGA NPs C) The graph shows the number of TCO-HUVECs interacted with NPs bound vWF- surface post flow condition. Data represented as Average ± SD with sample size (n) = 3. Significance is indicated as asterisk (*) when p value is < 0.05 with respect to TCO-HUVECs captured by Tz-Gp1bα PLGA NPs.*

### 3.3.5 *Ex Vivo* Evaluation of Tz-Gp1bα PLGA NPs Mediated Stem Cell Capture

The images of injured artery tissues treated sequentially with ICG loaded Tz-Gp1bα PLGA NPs and TCO-EPCs show that, as intended, the injured artery tissue attracts the accumulation of both Tz-Gp1bα PLGA NPs and TCO-EPCs (**Fig. 3.7A**). The accumulation of Tz-Gp1bα PLGA NPs is likely to contribute to the immobilization of TCO-HUVECs since both fluorescent images are overlapping with each other. The high specificity of such a pre-targeted cell delivery approach is supported by the quantitative difference of Tz-Gp1bα PLGA NPs and TCO-EPCs accumulation between injured and healthy tissues (**Fig. 3.7A-C**).

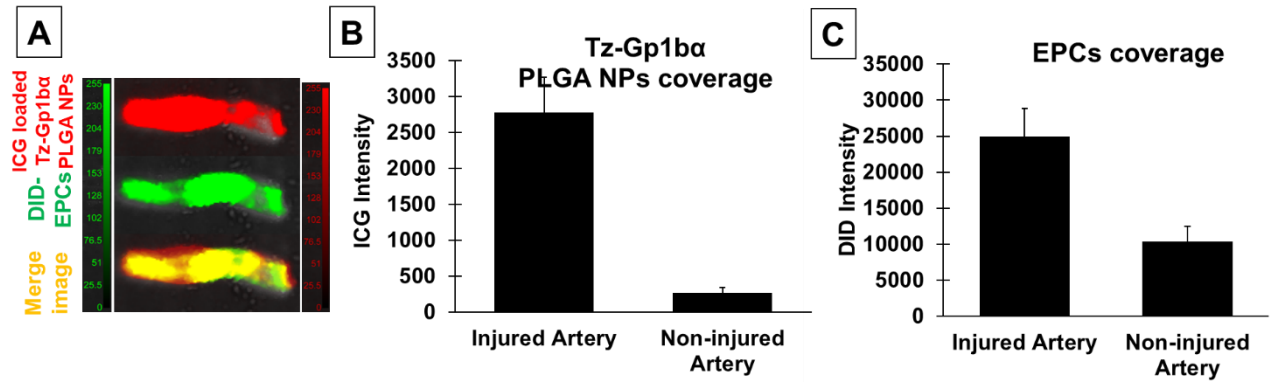


***Figure 3.7 Immobilization of EPCs on Ex Vivo injured rat carotid arteries.*** *A) The representative fluorescent images of ICG loaded Tz-Gp1bα PLGA NPs (red) immobilized TCO-EPCs (green) using rat injured carotid artery. A merge image shows the interaction of NPs with engineered cells (yellow). Quantitative data demonstrated Tz-functionalized PLGA NPs bound onto the injured arterial wall (B) and their capability to support subsequent capture of TCO-EPCs (C).*

## 3.4 DISCUSSION

Cell based therapies offer immense capabilities in regenerative medicine by supporting the restoration of tissue hemostasis and directing functional endogenous healing of damaged or diseased tissues. But one of the main challenges is the low number of cells recruited and retained at target sites after transplantation. As a result, cells can exert only minimal therapeutic benefits on the injured tissue leading to poor clinical outcomes. To circumvent this issue, researchers have modified the surface of cells to promote cell homing and engraftment at the treatment sites.[32, 128] For instance, Sarker et al. (2011) immobilized a ligand for E-selectin, sialyl Lewis X, on to the stem cells surface and demonstrated significantly improved cell interaction with inflamed tissue.[129] Different methods have been utilized to engineer the cell surface, and among them biorthogonal click chemistry based on a tetrazine (Tz)/trans-cyclooctene (TCO) reaction has recently garnered a lot of attention.[130, 131] Several studies have reported that cells engineered with click linkers resulted in more stable and robust cell adhesion to cells/tissues.[114, 132]

Our present work focused on a two-step approach utilizing biorthogonal click chemistry to improve the cell delivery and homing to treat an angioplasty induced vascular injury (**Fig. 3.1**). First, Tz tagged Gp1bα was conjugated on to PLGA nanoparticles to develop a multifunctional nanoparticle with targeting and cell capturing functionalities. These NPs mimic the natural injury targeting power of platelets via Gp1bα

interaction with vWF on the subendothelial layer, resulting in particle accumulation specifically to the injured arterial wall exposing Tz linkers attached to Gp1bα (**Fig. 3.1B**). Second, TCO tagged ECs were developed by modifying free amines on extracellular proteins and delivering them to the injured vasculature (**Fig. 3.1C**). Strong association of TCO on cells with Tz on NPs would allow ECs to capture and home on the treatment site to support *in situ* endothelial regeneration. We postulate that our two-step approach utilizing multifunctional nanoparticles and engineered cells to heal vascular injury will offer several advantages: (1) injury specific delivery of nanoparticles as well as therapeutic cells for regeneration, (2) cell homing utilizing biorthogonal chemistry to allow strong cell adhesion to tissues unlike conventional cell capturing methods based on antigen-antibody reaction, (3) nanoparticle formulation to allow us to incorporate growth factor molecules or therapeutic agents that may further assist in cell retention at diseased tissue, and (4) the platelet mimicking property of nanoparticles reduces interaction of platelets and other inflammatory cells in circulation to the injured arterial wall.

One of our goals in this work was to ensure that both the tagged molecules and functions of modified endothelial cells remain intact following their modification with Tz and TCO reagents, respectively. To verify this, we initially formulated ~170 nm uniform sized PLGA nanoparticles conjugated with Tz-modified Gp1bα. These Tz-Gp1bα PLGA NPs were very stable (Table 3.1) and showed superior cytocompatibility with HUVECs even at higher concentrations (**Fig. 3.2**). However, our preliminary studies have shown that increasing the amounts of Tz tagging on Gp1bα affected their functions to recognize or target the injured sites. We have seen almost a 50% decrease in NP adhesion towards vWF coated surfaces when 100 molar excess of Tz tagged on to Gp1bα (molar ratio of Gp1bα: Tz is 1:100) (Supplementary Fig. 3.1B). Despite this, we have observed that 50% of Tz-Gp1bα PLGA NPs (1:100) that were bound to vWF surfaces was enough to show significant improvement in cell capturing compared to Tz-Gp1bα PLGA NPs (1:25) and Gp1bα PLGA NPs. Therefore, we have utilized Tz-Gp1bα PLGA NPs (1:100) for further studies reported in this work. In addition, we have also observed that by increasing the amount of Tz-Gp1bα (1:100) conjugated on to PLGA NPs helps to recover 90% of protein functions to recognize the vWF surface when compared to naïve Gp1bα conjugated NPs (Supplementary Fig. 3.1D), and thereby, these Tz tagged NPs were able to immobilize more TCO-ECs to the targeted region (Supplementary Fig. 3.1E). Similar to our observations, Rahim et al. (2015) have reported that as 10 ug/ml

of anti-EGFR antibody was modified with 15 $PEG_4$-TCOs, their binding affinity to target cancer cells, A431, was dramatically reduced due to either decreased affinity or a population of permanently inactivated antibody.[133] However, when the antibody concentration was increased to 60 ug/ml, their binding function was almost fully recovered.

In parallel with modification of NPs, we have developed TCO tagged endothelial cells (TCO-ECs) by immobilizing TCO moieties on to free amines present on the extracellular membrane proteins (Supplementary Fig. 3.2A). With increasing the amount of TCO-$PEG_4$-NHS, the amount of tagging on cells has significantly increased (Supplementary Fig. 2B). Almost 93% of HUVECs have a certain amount of TCO groups present on their surface when they were modified using 10μM of TCO-$PEG_4$-NHS. Nevertheless, when cells were engineered using high concentrations of TCO-$PEG_4$-NHS (≥20μM), endothelial cell properties including proliferation and NO production were significantly affected. Hence 10μM of TCO-$PEG_4$-NHS was selected to incorporate TCO moieties onto the cell surface. These modified cells have no remarkable impact on cellular growth, NO release or other functions including LDL uptake and migratory response (**Fig. 3.3**). Following the modification, TCO groups on the HUVECs surface reduced to 34% after 24 hours of culture (Supplementary Fig. 2C), but these groups continued to retain on the cell surface and complexed with Tz moieties for almost 6 days (Supplementary Fig. 3.2D and E).

As previously noted, our main motivation for this research is to reduce the complications associated with the angioplasty/stenting procedure. The fast recovery of injured endothelium can significantly minimize the progression of restenosis and late-thrombotic events.[134] The click chemistry-based approach can overcome such limitations by allowing rapid and specific interaction of the engineered cells with the target regions. Our results have demonstrated that in the absence of any one of the click reagents either on HUVECs or PLGA NPs, no interaction occurred between them (Fig. 3.4). Furthermore, Tz-TCO interaction with NPs and HUVECs was completely abrogated when TCO sites on HUVECs were blocked using Tz-Cy5 prior to their treatment with Tz-Gp1bα PLGA NPs. Post click chemistry reaction, Tz-Gp1bα PLGA NPs were observed to occupy the sites on the surface of TCO-HUVECs as determined by flow cytometric analysis. Accordingly, almost 18% of TCO-HUVEC have NPs bound on their surface (Supplementary Fig. 3.3A) and more Tz sites on Tz-Gp1bα PLGA NPs were still available for further

reaction with TCO moieties (Supplementary Fig. 3.3B). The presence of these additional click chemistry mediated reactive sites following the initial reaction between cells and nanoparticles would allow us to utilize them as a depot system to deliver therapeutic payloads or track the transplanted cells *in situ.*

Lastly, Tz-modified PLGA NPs immobilized on to an injury mimicking surface have the potential to selectively capture TCO engineered ECs over unmodified cells as determined under static conditions (Fig. 3.5). Following the initial incubation with a vWF coated surface, almost complete coverage of Tz-Gp1bα PLGA NPs and Gp1bα PLGA NPs was observed, which reinstates our previous observation that the increased protein amount restores the binding affinity of Gp1bα to vWF. Furthermore, only Tz-Gp1bα PLGA NPs captured the engineered cells and a negligible interaction of NPs with cells was observed when either of the click chemistry reactive sites was absent on cells or PLGA NPs. Under flow conditions of 0.25dyn/cm$^2$, Tz-Gp1bα PLGA NPs selectively accumulated on to a vWF coated surface and subsequently captured and retained TCO-ECs from circulation effectively compared to their counterparts (Fig. 3.6). However, further studies optimizing the nanoparticles capability to retain and home the captured cells under physiological relevant shear stress need to be investigated. As a proof of concept for our approach, preliminary *ex vivo* studies have been performed. Accordingly, injured artery tissues treated sequentially with ICG loaded Tz-Gp1bα PLGA NPs and TCO-EPCs, as intended, showed that injured artery tissues attract the accumulation of both ICG loaded Tz-Gp1bα PLGA NPs and TCO-EPCs (Fig. 3.7A). The accumulation of ICG loaded Tz-Gp1bα PLGANPs is likely to contribute to the immobilization of TCO-EPCs since both fluorescent images overlap with each other. The high specificity of such a pre-targeted cell delivery approach is supported by the quantitative difference of ICG loaded Tz-Gp1bα PLGA NPs (Fig. 3.7B) and TCO-EPCs accumulation (Fig. 3.7C) between injured and healthy tissue.

In summary, in this work we have shown proof-of-concept application of bioorthogonal click chemistry in the field of regenerative medicine to efficiently deliver transplanted cells and support the functional recovery of injured tissue. TCO-engineered HUVECs maintained their functional properties and effectively captured Tz-Gp1bα PLGA NPs on to an injury mimicking surface under static and flow conditions. The long-term presence of click chemistry reactive groups on engineered cells enables us to further deliver a therapeutic payload to improve the growth and viability of the cells following transplantation. Our pre-targeting approach using Tz-Gp1bα PLGA NPs towards injured regions not only allows the specific homing

of engineered cells, but it can also reduce the inflammatory responses thereby supporting faster endothelial regeneration. NPs may further improve to carry growth factors that help in recruiting host stem cells as well as transplanted cells to the injured sites. Nevertheless, a substantial amount of work is needed to ensure the successful translation of our approach for practical use. For instance, the optimal size of Tz-Gp1bα PLGA NPs has yet to be determined. The diameter of the particle determines the efficiency of particle margination and retention towards injured vasculature from circulation. We have used ~170 nm sized NPs as a proof- of concept for our novel approach; however, future work will be performed to evaluate the effect of large sized NPs in targeting as well as capturing the cells in circulation. Furthermore, we must investigate the safety and efficacy of our strategy to support *in situ* reendothelialization using an *in vivo* injured artery model in animals.

### 3.5 CONCLUSIONS

Arterial wall injury post percutaneous coronary intervention (PCI) often leads to late vascular complications including restenosis and thrombosis. Rapid restoration of the loss of endothelium is a suitable solution that would help to overcome these issues. Cell targeted delivery to these injured sites by antibody immobilized stents exhibited only moderate success due to non-selective interaction with inflammatory cells and poor cell retention resulting in ineffective reconstitution of healthy vasculature. Recently, biorthogonal cycloaddition reaction with tetrazine and trans-cyclooctene was widely investigated to use for molecular imaging and cell-based diagnostics as it offers rapid, efficient, and strong binding. Herein, we show the concept of incorporating this highly selective biorthogonal click chemistry with nanotechnology and cell therapy to support endothelial cells homing and accelerated endothelial regeneration. We have developed PLGA nanoparticles tagged with tetrazine (Tz) to cloak on to the damaged arterial wall and capture trans-cyclooctene (TCO) modified endothelial cells from circulation to effectively treat angioplasty induced vascular injury. In our work, we have optimized the amount of TCO and Tz groups to incorporate onto endothelial cells and Gp1bα respectively without abrogating their biological activities. Our *in vitro* studies confirm the capability of TCO engineered cells to interact with injury targeted nanoparticles via a click chemistry reaction. Furthermore, pre-targeted nanoparticles successfully captured the engineered cells

under both static and flow conditions, which further reinforces the significance of our click chemistry-based approach to improve existing cell-based therapies for faster tissue healing and regeneration.

### 3.6 SUPPORTING INFORMATION

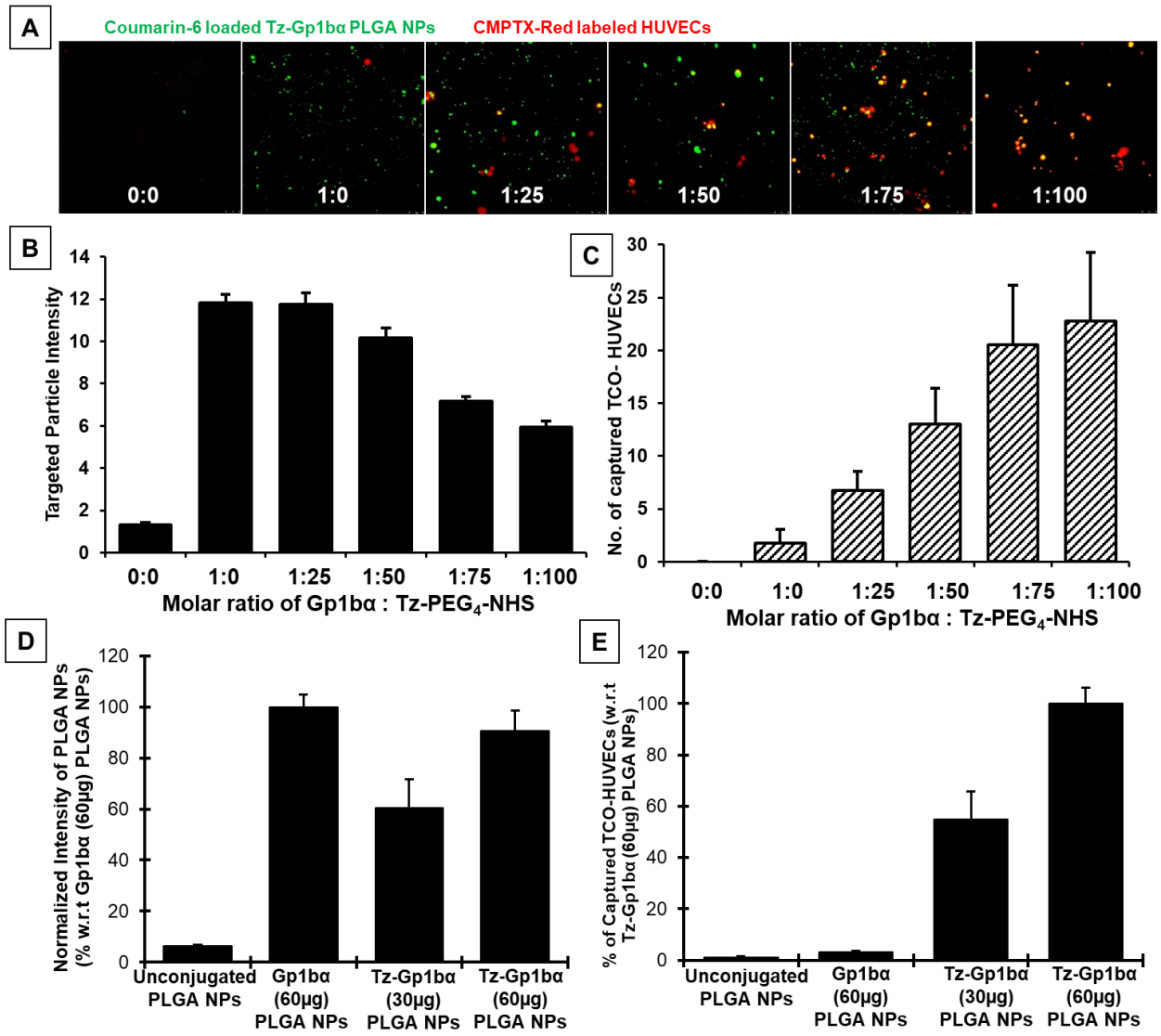


***Supplementary Figure 3.1 Development of Tz-Gp1bα conjugated PLGA NPs.*** *A) Fluorescent images show binding ability of Tz-Gp1bα PLGA NPs (green) on vWF coated surfaces and their subsequent capture of TCO-HUVECs (red) under static conditions. Various molar ratios of Tz with respect to Gp1bα were utilized to conjugate onto Coumarin 6 (C6) loaded PLGA NPs. HUVECs were stained with Cytotracker CMPTX red stain. B) Quantitative data represents the fluorescence intensities of C6-PLGA NPs that were bound to the vWF surface. C) Quantitative data demonstrates the number of TCO-HUVECs captured by Tz-Gp1bα PLGA NPs. Quantitative data representing the interaction of C6 PLGA NPs with the vWF coated surface as well as capture of TCO-HUVECs when increasing amounts of Tz-Gp1bα were used to conjugate onto the surface of C6 PLGA NPs as shown in D) and E) respectively. Data is represented as Average ± SD and significance was marked as an asterisk (*) when p value < 0.05.*

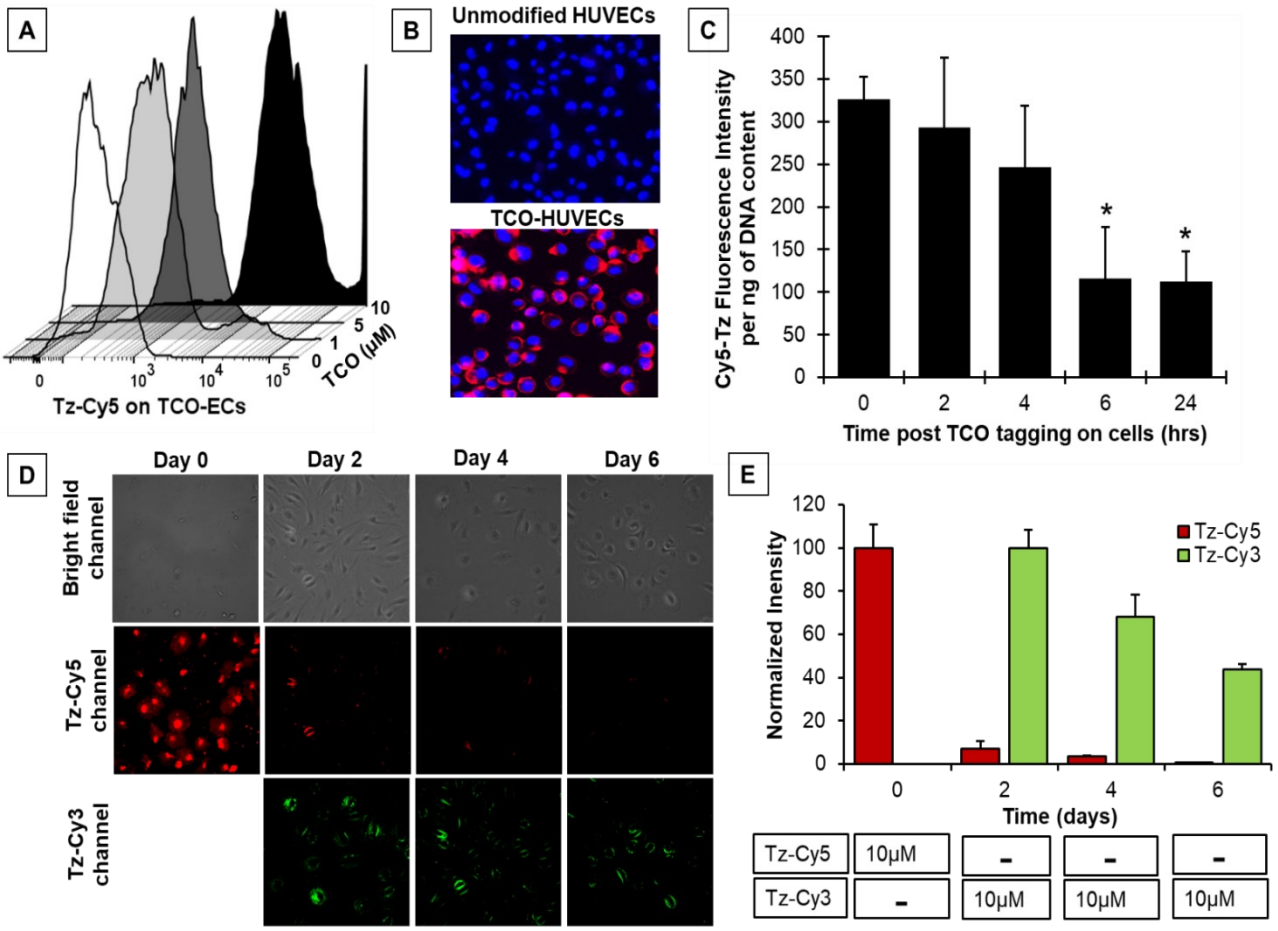


***Supplementary Figure 3.2 Development of TCO-HUVECs.*** *A) Flow cytometry analysis of HUVECs demonstrates a dose-dependent increase in TCO conjugation on the cells' surface. Almost 93% of HUVECs were tagged with TCO when treated with 10 μM of TCO-PEG$_4$-NHS. B) Fluorescent images confirm the coverage of TCO moieties on the HUVEC surface when treated with 10 μM of TCO-PEG$_4$-NHS. TCO-HUVECs and unmodified ones were treated with Tz-Cy5 (red) and cell nuclei were stained with NucBlue (blue). Scale bar represents 50 μm in length. C) Presence of TCO moieties on HUVECs cell surface post modification was quantified by tagging TCO-HUVECs at predetermined time points with Tz-Cy5. Following which, cells were lysed and fluorescence intensity of Cy5 as well as DNA content using Picogreen DNA assay were determined. D) Fluorescent images represent the retention of TCO groups on HUVECs surface over 6 days. On day 0, cells were labeled with Tz-Cy5 (red) and cultured until specified time points. At these time points, cells were further stained with Tz-Cy3 (green). Although fluorescence of Cy5 significantly decreased over time due to photobleaching, cell staining with Tz-Cy3 indicates that TCO sites were still available on the cell surface over 6 days post modification. E) Quantitative analysis of fluorescent intensities of Tz-Cy5 and Tz-Cy3 on the TCO-HUVECs over 6 days was measured using UV/Vis spectrophotometry. Data is represented as Average ± SD with n=4 and significance value is indicated as an asterisk (*) when p<0.05.*

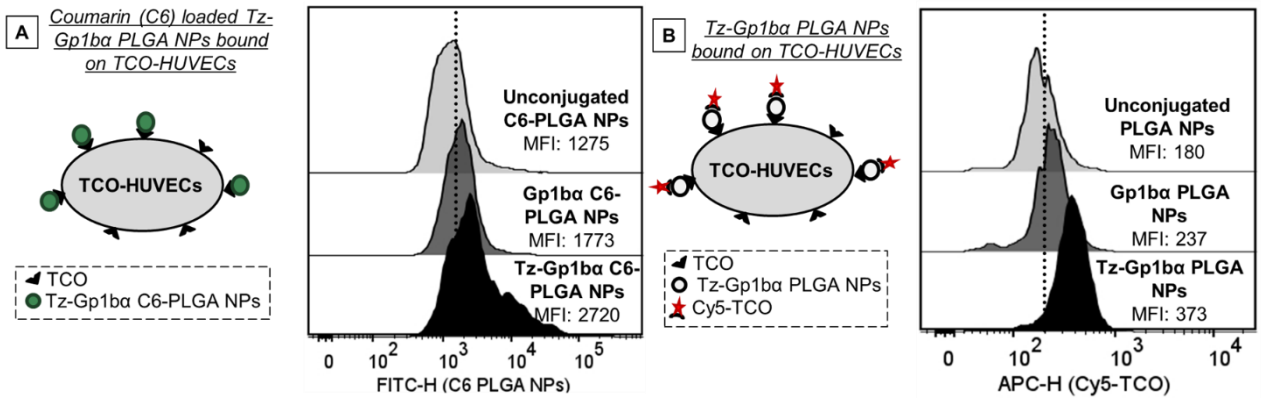


***Supplementary Figure 3.3 Tz/TCO mediated NPs-HUVECs interaction.*** *A) Schematic representation of TCO-HUVECs interaction with Tz-Gp1bα conjugated fluorescent PLGA NPs. Bound C6-PLGA NPs on the cell surface were quantified using flow cytometry. Median fluorescence intensity (MFI) of C6 PLGA NPs indicates click chemistry mediates a high interaction of NPs with engineered cells compared to its counterparts. Almost 18% more C6 PLGA NPs bound to TCO-HUVECs when NPs were modified with Tz-Gp1bα. B) Schematic representation of TCO-HUVECs interaction with Tz-Gp1bα conjugated PLGA NPs. Bound NPs were tagged with TCO-Cy5 and their fluorescence intensity was quantified using flow cytometry. MFI indicates a high number of Tz-Gp1bα PLGA NPs accumulated on the surface of TCO-HUVECs compared to Gp1bα PLGA NPs and unconjugated NPs.*

# Chapter 4. SUMMARY AND FUTURE STUDIES

Stenting and balloon angioplasty are common endovascular strategies used to open the occluded blood vessel. However, such interventions often damage the arterial wall, allowing activation and binding of circulating platelets to the exposed subendothelium that initiate inflammatory responses, ultimately leading to the development of restenosis. Although emerging drug eluting technologies have reduced the rates of endovascular complications, their long-term efficacy is hindered by late thrombosis and the catch-up phenomenon of restenosis.[135] It is now well known that ineffective reconstitution of the endothelial layer often results in these late stage complications. To overcome these limitations, several strategies involved with stem cell therapies and drug carriers have been developed. Previously, we have developed ~400 nm sized polymeric nano scaffolds that interface with the injured arterial endothelium via glycoprotein 1bα ligand and capture circulating EPCs via anti-CD34 antibodies.[46] These multifunctional nano systems cloaked the denuded endothelium, prevented platelet-mediated reactions, and reduced subsequent neointimal formation. Furthermore, they promoted rapid endothelial reconstruction by locally capturing EPCs and supporting their adhesion. Despite these achievements, the therapeutic potential of the nano scaffolds was not fully achieved as indicated by a decreased binding of EPCs to the injured artery after 7 and 21 days of transplantation, delayed intimal hyperplasia formation, as well as incomplete endothelial regeneration process. This might be associated with ineffective margination and retention of EPCs or nano scaffolds on the damaged vascular wall either due to hydrodynamic dislodging forces exerted on them by circulation or their poor tissue interactions.

In this work, we hypothesized that stable, biodegradable fluorescent nanoparticles could enable us to track the vascular carriers or nanoparticles labeled stem cells following *in vivo* delivery. This would allow us not only to track the nanocarriers or stem cells following transplantation, but also to estimate the required dosing of the therapeutic candidates to be administered at the injured site and assess the outcome of the therapy. Henceforth in Chapter 2, we have screened for three nature based, biodegradable polymers that have demonstrated intrinsic fluorescence for their potential to utilize as theranostic vascular carriers (**Aim 1)**. These polymers are BPLPL-PLGA50:50, BPLPL-PLGA75:25 and BPLPL-PLLA. Our fluorescent vascular carriers have sizes of ~150 nm and have shown to be highly stable, with desirable degradability

and release kinetics properties. BPLP-PLGA based NPs demonstrated superior hemocompatibility with blood cells. Furthermore, they did not cause any toxicity nor affected the normal functions of endothelial cells. NP-laden endothelial cells demonstrated fluorescent capability which enables them to be monitored for *in vivo* applications.

In Chapter 3, we took a different perspective of the application of nanoparticles other than as theranostic agents. Here, we developed nanoparticles that can mediate the homing of transplanted cells to the injured tissue and thereby support *in situ* endothelial regeneration following an arterial injury as occurs in PCI procedures (**Aim 2**). We have demonstrated that click chemistry utilizing a tetrazine (Tz) and transcyclooctene (TCO) reaction can provide a rapid and selective process to engage cells onto the subendothelium or injured arterial wall. Cellular engineering to incorporate TCO hooks on the cell surface has no impact on cell growth and function when the modification is performed at low concentrations. A multifunctional nanoparticles system can recognize the injury mimicking surface and capture engineered cells selectively under static and flow conditions. *Ex vivo* studies using an injured rat carotid artery have demonstrated the potential and feasibility of our approach to mediate cell homing via a click chemistry reaction. To summarize, our long-term objective of Aim 2 is to deliver our novel, multifunctional nanoparticles system that can engage in a click reaction with engineered stem cells transplanted following an injury and thereby improving the clinical outcome of PCI procedures. These stem cells can be bone marrow derived MSCs or EPCs from either autologous or allogenous sources.

Although, our fluorescent BPLPL based NPs showed the potential to be utilized as theranostic vascular carriers, a few challenges still need to be addressed. One of the limitations is that the intrinsic fluorescence of BPLPLs would not be strong enough to perform imaging in depth in tissues, thereby limiting the noninvasive tracking ability of NPs or NP-laden cells used for *in vivo* delivery. Thus, it would be necessary to combine other diagnostic imaging tools with BPLPL based NPs. Li et al. (2016) designed fluorescent nanobubbles by encapsulation of liquid tetradecafluorohexane within BPLPLs and demonstrated particle detection via *in vivo* ultrasound and *ex vivo* fluorescent imaging.[80] Another limitation of our study is that we did not demonstrate the feasibility of NPs or NP-laden cells imaging and detection using *ex vivo* tissue models, which needs to be addressed in our future studies. Our focus was given only

on optimizing the suitable BPLPLs in terms of their toxicity with endothelial cells and blood cells. Based on our results, BPLPL-PLGA based NPs would be ideal for our application for the treatment of cardiovascular diseases.

Our second approach utilizing NPs mediated cell capture in promoting tissue regeneration is innovative in various aspects; however, an *in vivo* study evaluating their efficacy in preventing the restenosis and intimal hyperplasia following balloon injury still needs to be investigated. Moreover, the retention and biodistribution of our multifunctional nanoparticle system on the arterial wall and other organs following *in vivo* delivery must be studied. In our project, we have utilized mature endothelial cells, HUVECs, as a model for endothelial progenitor cells (EPCs); however, for the successful clinical translation of our approach, we have to evaluate the effect of cell surface modification on the viability and function of EPCs. Following which, the fate of engineered cells after *in vivo* administration needs to be studied. TCO-EPCs must retain, proliferate, and differentiate into endothelial cells at the damaged site following their delivery to form a healthy vasculature. So, in our future studies, we will evaluate the extent of endothelial regeneration as well as their functions in terms of NO production and tight junction formation marked by ZO-1 expression.[136, 137] Additionally, the inflammatory responses that might be caused by the click chemistry reactions based on the presence of macrophages and neutrophils at the damaged artery following the treatment will also be conducted.[138, 139] Although, aforementioned *in vivo* studies were initially planned to be performed, due to the **COVID-19** pandemic, this could not be completed.

One of the concerns of our approach is the utilization of a non-specific reaction of NHS esters with the amines present on the cell surface to instill TCO moieties. Due to this, cellular viability and their functions are greatly impacted when treated with higher amounts of TCO-PEG-NHS. Therefore, to improve the amount of TCO groups on the cell surface as well as to maintain the superior cellular performance, alternative strategies need to be explored. Some of them are: (1) non-covalent incorporation of lipidated TCO groups; (2) combination of sialic acid glycoengineering with double click chemistry as previously reported,[114] where non-natural chemical groups (e.g. azide) are attached on the cellular glycans following with treatment of bifunctional crosslinkers like DBCO-PEG-TCO; and (3) incubation with ECs or EPCs specific antibodies tagged with TCO groups. Besides these, the influence of the NPs size on mediating

maximum availability of NPs (i.e Tz linkers) on the vasculature wall as well as their capability to promote subsequent capture of engineered cells must be studied. Lastly, localized delivery of engineered NPs to the artery may increase the availability of click reactive linkers available to interact with TCO modified endothelial cells. Hence, balloon or stent mediated delivery of nanoparticles may be optimal for our application, which also needs to be investigated in our future studies.

# REFERENCES


(1) Benjamin, E. J., Blaha, M. J., Chiuve, S. E., Cushman, M., Das, S. R., Deo, R., de Ferranti, S. D., Floyd, J., and Fornage, M. (2017) Heart disease and stroke statistics—2017 update: a report from the American Heart Association. *Circulation 135*, e146.

(2) Benjamin, E. J., Virani, S. S., Callaway, C. W., Chamberlain, A. M., Chang, A. R., Cheng, S., Chiuve, S. E., Cushman, M., Delling, F. N., and Deo, R. (2018) Heart disease and stroke statistics—2018 update: a report from the American Heart Association. *Circulation 137*, e67-e492.

(3) Mensah, G. A., and Brown, D. W. (2007) An Overview Of Cardiovascular Disease Burden In The United States. *Health Aff. 26*, 38-48.

(4) Mendis, S. (2017) Global progress in prevention of cardiovascular disease. *CDT 7*, S32-S38.

(5) Mehrpoya, A., Jalali, R., Jalali, A., and Namdari, M. (2018) Patient experiences of living with coronary stent. *J Vasc Nurs*.

(6) Bhatia, S. K. (2010) Coronary Artery Disease, in *Biomaterials for Clinical Applications* pp 23-49, Springer New York, New York, NY.

(7) Simon, A. S., and Vijayakumar, T. (2013) Molecular studies on coronary artery disease—a review. *Indian J Clin Biochem 28*, 215-226.

(8) Packard, R. R. S., and Libby, P. (2008) Inflammation in atherosclerosis: From vascular biology to biomarker discovery and risk prediction. *Clin. Chem. 54*, 24-38.

(9) Libby, P., and Theroux, P. (2005) Pathophysiology of Coronary Artery Disease. *Circulation 111*, 3481-3488.

(10) Malakar, A. K., Choudhury, D., Halder, B., Paul, P., Uddin, A., and Chakraborty, S. (2019) A review on coronary artery disease, its risk factors, and therapeutics. *J. Cell. Physiol. 234*, 16812-16823.

(11) Jovin, D. G., Katlaps, G. J., and Sumption, K. F. (2020) Coronary artery bypass graft markers: history, usage, and effects. *Gen Thorac Cardiovas 68*, 453-458.

(12) Mulukutla, S. R., Gleason, T. G., Sharbaugh, M., Sultan, I., Marroquin, O. C., Thoma, F., Smith, C., Toma, C., Lee, J. S., and Kilic, A. (2019) Coronary bypass versus percutaneous revascularization in multivessel coronary artery disease. *Ann. Thorac. Surg. 108*, 474-480.

(13) Braun, M. M., Stevens, W. A., and Barstow, C. H. (2018) Stable Coronary Artery Disease: Treatment. *Am Fam Physician 97*, 376-384.

(14) Hawkes, A. L., Nowak, M., Bidstrup, B., and Speare, R. (2006) Outcomes of coronary artery bypass graft surgery. *Vascular health and risk management 2*, 477-484.

(15) Camera, M., Brambilla, M., Canzano, P., Cavallotti, L., Parolari, A., Tedesco, C. C., Zara, C., Rossetti, L., and Tremoli, E. (2020) Association of microvesicles with graft patency in patients undergoing CABG surgery. *J Am Coll Cardiol 75*, 2819-2832.

(16) Patel, D. B., Shah, R., and Jovin, I. S. (2020) Improving outcomes of percutaneous coronary interventions in patients with stable ischemic heart disease. *J. Thorac. Dis. 12*, 1740-1749.

(17) Lee, D.-H., and de la Torre Hernandez, J. M. (2018) The Newest Generation of Drug-eluting Stents and Beyond. *Eur. Cardiol. 13*, 54-59.

(18) Borhani, S., Hassanajili, S., Ahmadi Tafti, S. H., and Rabbani, S. (2018) Cardiovascular stents: overview, evolution, and next generation. *Prog. Biomater. 7*, 175-205.

(19) Torrado, J., Buckley, L., Durán, A., Trujillo, P., Toldo, S., Valle Raleigh, J., Abbate, A., Biondi-Zoccai, G., and Guzmán, L. A. (2018) Restenosis, stent thrombosis, and bleeding complications: Navigating between scylla and charybdis. *J Am Coll Cardiol 71*, 1676-1695.

(20) Husted, S. E., Ziegler, B. K., and Kher, A. (2006) Long-term anticoagulant therapy in patients with coronary artery disease. *Eur Heart J 27*, 913-919.

(21) Wersäll, A., Golebiewska, E. M., and Poole, A. W. (2017) Platelet secretion, in *Platelets in Thrombotic and Non-Thrombotic Disorders* pp 637-649, Springer.

(22) Wilentz, J. R., Sanborn, T. A., Haudenschild, C. C., Valeri, C., Ryan, T., and Faxon, D. (1987) Platelet accumulation in experimental angioplasty: time course and relation to vascular injury. *Circulation 75*, 636-642.

(23) Ed Rainger, G., Chimen, M., Harrison, M. J., Yates, C. M., Harrison, P., Watson, S. P., Lordkipanidzé, M., and Nash, G. B. (2015) The role of platelets in the recruitment of leukocytes during vascular disease. *Platelets 26*, 507-520.

(24) Cornelissen, A., and Vogt, F. J. (2019) The effects of stenting on coronary endothelium from a molecular biological view: Time for improvement? *J Cell Mol Med 23*, 39-46.
(25) Finn, A. V., Joner, M., Nakazawa, G., Kolodgie, F., Newell, J., John, M. C., Gold, H. K., and Virmani, R. (2007) Pathological correlates of late drug-eluting stent thrombosis: strut coverage as a marker of endothelialization. *Circulation 115*, 2435-41.
(26) Joner, M., Finn, A. V., Farb, A., Mont, E. K., Kolodgie, F. D., Ladich, E., Kutys, R., Skorija, K., Gold, H. K., and Virmani, R. (2006) Pathology of drug-eluting stents in humans: delayed healing and late thrombotic risk. *J Am Coll Cardiol 48*, 193-202.
(27) Duan, Y., Yu, S., Xu, P., Wang, X., Feng, X., Mao, Z., and Gao, C. (2019) Co-immobilization of CD133 antibodies, vascular endothelial growth factors, and REDV peptide promotes capture, proliferation, and differentiation of endothelial progenitor cells. *Acta Biomater 96*, 137-148.
(28) Lee, J. M., Choe, W., Kim, B. K., Seo, W. W., Lim, W. H., Kang, C. K., Kyeong, S., Eom, K. D., Cho, H. J., Kim, Y. C., Hur, J., Yang, H. M., Cho, H. J., Lee, Y. S., and Kim, H. S. (2012) Comparison of endothelialization and neointimal formation with stents coated with antibodies against CD34 and vascular endothelial-cadherin. *Biomaterials 33*, 8917-27.
(29) Sedaghat, A., Sinning, J. M., Paul, K., Kirfel, G., Nickenig, G., and Werner, N. (2013) First in vitro and in vivo results of an anti-human CD133-antibody coated coronary stent in the porcine model. *Clin Res Cardiol 102*, 413-25.
(30) Uthamaraj, S., Tefft, B. J., Hlinomaz, O., Sandhu, G. S., and Dragomir-Daescu, D. (2015) Ferromagnetic bare metal stent for endothelial cell capture and retention. *J Vis Exp*, 53100.
(31) Polyak, B., Medved, M., Lazareva, N., Steele, L., Patel, T., Rai, A., Rotenberg, M. Y., Wasko, K., Kohut, A. R., Sensenig, R., and Friedman, G. (2016) Magnetic nanoparticle-mediated targeting of cell therapy reduces in-stent stenosis in injured arteries. *Acs Nano 10*, 9559-9569.
(32) Kuriakose, A. E., Pandey, N., Shan, D., Banerjee, S., Yang, J., and Nguyen, K. T. (2019) Characterization of photoluminescent polylactone-based nanoparticles for their applications in cardiovascular diseases. *Front Bioeng Biotechnol 7*, 353.
(33) Karimi, M., Zare, H., Bakhshian Nik, A., Yazdani, N., Hamrang, M., Mohamed, E., Sahandi Zangabad, P., Moosavi Basri, S. M., Bakhtiari, L., and Hamblin, M. R. (2016) Nanotechnology in diagnosis and treatment of coronary artery disease. *Nanomedicine-UK 11*, 513-530.
(34) Chan, J. M., Rhee, J.-W., Drum, C. L., Bronson, R. T., Golomb, G., Langer, R., and Farokhzad, O. C. (2011) In vivo prevention of arterial restenosis with paclitaxel-encapsulated targeted lipid-polymeric nanoparticles. *Proc. Natl. Acad. Sci. U.S.A. 108*, 19347-19352.
(35) Kona, S., Dong, J.-F., Liu, Y., Tan, J., and Nguyen, K. T. (2012) Biodegradable nanoparticles mimicking platelet binding as a targeted and controlled drug delivery system. *Int. J. Pharm. 423*, 516-524.
(36) Danenberg, H. D., Golomb, G., Groothuis, A., Gao, J., Epstein, H., Swaminathan, R. V., Seifert, P., and Edelman, E. R. (2003) Liposomal alendronate inhibits systemic innate immunity and reduces in-stent neointimal hyperplasia in rabbits. *Circulation 108*, 2798-804.
(37) Hu, C.-M. J., Fang, R. H., Wang, K.-C., Luk, B. T., Thamphiwatana, S., Dehaini, D., Nguyen, P., Angsantikul, P., Wen, C. H., Kroll, A. V., Carpenter, C., Ramesh, M., Qu, V., Patel, S. H., Zhu, J., Shi, W., Hofman, F. M., Chen, T. C., Gao, W., Zhang, K., Chien, S., and Zhang, L. (2015) Nanoparticle biointerfacing by platelet membrane cloaking. *Nature 526*, 118-121.
(38) Xu, J., Zhang, Y., Xu, J., Liu, G., Di, C., Zhao, X., Li, X., Li, Y., Pang, N., Yang, C., Li, Y., Li, B., Lu, Z., Wang, M., Dai, K., Yan, R., Li, S., and Nie, G. (2020) Engineered nanoplatelets for targeted delivery of plasminogen activators to reverse thrombus in multiple mouse thrombosis models. *J. Adv. Mater. 32*, 1905145.
(39) Anselmo, A. C., Modery-Pawlowski, C. L., Menegatti, S., Kumar, S., Vogus, D. R., Tian, L. L., Chen, M., Squires, T. M., Sen Gupta, A., and Mitragotri, S. (2014) Platelet-like nanoparticles: mimicking shape, flexibility, and surface biology of platelets to target vascular injuries. *Acs Nano 8*, 11243-53.
(40) Iyer, R., Kuriakose, A. E., Yaman, S., Su, L.-C., Shan, D., Yang, J., Liao, J., Tang, L., Banerjee, S., and Xu, H. (2019) Nanoparticle eluting-angioplasty balloons to treat cardiovascular diseases. *Int. J. Pharm. 554*, 212-223.
(41) Flores, A. M., Ye, J., Jarr, K. U., Hosseini-Nassab, N., Smith, B. R., and Leeper, N. J. (2019) Nanoparticle therapy for vascular diseases. *Arterioscler Thromb Vasc Biol 39*, 635-646.

(42) Chorny, M., Fishbein, I., Yellen, B. B., Alferiev, I. S., Bakay, M., Ganta, S., Adamo, R., Amiji, M., Friedman, G., and Levy, R. J. (2010) Targeting stents with local delivery of paclitaxel-loaded magnetic nanoparticles using uniform fields. *Proc. Natl. Acad. Sci. U.S.A. 107*, 8346-8351.
(43) Korin, N., Kanapathipillai, M., Matthews, B. D., Crescente, M., Brill, A., Mammoto, T., Ghosh, K., Jurek, S., Bencherif, S. A., Bhatta, D., Coskun, A. U., Feldman, C. L., Wagner, D. D., and Ingber, D. E. (2012) Shear-activated nanotherapeutics for drug targeting to obstructed blood vessels. *Science 337*, 738-742.
(44) Polyak, B., Medved, M., Lazareva, N., Steele, L., Patel, T., Rai, A., Rotenberg, M. Y., Wasko, K., Kohut, A. R., and Sensenig, R. (2016) Magnetic nanoparticle-mediated targeting of cell therapy reduces in-stent stenosis in injured arteries. *Acs Nano 10*, 9559-9569.
(45) Vosen, S., Rieck, S., Heidsieck, A., Mykhaylyk, O., Zimmermann, K., Bloch, W., Eberbeck, D., Plank, C., Gleich, B., Pfeifer, A., Fleischmann, B. K., and Wenzel, D. (2016) Vascular repair by circumferential cell therapy using magnetic nanoparticles and tailored magnets. *Acs Nano 10*, 369-376.
(46) Su, L. C., Xu, H., Tran, R. T., Tsai, Y. T., Tang, L., Banerjee, S., Yang, J., and Nguyen, K. T. (2014) In situ re-endothelialization via multifunctional nanoscaffolds. *Acs Nano 8*, 10826-36.
(47) Deb, S., Ghosh, K., and Shetty, S. D. (2015) Nanoimaging in cardiovascular diseases: Current state of the art. *Indian J Med Res 141*, 285-298.
(48) Garcia, J., Liu, S. Z., and Louie, A. Y. (2017) Biological effects of MRI contrast agents: gadolinium retention, potential mechanisms and a role for phosphorus. *Phiols T R Soc A 375*, 20170180.
(49) Pellico, J., Ellis, C. M., and Davis, J. J. (2019) Nanoparticle-based paramagnetic contrast agents for magnetic resonance imaging. *Contrast media & molecular imaging 2019*, 1845637-1845637.
(50) Menon, J. U., Jadeja, P., Tambe, P., Thakore, D., Zhang, S., Takahashi, M., Xie, Z., Yang, J., and Nguyen, K. T. (2016) Polymeric nanoparticles as dual-imaging probes for cancer management. *Biomater. biomech. bioeng. 3*, 129-140.
(51) Chen, W., Cormode, D. P., Fayad, Z. A., and Mulder, W. J. M. (2011) Nanoparticles as magnetic resonance imaging contrast agents for vascular and cardiac diseases. *Wiley Interdiscip. Rev. Nanomed. Nanobiotechnol. 3*, 146-161.
(52) Chandarana, M., Curtis, A., and Hoskins, C. (2018) The use of nanotechnology in cardiovascular disease. *Appl. Nanosci. 8*, 1607-1619.
(53) Park, J. H., Dehaini, D., Zhou, J., Holay, M., Fang, R. H., and Zhang, L. (2020) Biomimetic nanoparticle technology for cardiovascular disease detection and treatment. *Nanoscale Horiz 5*, 25-42.
(54) Goradel, N. H., Hour, F. G.-., Negahdari, B., Malekshahi, Z. V., Hashemzehi, M., Masoudifar, A., and Mirzaei, H. (2018) Stem cell therapy: A new therapeutic option for cardiovascular diseases. *J. Cell. Biochem. 119*, 95-104.
(55) Sun, R., Li, X., Liu, M., Zeng, Y., Chen, S., and Zhang, P. (2016) Advances in stem cell therapy for cardiovascular disease (Review). *Int. J. Mol. Med. 38*, 23-29.
(56) Chen, H., Wang, X., Zhou, Q., Xu, P., Liu, Y., Wan, M., Zhou, M., and Mao, C. (2017) Preparation of vascular endothelial cadherin loaded-amphoteric copolymer decorated coronary stents for anticoagulation and endothelialization. *Langmuir 33*, 13430-13437.
(57) Chen, Z., Li, Q., Chen, J., Luo, R., Maitz, M. F., and Huang, N. (2016) Immobilization of serum albumin and peptide aptamer for EPC on polydopamine coated titanium surface for enhanced in-situ self-endothelialization. *Mater Sci Eng C Mater Biol Appl 60*, 219-229.
(58) Povsic, T. J., and Goldschmidt-Clermont, P. J. (2008) Endothelial progenitor cells: markers of vascular reparative capacity. *Ther Adv Cardiovasc Dis. 2*, 199-213.
(59) Adams, William J., Zhang, Y., Cloutier, J., Kuchimanchi, P., Newton, G., Sehrawat, S., Aird, William C., Mayadas, Tanya N., Luscinskas, Francis W., and García-Cardeña, G. (2013) Functional vascular endothelium derived from human induced pluripotent stem cells. *Stem Cell Rep 1*, 105-113.
(60) Giordano, S., Zhao, X., Xing, D., Hage, F., Oparil, S., Cooke, J. P., Lee, J., Nakayama, K. H., Huang, N. F., and Chen, Y. F. (2016) Targeted delivery of human iPS-ECs overexpressing IL-8 receptors inhibits neointimal and inflammatory responses to vascular injury in the rat. *Am J Physiol Heart Circ Physiol 310*, H705-15.
(61) Wang, C.-H., Cherng, W.-J., Yang, N.-I., Kuo, L.-T., Hsu, C.-M., Yeh, H.-I., Lan, Y.-J., Yeh, C.-H., and Stanford, W. L. (2008) Late-outgrowth endothelial cells attenuate intimal hyperplasia

contributed by mesenchymal stem cells after vascular injury. *Arterioscler Thromb Vasc Biol 28*, 54-60.

(62) Chang, H.-K., Kim, P.-H., Kim, D. W., Cho, H.-M., Jeong, M. J., Kim, D. H., Joung, Y. K., Lim, K. S., Kim, H. B., Lim, H. C., Han, D. K., Hong, Y. J., and Cho, J.-Y. (2018) Coronary stents with inducible VEGF/HGF-secreting UCB-MSCs reduced restenosis and increased re-endothelialization in a swine model. *Exp Mol Med 50*, 114.

(63) Li, Z., Shen, D., Hu, S., Su, T., Huang, K., Liu, F., Hou, L., and Cheng, K. (2018) Pretargeting and bioorthogonal click chemistry-mediated endogenous stem cell homing for heart repair. *Acs Nano 12*, 12193-12200.

(64) Adamo, R. F., Fishbein, I., Zhang, K., Wen, J., Levy, R. J., Alferiev, I. S., and Chorny, M. (2016) Magnetically enhanced cell delivery for accelerating recovery of the endothelium in injured arteries. *J Control Release 222*, 169-175.

(65) Kuriakose, A. E., Nguyen, T. P., Noukeu, L. C., Sabhani, M. K., Weidanz, J. A., Le, D. Q., and Nguyen, K. T. (2019) Stem cells as drug delivery vehicles, in *Encyclopedia of Tissue Engineering and Regenerative Medicine* (Reis, R. L., Ed.) pp 197-210, Academic Press, Oxford.

(66) Lo, C. Y., Antonopoulos, A., Dell, A., Haslam, S. M., Lee, T., and Neelamegham, S. (2013) The use of surface immobilization of P-selectin glycoprotein ligand-1 on mesenchymal stem cells to facilitate selectin mediated cell tethering and rolling. *Biomaterials 34*, 8213-8222.

(67) Tang, J., Su, T., Huang, K., Dinh, P.-U., Wang, Z., Vandergriff, A., Hensley, M. T., Cores, J., Allen, T., Li, T., Sproul, E., Mihalko, E., Lobo, L. J., Ruterbories, L., Lynch, A., Brown, A., Caranasos, T. G., Shen, D., Stouffer, G. A., Gu, Z., Zhang, J., and Cheng, K. (2018) Targeted repair of heart injury by stem cells fused with platelet nanovesicles. *Nat. Biomed. Eng. 2*, 17-26.

(68) Wang, J., and Jokerst, J. V. (2016) Stem cell imaging: Tools to improve cell delivery and viability. *Stem Cells Int 2016*, 16.

(69) Yang, J., Zhang, Y., Gautam, S., Liu, L., Dey, J., Chen, W., Mason, R. P., Serrano, C. A., Schug, K. A., and Tang, L. (2009) Development of aliphatic biodegradable photoluminescent polymers. *Proc. Natl. Acad. Sci. U.S.A. 106*, 10086-10091.

(70) Hu, J., Guo, J., Xie, Z., Shan, D., Gerhard, E., Qian, G., and Yang, J. (2016) Fluorescence imaging enabled poly(Lactide-co-glycolide). *Acta Biomater 29*, 307-319.

(71) Xie, Z., Zhang, Y., Liu, L., Weng, H., Mason, R. P., Tang, L., Nguyen, K. T., Hsieh, J.-T., and Yang, J. (2014) Development of intrinsically photoluminescent and photostable polylactones. *Adv. Mater. Weinheim 26*, 4491-4496.

(72) Xie, Z., Kim, J. P., Cai, Q., Zhang, Y., Guo, J., Dhami, R. S., Li, L., Kong, B., Su, Y., Schug, K. A., and Yang, J. (2017) Synthesis and characterization of citrate-based fluorescent small molecules and biodegradable polymers. *Acta Biomater 50*, 361-369.

(73) Marques, M. R., Loebenberg, R., and Almukainzi, M. (2011) Simulated biological fluids with possible application in dissolution testing. *Dissolution Technol 18*, 15-28.

(74) Honary, S., and Zahir, F. (2013) Effect of zeta potential on the properties of nano-drug delivery systems-a review (Part 2). *Trop J Pharm Res 12*, 265-273.

(75) Cerda-Cristerna, B. I., Flores, H., Pozos-Guillen, A., Perez, E., Sevrin, C., and Grandfils, C. (2011) Hemocompatibility assessment of poly(2-dimethylamino ethylmethacrylate) (PDMAEMA)-based polymers. *J Control Release 153*, 269-77.

(76) Merten, M., and Thiagarajan, P. (2000) P-selectin expression on platelets determines size and stability of platelet aggregates. *Circulation 102*, 1931-1936.

(77) Zilla, P., Fasol, R., Hammerle, A., Yildiz, S., Kadletz, M., Laufer G, G., Wollenek, G., Seitelberger, R., and Deutsch, M. (1987) Scanning electron microscopy of circulating platelets reveals new aspects of platelet alteration during cardiopulmonary bypass operations. *Tex Heart I J 14*, 13-21.

(78) Braeken, Y., Cheruku, S., Ethirajan, A., and Maes, W. (2017) Conjugated polymer nanoparticles for bioimaging. *Materials 10*, 1420.

(79) Zhang, Y. S., and Yao, J. (2018) Imaging biomaterials-tissue interactions. *Trends Biotechnol. 36*, 403-414.

(80) Li, J., Tian, Y., Shan, D., Gong, A., Zeng, L., Ren, W., Xiang, L., Gerhard, E., Zhao, J., Yang, J., and Wu, A. (2017) Neuropeptide Y Y1 receptor-mediated biodegradable photoluminescent nanobubbles as ultrasound contrast agents for targeted breast cancer imaging. *Biomaterials 116*, 106-117.

(81) Lazzari, S., Moscatelli, D., Codari, F., Salmona, M., Morbidelli, M., and Diomede, L. (2012) Colloidal stability of polymeric nanoparticles in biological fluids. *J Nanopart Res 14*, 920-920.
(82) Singh, N. A., Mandal, A. K. A., and Khan, Z. A. (2017) Fabrication of PLA-PEG nanoparticles as delivery systems for improved stability and controlled release of catechin. *J Nanomater 2017*, 9.
(83) Liu, R., Huang, S.-S., Wan, Y.-H., Ma, G.-H., and Su, Z.-G. (2006) Preparation of insulin-loaded PLA/PLGA microcapsules by a novel membrane emulsification method and its release in vitro. *Colloids Surfaces B 51*, 30-38.
(84) Tran, R. T., Zhang, Y., Gyawali, D., and Yang, J. (2009) Recent developments on citric acid derived biodegradable elastomers. *Recent Pat Biomed Eng 2*, 216-227.
(85) Zhang, Y., Tran, R. T., Qattan, I. S., Tsai, Y.-T., Tang, L., Liu, C., and Yang, J. (2013) Fluorescence imaging enabled urethane-doped citrate-based biodegradable elastomers. *Biomaterials 34*, 4048-4056.
(86) Le, D. Q., Kuriakose, A. E., Nguyen, D. X., Nguyen, K. T., and Acharya, S. (2017) Hybrid nitric oxide donor and its carrier for the treatment of peripheral arterial diseases. *Sci. Rep 7*, 8692-8692.
(87) Montiel-Dávalos, A., Ventura-Gallegos, J. L., Alfaro-Moreno, E., Soria-Castro, E., García-Latorre, E., Cabañas-Moreno, J. G., Ramos-Godinez, M. d. P., and López-Marure, R. (2012) $TiO_2$ nanoparticles induce dysfunction and activation of human endothelial cells. *Chem. Res. Toxicol 25*, 920-930.
(88) Cao, Y. (2018) The toxicity of nanoparticles to human endothelial cells. *Adv Exp Med Biol 1048*, 59-69.
(89) Astanina, K., Simon, Y., Cavelius, C., Petry, S., Kraegeloh, A., and Kiemer, A. K. (2014) Superparamagnetic iron oxide nanoparticles impair endothelial integrity and inhibit nitric oxide production. *Acta Biomater 10*, 4896-4911.
(90) Duan, J., Yu, Y., Yu, Y., Li, Y., Wang, J., Geng, W., Jiang, L., Li, Q., Zhou, X., and Sun, Z. (2014) Silica nanoparticles induce autophagy and endothelial dysfunction via the PI3K/Akt/mTOR signaling pathway. *Int J Nanomedicine 9*, 5131-5141.
(91) Wang, X., Zachman, A. L., Chun, Y. W., Shen, F.-W., Hwang, Y.-S., and Sung, H.-J. (2014) Polymeric stent materials dysregulate macrophage and endothelial cell functions: implications for coronary artery stent. *Int. J. Cardiol. 174*, 688-695.
(92) Liu, X., and Ma, P. X. (2010) The nanofibrous architecture of poly(L-lactic acid)-based functional copolymers. *Biomaterials 31*, 259-69.
(93) Xu, H., Deshmukh, R., Timmons, R., and Nguyen, K. T. (2011) Enhanced endothelialization on surface modified poly(L-lactic acid) substrates. *Tissue Eng Part A 17*, 865-76.
(94) Menon, J. U., Ravikumar, P., Pise, A., Gyawali, D., Hsia, C. C. W., and Nguyen, K. T. (2014) Polymeric nanoparticles for pulmonary protein and DNA delivery. *Acta Biomateria 10*, 2643-2652.
(95) Wadajkar, A. S., Kadapure, T., Zhang, Y., Cui, W., Nguyen, K. T., and Yang, J. (2012) Dual-imaging enabled cancer-targeting nanoparticles. *Adv. Healthc. Mater 1*, 450-456.
(96) Lesniak, A., Campbell, A., Monopoli, M. P., Lynch, I., Salvati, A., and Dawson, K. A. (2010) Serum heat inactivation affects protein corona composition and nanoparticle uptake. *Biomaterials 31*, 9511-9518.
(97) Pelaz, B., del Pino, P., Maffre, P., Hartmann, R., Gallego, M., Rivera-Fernández, S., de la Fuente, J. M., Nienhaus, G. U., and Parak, W. J. (2015) Surface functionalization of nanoparticles with polyethylene glycol: Effects on protein adsorption and cellular uptake. *Acs Nano 9*, 6996-7008.
(98) Yang, J., Webb, A. R., and Ameer, G. A. (2004) Novel citric acid-based biodegradable elastomers for tissue engineering. *J. Adv. Mater. 16*, 511-516.
(99) Tran, R. T., Yang, J., and Ameer, G. A. (2015) Citrate-based biomaterials and their applications in regenerative engineering. *Annu. Rev. Mater. Res. 45*, 277-310.
(100) Motlagh, D., Allen, J., Hoshi, R., Yang, J., Lui, K., and Ameer, G. (2007) Hemocompatibility evaluation of poly(diol citrate) in vitro for vascular tissue engineering. *J. Biomed. Mater. Res. A 82A*, 907-916.
(101) Meng, B., Wang, X., Cui, F., Dong, H., and Yu, F. (2004) A new method of heparinizing PLLA film by surface entrapment. *J Bioact Compat Pol 19*, 131-143.
(102) Okamura, Y., Schmidt, R., Raschke, I., Hintze, M., Takeoka, S., Egner, A., and Lang, T. (2011) A few immobilized thrombins are sufficient for platelet spreading. *Biophys. J. 100*, 1855-1863.

(103) Rudolph, A., Teske, M., Illner, S., Kiefel, V., Sternberg, K., Grabow, N., Wree, A., and Hovakimyan, M. (2015) Surface modification of biodegradable polymers towards better biocompatibility and lower thrombogenicity. *PLOS ONE 10*, e0142075.
(104) Nguyen, K. T., Su, S. H., Sheng, A., Wawro, D., Schwade, N. D., Brouse, C. F., Greilich, P. E., Tang, L., and Eberhart, R. C. (2003) In vitro hemocompatibility studies of drug-loaded poly-(L-lactic acid) fibers. *Biomaterials 24*, 5191-201.
(105) Meiring, M., Khemisi, M., Laker, L., Dohmen, P. M., and Smit, F. E. (2017) Tissue engineered small vessel conduits - the anti-thrombotic effect of re-endothelialization of decellularized baboon arteries: A preliminary experimental study. *Med. Sci. Monit. Basic Res. 23*, 344-351.
(106) Guo, H. F., Dai, W. W., Qian, D. H., Qin, Z. X., Lei, Y., Hou, X. Y., and Wen, C. (2017) A simply prepared small-diameter artificial blood vessel that promotes in situ endothelialization. *Acta Biomater 54*, 107-116.
(107) Ullah, M., Liu, D. D., and Thakor, A. S. (2019) Mesenchymal stromal cell homing: Mechanisms and strategies for improvement. *iScience 15*, 421-438.
(108) Liu, B. (2019) Bio-orthogonal click chemistry for in vivo bioimaging. *Trends Chem. 1*, 763-778.
(109) McKay, C. S., and Finn, M. G. (2014) Click chemistry in complex mixtures: bioorthogonal bioconjugation. *Chemistry & biology 21*, 1075-1101.
(110) Borrmann, A., and van Hest, J. C. (2014) Bioorthogonal chemistry in living organisms. *Chem. Sci. 5*, 2123-2134.
(111) Patterson, D. M., Nazarova, L. A., and Prescher, J. A. (2014) Finding the right (bioorthogonal) chemistry. *ACS Chem. Biol. 9*, 592-605.
(112) Feng, Y., Wu, Y., Zuo, J., Tu, L., Que, I., Chang, Y., Cruz, L. J., Chan, A., and Zhang, H. (2019) Assembly of upconversion nanophotosensitizer in vivo to achieve scatheless real-time imaging and selective photodynamic therapy. *Biomaterials 201*, 33-41.
(113) Shao, H., Chung, J., Balaj, L., Charest, A., Bigner, D. D., Carter, B. S., Hochberg, F. H., Breakefield, X. O., Weissleder, R., and Lee, H. (2012) Protein typing of circulating microvesicles allows real-time monitoring of glioblastoma therapy. *Nat. Med. 18*, 1835-1840.
(114) Koo, H., Choi, M., Kim, E., Hahn, S. K., Weissleder, R., and Yun, S. H. (2015) Bioorthogonal click chemistry-based synthetic cell glue. *Small 11*, 6458-66.
(115) Yazdani, A., Bilton, H., Vito, A., Genady, A. R., Rathmann, S. M., Ahmad, Z., Janzen, N., Czorny, S., Zeglis, B. M., Francesconi, L. C., and Valliant, J. F. (2016) A bone-seeking trans-cyclooctene for pretargeting and bioorthogonal chemistry: A proof of concept study using 99mtc- and 177lu-labeled tetrazines. *J. Med. Chem. 59*, 9381-9389.
(116) Zlitni, A., Janzen, N., Foster, F. S., and Valliant, J. F. (2014) Catching bubbles: targeting ultrasound microbubbles using bioorthogonal inverse-electron-demand Diels–Alder reactions. *Angewandte Chemie 126*, 6577-6581.
(117) Zeglis, B. M., Sevak, K. K., Reiner, T., Mohindra, P., Carlin, S. D., Zanzonico, P., Weissleder, R., and Lewis, J. S. (2013) A pretargeted PET imaging strategy based on bioorthogonal Diels–Alder click chemistry. *J. Nucl. Med 54*, 1389-1396.
(118) Xu, H., Kona, S., Su, L.-C., Tsai, Y.-T., Dong, J.-F., Brilakis, E. S., Tang, L., Banerjee, S., and Nguyen, K. T. (2013) Multi-ligand poly(L-lactic-co-glycolic acid) nanoparticles inhibit activation of endothelial cells. *J. Cardiovasc. Transl. Res. 6*, 570-578.
(119) Patel, R. H., Wadajkar, A. S., Patel, N. L., Kavuri, V. C., Nguyen, K. T., and Liu, H. (2012) Multifunctionality of indocyanine green-loaded biodegradable nanoparticles for enhanced optical imaging and hyperthermia intervention of cancer. *J Biomed Opt 17*, 046003.
(120) El-Sharkawey, A. (2016) *Calculate the Corrected Total Cell Fluorescence (CTCF)*.
(121) Chen, S., Segal, M., and Agarwal, A. (2004) “Lumen digestion” technique for isolation of aortic endothelial cells from heme oxygenase-1 knockout mice. *Biotechniques 37*, 84-89.
(122) Vasile, E., Simionescu, M., and Simionescu, N. (1983) Visualization of the binding, endocytosis, and transcytosis of low-density lipoprotein in the arterial endothelium in situ. *J Cell Biol 96*, 1677-89.
(123) Parthasarathy, S., Raghavamenon, A., Garelnabi, M. O., and Santanam, N. (2010) Oxidized low-density lipoprotein. *Methods Mol. Biol. 610*, 403-417.
(124) Pentikäinen, M. O., Öörni, K., Ala-Korpela, M., and Kovanen, P. T. (2000) Modified LDL – trigger of atherosclerosis and inflammation in the arterial intima. *J. Intern. Med. 247*, 359-370.

(125) Alique, M., Luna, C., Carracedo, J., and Ramírez, R. (2015) LDL biochemical modifications: a link between atherosclerosis and aging. *Food & nutrition research 59*, 29240-29240.
(126) Steinberg, D. (1998) Oxidative Modification of LDL and Atherogenesis, in *Multiple Risk Factors in Cardiovascular Disease: Strategies of Prevention of Coronary Heart Disease, Cardiac Failure, and Stroke* (Gotto, A. M., Lenfant, C., Paoletti, R., Catapano, A. L., and Jackson, A. S., Eds.) pp 141-147, Springer Netherlands, Dordrecht.
(127) Fournet-Bourguignon, M.-P., Castedo-Delrieu, M., Bidouard, J.-P., Leonce, S., Saboureau, D., Delescluse, I., Vilaine, J.-P., and Vanhoutte, P. M. (2000) Phenotypic and functional changes in regenerated porcine coronary endothelial cells. *Circ. Res. 86*, 854-861.
(128) De Becker, A., and Riet, I. V. (2016) Homing and migration of mesenchymal stromal cells: How to improve the efficacy of cell therapy? *World J Stem Cells 8*, 73-87.
(129) Sarkar, D., Spencer, J. A., Phillips, J. A., Zhao, W., Schafer, S., Spelke, D. P., Mortensen, L. J., Ruiz, J. P., Vemula, P. K., Sridharan, R., Kumar, S., Karnik, R., Lin, C. P., and Karp, J. M. (2011) Engineered cell homing. *Blood 118*, e184-e191.
(130) Csizmar, C. M., Petersburg, J. R., and Wagner, C. R. (2018) Programming cell-cell interactions through non-genetic membrane engineering. *Cell Chem Biol 25*, 931-940.
(131) Takayama, Y., Kusamori, K., and Nishikawa, M. (2019) Click chemistry as a tool for cell engineering and drug delivery. *Molecules 24*, 172.
(132) Koo, H., Hahn, S. K., and Yun, S. H. (2016) Controlled detachment of chemically glued cells. *Bioconjug Chem 27*, 2601-2604.
(133) Rahim, M. K., Kota, R., and Haun, J. B. (2015) Enhancing reactivity for bioorthogonal pretargeting by unmasking antibody-conjugated trans-cyclooctenes. *Bioconjugate Chem 26*, 352-360.
(134) Cheng, M., Guan, X., Li, H., Cui, X., Zhang, X., Li, X., Jing, X., Wu, H., and Avsar, E. (2013) Shear stress regulates late EPC differentiation via mechanosensitive molecule-mediated cytoskeletal rearrangement. *PLOS ONE 8*, e67675-e67675.
(135) Sun, J., Kang, X., and Li, T. (2015) Vascular restoration: Is there a window of opportunity? *Med Hypotheses 85*, 972-5.
(136) Zhang, Y., and Yang, W.-X. (2016) Tight junction between endothelial cells: the interaction between nanoparticles and blood vessels. *Beilstein J. Nanotechnol. 7*, 675-684.
(137) Qin, M., Guan, X., Wang, H., Zhang, Y., Shen, B., Zhang, Q., Dai, W., Ma, Y., and Jiang, Y. (2017) An effective ex-vivo approach for inducing endothelial progenitor cells from umbilical cord blood CD34+ cells. *Stem Cell Res Ther 8*, 25.
(138) Mickelson, J. K., Lakkis, N. M., Villarreal-Levy, G., Hughes, B. J., and Smith, C. W. (1996) Leukocyte activation with platelet adhesion after coronary angioplasty: a mechanism for recurrent disease? *J Am Coll Cardiol 28*, 345-353.
(139) Melero-Martin, J. M., Khan, Z. A., Picard, A., Wu, X., Paruchuri, S., and Bischoff, J. (2007) In vivo vasculogenic potential of human blood-derived endothelial progenitor cells. *Blood 109*, 4761-4768.

## PUBLICATIONS AND POSTER PRESENTATIONS

1) Inyang E, **Kuriakose AE**, Chen B, Nguyen KT, Cho M. Engineering delivery of nonbiologics using poly(lactic-*co*-glycolic acid) nanoparticles for repair of disrupted brain endothelium. *ACS Omega*. 2020 Jun 23;5(24):14730-14740. PubMed Central PMCID: PMC7315588.

2) **Kuriakose AE**, Pandey N, Shan D, Banerjee S, Yang J, Nguyen KT. Characterization of photoluminescent polylactone-based nanoparticles for their applications in cardiovascular diseases. *Front Bioeng Biotechnol.* 2019; 7:353. PubMed Central PMCID: PMC6886382.

3) **Kuriakose AE**, Hu W, Nguyen KT, Menon JU. Scaffold-based lung tumor culture on porous PLGA microparticle substrates. *PLoS One*. 2019;14(5): e0217640. PubMed Central PMCID: PMC6544352.

4) Iyer R, **Kuriakose AE**, Yaman S, Su LC, Shan D, Yang J, Liao J, Tang L, Banerjee S, Xu H, Nguyen KT. Nanoparticle eluting-angioplasty balloons to treat cardiovascular diseases. *Int J Pharm*. 2019 Jan 10; 554:212-223. PubMed Central PMCID: PMC6489505.

5) Xu C, **Kuriakose AE**, Truong D, Punnakitikashem P, Nguyen KT, Hong Y. Enhancing anti-thrombogenicity of biodegradable polyurethanes through drug molecule incorporation. *J Mater Chem B*. 2018 Nov 28;6(44):7288-7297. PubMed Central PMCID: PMC6424506.

6) Yu L, Scherlag BS, Dormer K, Rutel I, Huang B, Zhou X, **Kuriakose AE**, Nguyen KK, Po S. Targeted ganglionated plexi denervation using magnetic nanoparticles carrying calcium chloride payload. *JACC Clin Electrophysiol.* 2018 Oct;4(10):1347-1358. PubMed Central PMCID: PMC6598434.

7) Menon JU, **Kuriakose AE**, Iyer R, Hernandez E, Gandee L, Zhang S, Takahashi M, Zhang Z, Saha D, Nguyen KT. Dual-drug containing core-shell nanoparticles for lung cancer therapy. *Sci Rep*. 2017 Oct 16;7(1):13249. PubMed Central PMCID: PMC5643549.

8) Le DQ, **Kuriakose AE**, Nguyen DX, Nguyen KT, Acharya S. Hybrid nitric oxide donor and its carrier for the treatment of peripheral arterial diseases. *Sci Rep*. 2017 Aug 18;7(1):8692. PubMed Central PMCID: PMC5562917.

9) **Kuriakose, A. E.**, Nguyen, T. P., Noukeu, L. C., Sabhani, M. K., Weidanz, J. A., Le, D. Q., and Nguyen, K. T. (2019) Stem Cells as Drug Delivery Vehicles, in *Encyclopedia of Tissue Engineering and Regenerative Medicine* (Reis, R. L., Ed.) pp 197-210, Academic Press, Oxford.

10) Kyung KM, **Kuriakose AE**, Truong TD, Zhou J, Nguyen KT, Tang L. Enhanced endothelial cell delivery for repairing injured endothelium via pretargeting approach and bioorthogonal chemistry. *ACS Biomaterials Science and Engineering*. (currently in the review process)

11) **Kuriakose AE**, Zou J, Tran V, Nguyen KT, Tang L. Nanomatchmakers to promote rapid EPCs homing and regeneration following PCI. (work in progress)

12) Messerschmidt, V, **Kuriakose, AE**, Nguyen, KT, Lee, J, Therapeutic PLGA nanoparticles to recover endocardial notch signaling. (work in progress)

13) Pandey, N., Soto Garcia, L., **Kuriakose, AE**., Joseph, T., Liao, J, Zimmern, P., Nguyen, KT., Hong, Y., Antimicrobial nanocomposite adhesives for wound healing. (work in progress)

### ***Poster Sessions:***

1) Pandey, N., Soto Garcia, L., **Kuriakose, AE**., Joseph, T., Liao, J, Zimmern, P., Nguyen, KT., Hong, Y., Antimicrobial Nanocomposite Adhesives for Wound Healing. BMES 2019, Philadelphia, PA

2) **Kuriakose, AE**., Yaman, S., Banerjee, S., Nguyen, KT., Development of Engineered Cell Therapy Using Gp1bα Expressing Endothelial Cells Loaded with LipoxinA4 Eluting Nanoparticles. BMES 2019, Philadelphia, PA

3) Messerschmidt, V., **Kuriakose, A.**, Nguyen, K., Lee, J., mRNA Delivery via PLGA Nanoparticles to Recover Endocardial Notch Signaling. American Heart Association's Basic Cardiovascular Science Conference 2019, Boston, MA

4) Inyang, E., **Kuriakose, A.**, Chen, B., Nguyen, K., Cho, M., Theragnostic Nano-device to Detect and Regenerate Disrupted Brain Endothelium by Mechanical Trauma. BMES 2019, Philadelphia, PA

5) **Kuriakose A**, Perez P, Pandey N, Shan D, Yang J, Nguyen KT. Effects of Synthesis Parameters on the Size of Biodegradable Fluorescent Nanoparticles. BMES 2017, Phoenix, AZ

6) **Kuriakose A**, Rajnikant P, Xie Z, Yang J, Banarjee S, Nguyen KT**.** Photoluminescent Polylactones Based Nanoscaffolds for Enhancing Reendothelialization. ATVB/PVD 2017, Minneapolis, MN

7) Le D, **Kuriakose A**, Nguyen T, Raphel J, Nguyen KT, Acharya S. Hybrid Nitric Oxide and Antioxidant Small Molecule and its Nanocarrier for Peripheral Arterial Disease Treatment. BioNorth Texas Innovation IC3 2017, Arlington, TX

8) **Kuriakose** A, Priyesh Rajnikant, Upasana Mali, Zhiwei Xie, Jian Yang, Subhash Banerjee, Kytai Nguyen. Nanoscaffolds using photoluminescent-polylactones to prevent restenosis after PCI. BMES, 2016, Minneapolis, MN

9) Le, D, **Kuriakose A**, Acharya S, Nguyen KT. Development of Novel Antioxidant-Nitric Oxide Donor Hybrid Compound, and its Carrier for PAD Treatment. BMES, 2016, Minneapolis, MN

10) **Kuriakose AE**, Rajnikant P, Mali U, Xie Z, Yang J, Subhash Banerjee, Kytai Nguyen. Nano-scaffold for *in situ* Endothelial Regeneration after PCI. NANOSMAT-USA, 2016, the University of Texas at Arlington, TX

11) **Kuriakose AE**, Menon JU, Nguyen KT. Three-dimensional *in vitro* lung tumor models for cancer drug screening. ACES 2015, the University of Texas at Arlington, Arlington, TX

12) Iyer R, **Kuriakose AE**, Yaman S, Nguyen KT. Screening of Nanoparticles and Nanoparticle Delivery Strategies for Treatment of Atherosclerosis via Coated Angioplasty Balloons. BMES 2015, Tampa, FL

13) **Kuriakose AE**, Menon JU, Nguyen KT. Porous Microspheres for Cell Delivery in Tissue Regeneration. BMES 2014, San Antonio, TX

14) **Kuriakose AE**, Menon JU, Pokhrel K, Sharma A, Hong Y, Nguyen KT. Porous Poly Urethane Microspheres as a 3-D Culture Model for In Vitro Drug Screening. BMES 2014, San Antonio, TX

15) Menon JU, **Kuriakose AE**, Hernandez E, Gandee L, Zhang S, Takahashi M, Zhang Z, Saha D, Nguyen KT. Development of MultiFunctional Core-Shell NPs for Targeted Lung Cancer Dual Therapy. BMES 2014, San Antonio,TX

## BIOGRAPHY

Aneetta E. Kuriakose was born in Kerala, India and raised there until she and her family moved to Saudi Arabia. She completed her secondary schooling at the International Indian Embassy School inDammam, Saudi Arabia. Following this, Aneetta came to the United States and enrolled in a dual degree program with a Bachelor of Science in Biology and a Master of Science in Biomedical Engineering at UT Arlington from September 2009 to August 2013. During this time, Aneetta joined Dr. Kytai T. Nguyen's lab and her primary research interest was using nanoparticles to treat lung cancer. Her main research topic involved the development of an *in vitro* three-dimensional cell culture model to screen and test the efficacy of anti-cancer drugs. During this time, Aneetta was also accepted into the National Science Foundation's REU (Research Experience for Undergraduates) summer program at UT Arlington under the direction of Dr. Manfred Huber. In this program, Aneetta developed a Smart Mug that read and recorded vital health parameters for elderly patients. Later in Fall 2014, Aneetta joined the Ph.D. program in Bioengineering at UT Arlington under the guidance of Dr. Nguyen. Here, Aneetta gained her experience in developing nanoparticle based therapeutic modalities for cardiovascular disease applications. Her major research interest includes development of a multifunctional nanoparticle system that can function as an imaging tool as well as support tissue regeneration following percutaneous coronary interventions. Other research interests include the development of nanoparticle-based DNA and small molecule delivery for the treatment of cardiovascular diseases and childhood sarcoma. Also, she gained expertise in fabrication of stimuli-responsive nanoparticles for the treatment and imaging of lung cancer and arterial fibrillation. During her Ph.D. career at UTA, Aneetta has maintained membership in the Society for Biomaterials and the Biomedical Engineering Society, and has presented her research at over 10 national and local conferences. She has also published 8 papers in peer-reviewed journals and 1 book chapter, in addition to an article in submission for a review process and three other articles in preparation for submission. She has mentored 2 high school students, 2 undergraduate students and 5 graduate students in research. During her Ph.D. program at UTA, Aneetta was financially supported by GAANN, STEM GRA, NIH T32 fellowships as well as a NIH F31 predoctoral fellowship.